Synaptic Circuitry of Ganglion Cells in the Mammalian Retina

Dissertation
Zur Erlangung des Grades
"Doktor der Naturwissenschaften"

Am Fachbereich Biologie
Der Johannes Gutenberg-Universität Mainz

Sonja Neumann
geb. in Wiesbaden

Mainz, Oktober 2014

Dekan:

1. Berichterstatter:

2. Berichterstatter:

Datum der mündlichen Prüfung: 16.04.2015

D77

Contents

List of Figures

List of Tables

Abbreviations

°C	Degree Celsius
$\lambda_{[abs]}$	absorbtion wavelength
$\lambda_{[exc]}$	excitation wavelength
$\lambda_{[max]}$	maximal absorption wavelength
τ	τ decay time constant
µl	microliter
µm	micrometer
A cell	Alpha ganglion cell
$A_{(OFF\text{-}S)}$	sustained OFF-Alpha ganglion cell
$A_{(OFF\text{-}T)}$	transient OFF-Alpha ganglion cell
$A_{(ON\text{-}S)}$	sustained OFF-Alpha ganglion cell
A. dest.	distilled water
AA	amino acid
AC	amacrine cell
ANOVA	analysis of variance
BB	blue- (S-ON) bipolar cell
BC	bipolar cell
BSA	bovine serum albumin
B-type	ganglion cell types with small dendritic trees
C	cone photoreceptor
CaBP	calbindin (calcium binding protein)
CCK	cholecystokinin
ch	chicken
ChAT	choline acetyl transferase
CreER	Cre-recombinase-oestrogene receptor fusion protein
CtBP2	C-terminal binding protein 2
Cy3	Indocarbocyanine (flourophore)
Cy5	Indodicarbocyanine (fluorophore)
D2	bistratified ganglion cell type in mouse retina
DB	diffuse bipolar
DIC	differential interference contrast

dk	donkey
DSGC	direction-selective ganglion cell
$F(ab)_2$	Fragment of the 2 antigen binding sites of antibodies
FMB	flat (OFF-) midget bipolar cell
GABA	gamma-amino butyric acid
$GABA_A$	$GABA_A$ receptor (ionotropic)
$GABA_AR\alpha$	$GABA_A$ receptor subunit α
GC	ganglion cell
GCL	ganglion cell layer
GFP	green fluorescent protein
GFP-O	transgenic mouseline expressing GFP in some retinal ganglion and amacrine cells
GLT-1	glutamate transporter 1 (also excitatory amino acid transporter 2)
GlyR	glycine receptor
GlyRα	glycine receptor subunit α
gt	goat
H	horizontal cell
h	hour
HC	horizontal cell
IB	invaginating (ON-) bipolar cell
IgG	immunoglobuline G
IMB	invaginating (ON-) midget bipolar cell
INL	inner nuclear layer
IPL	inner plexiform layer
ipRGC	intrinsically photosensitive retinal ganglion cell
IS	inner segments of photoreceptors
IS/OS	inner and outer segments of photoreceptors
Jam-B	junctional adhesion molecule B
Jam-B mouse	transgenic mouseline expressing YFP in asymmetric monostratified ganglion cells (OFF direction-selective (C6) ganglion cells)
L-cones	long-wavelength sensitive cones
LGN	lateral geniculate nucleus
L-opsin	opsin most sensitive to long-wavelength (red) light
M-/L- cones	cone photoreceptors expressing M- or L-opsin
M1	outer-stratifying, melanopsin expressing ganglion cell type 1 (M1 ipRGC)
M2	inner-stratifying, melanopsin expressing ganglion cell type 2 (M2 ipRGC)

mBC	midget bipolar cell
M-cones	middle-wavelength sensitive cones
Mk	macaque
M-opsin	opsin most sensitive to middle-wavelength (green) light
ms	mouse
NDS	normal donkey serum
NFL	nerve fiber layer
NGS	normal goat serum
NHS	normal horse serum
ns	not significant
NTA	non-triad associated
ONL	outer nuclear layer
OPL	outer plexiform layer
OS	outer segments of photoreceptors
PB	phosphate buffer
PBS	phophate buffered saline
PCR	polymerase chain reaction
PFA	paraformaldehyd
PNA	peanut agglutinin
PR	photoreceptor
R	rod
rb	rabbit
RB	rod bipolar cell
rb	rabbit
Rec	recoverin
S1−5	Sublamina 1−5
S-cones	short-wavelength sensitive cones
sh	sheep
S-ON BC (BB)	ON-bipolar cell type selectively contacting S-cones (blue- or blue-ON bipolar cell (BB))
S-opsin	opsin most sensitive to short-wavelength (blue) light
Syt2	synaptotagmin-2
TA	triad associated
Tx	Triton X-100 (detergent)
UV	ultraviolet
YFP	yellow fluorescent protein

Chapter 1

Introduction

1.1 Vision sense and the retina

Vision is one of our most crucial senses. It provides the individual with precise information about its environment and thereby allows orientation and navigation. In addition to these image forming functions, which are also known as "conscious" vision, there are more subtle functions of vision, such as the adjustment of the individual to diurnal rhythms and the overall brightness of its environment. All of these functions, image forming and non-image forming, are processed in different visual areas of the brain. However, the first steps of this processing occur already inside of the eyes.

The retina is a thin layer of sensory neural tissue lining the back of the eye, which is formed by five major neural cell classes (photoreceptors, horizontal-, bipolar-, amacrine and ganglion cells) and glial cells (Müller cells, astrocytes and microglia). These cells are arranged in several distinct layers: The nuclear layers, where the cell bodies recide and the plexiform layers, where synaptic connections between the cells are built (Fig. 1.1). Vertebrates possess a so-called inverted retina, meaning that the light has to pass through all layers of the retina before it reaches the actual sensory cells of the retina, the **photoreceptors** (Fig. 1.1 A, yellow arrow). With their photopigments, called opsins, photoreceptor cells detect photons of the light passing through the pupil and the optic apparatus of the eye. The opsins are located in specialised membrane intrusions of their outer segments, which are in contact with the pigment epithelium. The detection of photons by opsin molecules in the photoreceptor

leads, via a sophisticated transduction cascade, to a change of the excitation state of the photoreceptors and hence a change in its neurotransmitter release. The somata of the photoreceptors form the outermost layer of cell bodies of the retina, the **outer nuclear layer** (ONL). Their axon terminals (pedicles in case of cone- and spherules in case of rod photoreceptors) are part of the **outer plexiform layer** (OPL), where they contact horizontal and bipolar cells.

Horizontal cells are GABAergic (gamma amino butyric acid) interneurons. Their neurites are located within the OPL where they modulate the responses to light of the photoreceptors via lateral inhibition (reviewed by Euler *et al.*, 2014). Their cell bodies are located in the outermost part of the second layer of cell bodies in the retina – the **inner nuclear layer** (INL). Depending on the species one or two anatomical types of horizontal cells, named A-type and B-type horizontal cells, are known in mammals (Peichl, 1998). A-type horizontal cells contact only cone photoreceptors, whereas the B-type horizontal cells receive additional input from rod photoreceptors onto their axonal processes (Peichl & Gonzalez-Soriano, 1994; Hack & Peichl, 1999; reviewed by Peichl, 1998). The primate retina in contrast contains two axon bearing horizontal cell types, H1 and H2 horizontal cells. H1 cells connect to rods with their axon and receive input from middle- and long-wavelength sensitive cones (M- and L-cones). H2 cells by contrast receive input predominantly from short-wavelength sensitive cones (S-cones) (Kolb *et al.*, 1980; Dacey *et al.*, 1996). Their connections to different cone types indicate their different roles in processing of chromatic signals.

Bipolar cells, in contrast, are glutamatergic interneurons involved in the vertical retinal pathway. Depending on the species, 10 to 15 distinct types of bipolar cells are known, which differ in their morphology and physiological properties (reviewed by Masland, 2001a and Euler *et al.*, 2014). The cell bodies of bipolar cells occupy the middle layers of the INL. Their dendrites reach to the OPL where they receive synaptic input from photoreceptors. This signal is transferred to amacrine and ganglion cells in the second synaptic layer of the retina, the **inner plexiform layer** (IPL). The IPL can be subdivided into five distinct strata of equal thickness (sublamina S1 – S5) according to Ramón y Cajal (1892) or is subdivided with regards on physiological function, into two strata, the outer sublamina a or OFF-layer (corresponding to S1 and S2) and

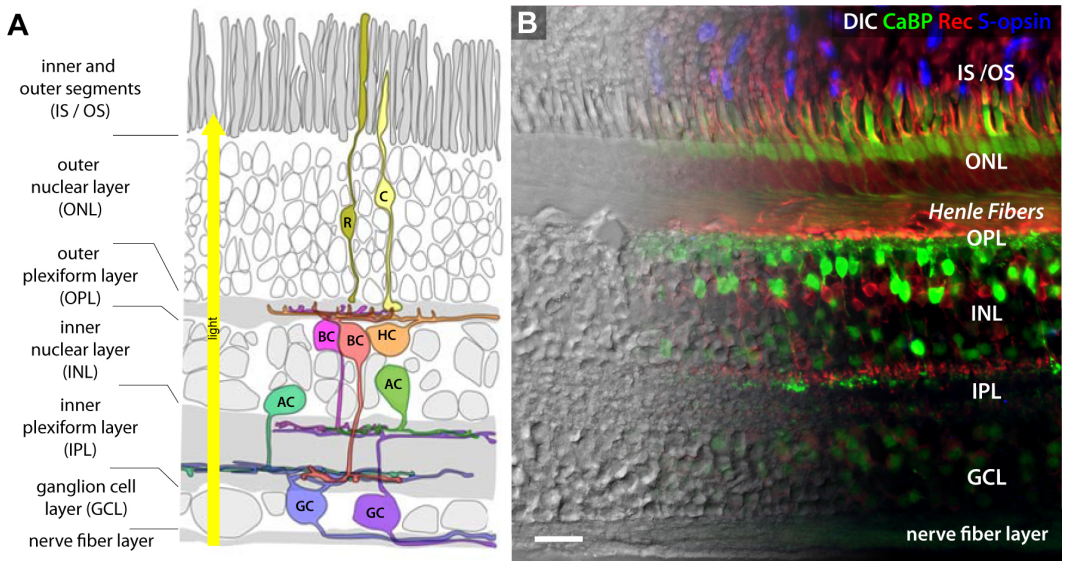

Figure 1.1: The mammalian retina. (A) Scheme of a section through a mouse retina. Layers are indicated on the left. Examples of the neuronal cell classes are highlighted in different colours (rod and cone photoreceptors (R and C), horizontal, bipolar, amacrine and ganlion cells (HC, BC, AC and GC). Light has to pass through all retinal layers before it reaches the outer segments of the photoreceptors (arrow). **(B)** Vertical section through a part of central primate retina, immunostained against different cell markers (Calbindin (CaBP), Recoverin (Rec) and S-opsin), partially overlaid with the differential interference contrast (DIC) image of the section showing the retinal layers. CaBP labelled Cs, HCs and BCs; Rec labelled Rs, Cs and flat midget bipolar cells (FMBs); S-opsin labelled the outer segments of S-cones. Layers are indicated on the right. The Henle fibers as well as multiple layers GC somata are a specialisation of the central primate retina. Scale bar: 25 µm.
(A: Modified from Euler *et al.*, 2009. B: Own unpublished data.)

the inner sublamina b or ON-layer corresponding to S3 – S5. A general scheme is that cells responding to light offset are connected in sublamina a, whereas cells responding to the onset of light stratify in sublamina b (Famiglietti & Kolb, 1976).

Amacrine cells form the second group of inhibitory interneurons within the retina and modulate the responses of bipolar and ganglion cells. They are the most diverse cell class in the mammalian retina (Masland, 2001a). Two major sub-classes are distinguished, the glycinergic small-field and the GABAergic wide-field amacrine cells. The cell bodies of the majority of amacrine cells are located in the inner tiers of the INL; the somata of some wide-field amacrine cells, however, are displaced in the ganglion cell layer.

Ganglion cells are the output elements of the retina and a plethora of functional as well as morphologically distinct types exist (reviewed by Masland, 2001a; Rockhill *et al.*, 2002; Wässle, 2004; please refer also to subsection 1.1.4). They receive the signals derived from the photoreceptors via bipolar cells and are modulated by amacrine cells on their dendrites within the IPL. Together with the cell bodies of displaced amacrine cells somata of ganglion cells form the innermost nuclear layer of the retina: the **ganglion cell layer** (GCL). Some cell bodies, however, are displaced into the inner INL. The ganglion cell axons form the **nerve fiber layer** (NFL) and exit the retina at the optic disc, where they form the optic nerve. The ganglion cells project to higher retino-recipient brain areas and transmit visual signals for further processing.

In summary, the retina possesses two general pathways: the **vertical pathway**, which is mediated by glutamate and describes the connection from photoreceptors to bipolar cells to ganglion cells and the **lateral pathway**, which describes the inhibitory modulation by GABAergic horizontal cells in the OPL as well as the modulation by GABAergic and glycinergic amacrine cells in the IPL.

1.1.1 The classical photoreceptors: Rods and Cones

The mammalian retina contains two classes of photoreceptors (duplex retina), which are responsible for image forming vision, the rods and cones. The ratio of rods and cones varies strongly between the different mammalian species, but is often correlated with the animals´ habitat and the temporal niche (primate: Wikler & Rakic, 1990; reviewed by Peichl, 2005). Rods and cones differ in their light sensitivity, kinetics and spectral tuning.

Rods are highly light sensitive and are even capable of single photon detection (reviewed by Wässle, 2004). Hence, rods mediate vision under scotopic light conditions, e.g. by night. Retinae of nocturnal animals are therefore often rod dominated. The rod photopigment, rhodopsin, is located in specialised membrane intrusions, called discs, in their outer segments. The maximal absorption (λ_{max}) of rhodopsin peaks close to light of 500 nm wavelength (Bowmaker & Dartnall, 1980a, reviewed by Hunt & Peichl, 2013).

Cones are less light sensitive than rods and mediate vision at higher light levels (photopic conditions), in which rods are saturated. Cones also exhibit

faster response kinetics, enabling them to contribute to vision of high temporal resolutions (*turtle:* Baylor & Hodgkin, 1973; Schnapf & Copenhagen, 1982; *salamander:* Cadetti *et al.*, 2005; *mouse:* Nikonov *et al.*, 2006). In contrast to rods, multiple cone types exist, which differ in their tuning to different spectra of light, enabling the organism to colour (chromatic) discrimination. This difference in their spectral tuning is based on the expression of different opsin molecules with distinct spectral absorption maxima. Most eutherian mammalian species possess two different cone types, one expressing an opsin most sensitive to short-wavelength light (S-opsin; range: $[\lambda_{max} = 365 - 450\,nm]$) and hence referred to as S-cones and one cone type expressing an opsin most sensitive for light of longer wavelengths (range: $[\lambda_{max} = 510 - 565\,nm]$), which are generally referred to as middle-wavelength sensitive cones (M-cones) (Bowmaker & Hunt, 2006)[1]. Hence, these animals are dichromates.

Some primate species are capable of trichromatic vision as a result of the expression of three cone opsins with distinct absorption spectra: S-opsin, which is most sensitive to short- ($[\lambda_{max} \approx 410 - 420\,nm]$), M-opsin, most sensitive to middle- ($[\lambda_{max} \approx 520 - 535\,nm]$) and L-opsin, which is most sensitive to long-wavelength light ($[\lambda_{max} \approx 560 - 575\,nm]$). According to the opsin type they express, S-, M- and L-cones are distinguished in retinae of trichromatic primates (Bowmaker & Dartnall, 1980b; Bowmaker *et al.*, 1980).

A common feature shared by both photoreceptor classes, rods and cones, is their constant release of glutamate in darkness, which is reduced upon the detection of light. The absorption of photons by the photopigments results in the start of a molecular signalling cascade, leading to the closure of sodium and potassium channels, which in turn hyperpolarises the cell and reduces the neurotransmitter release. This reduction of neurotransmitter release, however, leads to different responses in the downstream bipolar cells.

[1] It is noteworthy that the sensitivity of cone photoreceptors in several rodent species are shifted to shorter wavelengths, compared to other species. The sensitivity of mouse S-cones for example peaks in the UV-spectrum around 360 nm, whereas it recides in the blue spectrum of light around $420 - 450$ nm in other species. This difference in the spectral sensitivity exists also in M-cones. Their spectral sensitivity lies around $[\lambda_{max} = 510\,nm]$ in mice and in a range of about $[\lambda_{max} = 530 - 560\,nm]$ in carnivores and primates (reviewed by Bowmaker & Hunt, 2006 and Peichl, 2005)

1.1.2 Bipolar cells

Bipolar cells relay the signals of photoreceptors to ganglion cells and are functionally divided in OFF- and ON-bipolar cells.

OFF-bipolar cells express ionotropic glutamate receptors on their dendritic tips, which are located on the base of the cone pedicles. They respond to the offset of light following an increase of glutamate released by photoreceptors and are hence sign-conserving.

ON-bipolar cells, in contrast, express metabotropic glutamate receptors on their dendritic tips and are depolarised at the onset of light, caused by a reduction of the glutamate release from the photoreceptors in response to light. ON-bipolar cells make invaginating contacts (see section 1.2) beneath the synaptic ribbons of the photoreceptor terminals (cone pedicles and rod spherules) with their dendrite. It was also demonstrated that some ON-bipolar cells make additional basal contacts to the cone pedicle, but the majority of their contacts are invaginating (Hopkins & Boycott, 1997).

This dichotomy of bipolar cells is also reflected by the anatomy of their axon terminals (Famiglietti & Kolb, 1976). Axon terminals of OFF-bipolar cells stratify within the **OFF-layer**. Within these strata they provide synaptic input onto the dendritic trees of ganglion cells, which in turn also respond to the offset of light. ON-bipolar cells possess axon terminals, which are located within the **ON-layer**. Within these layers ON-bipolar cells provide input to ganglion cells also responding to the onset of light. Depending on the species about 4 – 5 types of OFF- and 5 – 6 types of ON-cone bipolar cells and one type of rod bipolar cell are described in mammals (Fig. 1.2).

A further criterion to distinguish cone bipolar cell types is the specificity of their **contacts to cone** photoreceptors. Most cone bipolar cells contact all cone photoreceptors within their dendritic field. However, since S-cones contribute only 5 – 10 % of all cones in most mammalian species, the input onto bipolar cells receiving mixed cone input is dominated by M- and L-cones in primates, or M-cones in dichromatic species. Blue light signals detected by S-cones are transferred through the retina by specialised bipolar cells, which selectively contact S-cones. Such S-cone selective bipolar cells were described in several mammalian species, including mice and primates (*mouse:* Haverkamp

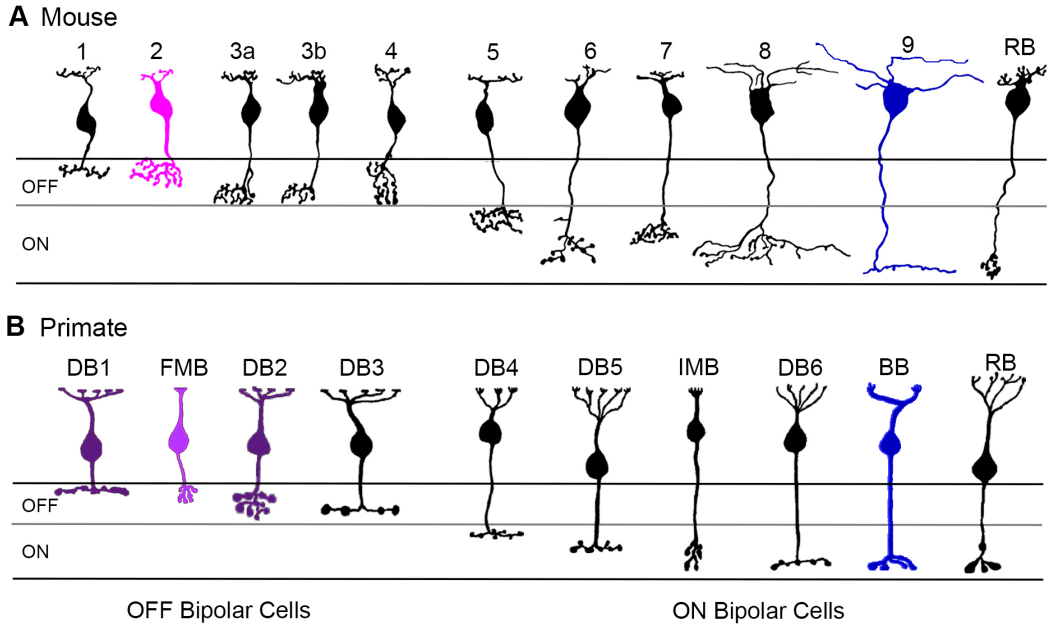

Figure 1.2: Bipolar cell types in mouse (A) and macaque (B) retina. Bipolar cell types are indicated above the cells (type 1−9 in mouse, diffuse bipolar cell (DB) type 1−6, flat- and invaginating midget bipolars (FMBs and IMBs, respectively), S-ON (blue-) bipolar cells (BB) in macaque, rod bipolar cells (RBs) in both species). In mouse retina type 1 bipolar cells are labelled by antibodies against synaptotagmin-2 (magenta). In the macaque retina FMBs, DB1 and DB2 cells are labelled by antibodies against the glutamate transporter-1 (GLT-1) (purple), whereas antibodies against recoverin (Rec) label FMBs only (light purple). S-cone selective ON- bipolar cells are marked in blue (both species). (Modified from Ghosh *et al.*, 2004.)

et al., 2005; *primate:* Mariani, 1984), suggesting that they form an ancient retinal pathway. These bipolar cells are ON-bipolar cells, which make invaginating contacts with the S-cone pedicles and stratify with their axon terminals within the ON-layer of the IPL. Hence these cells are referred to as **S-ON bipolar cells** in the following text. Selective contacts between S-cones and OFF-bipolar cells are still controversially discussed and are described in more detail in subsections 1.4.2 and 1.4.3.

The central primate retina contains an additional complexity regarding the specificity of connections between cones and bipolar cells. Most bipolar cell types sample synaptic input from multiple cone types in their dendritic field, and are hence called diffuse bipolar cells (DBs). Primates possess a bipolar cell

type connected only to a single cone and a single ganglion cell, the so-called **midget bipolar cell**. Midget bipolar cells exist in an OFF- (flat midget bipolar cells, FMBs) and an ON-variant (invaginating midget bipolar cells, IMBs). This one-to-one connection allows transferring high acuity and colour selective signals to higher brain areas, in case of midget ganglion cells to the dorsal lateral geniculate nucleus (LGN). This circuit is well established for M- and L-cones leading to green-red colour opponency and exists in an ON- and OFF-circuit. However, the existence of a midget system connected to S-cones is still on debate (see 1.4.2 and 1.4.3).

1.1.3 Amacrine cells

Amacrine cells are inhibitory interneurons of the inner retina, which receive glutamatergic synaptic input from bipolar cells and inhibitory inputs from other amacrine cells within the IPL. In turn, amacrine cells provide synaptic output to ganglion cells, bipolar cells as well as other amacrine cells and thereby controll the output from bipolar cells onto ganglion cells or directly modulate ganglion cell responses. Most amacrine cells use glycine or GABA as their neurotransmitter and are thought to modulate the responses of target cells via inhibitory synaptic input. A plethora of different amacrine cell types has been described morphologically and functionally in various species (Masland, 2001a). However, they can be coarsely sub-divided into wide-field amacrine and small-field amacrine cells.

Wide-field amacrine cells are characterised by large monostratified dendritic arbors, which are restricted to narrow sublaminae of the IPL. The stratification depth depends on the cell type and hints in which retinal pathway the cells are involved. Because of their wide dendritic trees and narrow stratification, wide-field amacrine cells are generally thought to be involved in lateral modulations of retinal circuits. As their primary neurotransmitter, wide-field amacrine cells use GABA and can be immunohistochemically labelled using antibodies against GABA or its synthesising enzyme glutamic acid decarboxylase, often abbreviated as GAD. However, many of the GABAergic amacrine cells contain an additional neuromodulator as secondary transmitter, such as acetylcholine, substance P, neuropeptide Y or serotonin (reviewed by Zhang & McCall, 2012). As a special case, however, appear the dopaminergic amacrine

cells (type 1), which were shown to lack immunoreactivity to GABA, but are positive for glutamate (Anderson *et al.*, 2011). Dopaminergic amacrine cells stratify within the OFF-layer of the IPL and respond to the onset of light (Zhang *et al.*, 2007).

Small-field amacrine cells, in contrast, use glycine as their neurotransmitter and their dendritic trees occupy only small lateral areas (10 – 100 µm in diameter) within the IPL. Vertically, however, their dendrites commonly span several sublaminae of the IPL. Morphologically, small-field amacrine cells are a highly diverse group, which often possess bistratified trees and are involved in crossover inhibition between retinal ON- and OFF-layers. Thereby, they form crucial elements of many retinal pathways. The **AII amacrine cells** for example, are involved in the scotopic rod pathway. They receive input from rod bipolar cells and convey these signals via inhibitory synapses onto OFF-bipolar cells and via electrical synapses (gap junctions) onto cone ON-bipolar cells (newly analysed by Marc *et al.* (2014)). Another example are small-field amacrine cells, which receive synaptic input from S-ON bipolar cells and mediate S-OFF signals (Chen & Li, 2012; Mills *et al.*, 2014; Sher & DeVries, 2012; see also subsection 1.4.3 and Fig. 1.6 B).

Cells postsynaptic to amacrine cells express distinct subtypes of GABA or glycine receptors, which differ in their kinetic properties. In most cases the receptor types expressed hint to the involvement of these cells in certain retinal pathways (see also section 1.3).

1.1.4 Ganglion cells

Ganglion cells are the retinal output elements. They receive glutamatergic synaptic input from bipolar cells and are modulated by inhibitory synaptic input from glycinergic and GABAergic amacrine cells. In turn the ganglion cells send their signal via their axons through the optic nerve to higher brain areas, such as the LGN or the suprachiasmatic nucleus, for further processing.

About 10 – 15 different types of ganglion cells with different morphological and physiological properties have been described in the mammalian retina (Wässle, 2004). Important **anatomical** features used to determine the ganglion cell type are the stratification depth of the dendrites in the IPL, the branching pattern of the dendrites, and the size of the dendritic field. The

dendritic field size, however, should be used for classification with regard of the eccentricity of the respective cells. In primate retina, the extension of the dendritic field of retinal cells varies depending on the cells distance to the fovea, with cells of large dendritic trees in the periphery and small ones within and close to the fovea. Similar variations were also observed in other species, such as the cat and rabbit (*cat:* Stein *et al.*, 1996; Berson *et al.*, 1998, 1999, and Isayama *et al.*, 2000; *rabbit:* Peichl *et al.*, 1987b). For other mammals a more homogenous distribution of cells was assumed, a recent study by Bleckert *et al.* (2014), however, demonstrated a significant change of the dendritic tree sizes of certain ganglion cell types in the mouse retina.

Physiologically, ganglion cells form a highly diverse group. In a first attempt ganglion cells can be divided into **ON- and OFF-**ganglion cells which respond to light onset or offset only. This division correlates in most cases with the stratification depth of the dendritic tree within the IPL. Ganglion cells responding to the offset of light stratify in OFF-layer of the IPL, where they receive their driving input from OFF-bipolar cells. Ganglion cells responding to the onset of light, in contrast, branch within the ON-layer and receive input from ON-bipolar cells[2] (see also subsection 1.1.2). Bistratified ganglion cells with dendritic trees branching in both layers display ON/OFF-responses to appropriate stimulation.

A further property to distinguish physiological types of ganglion cells is the division into **transient and sustained** ganglion cells. Alpha ganglion cells exist in ON- and OFF-populations. These cells are morphologically characterised by large somas and dendritic trees with radiate branching and were found in many species (Peichl *et al.*, 1987a). In mouse retina Alpha ganglion cells stratifying in the OFF-layer of the IPL (A_{OFF}) cells), for example, were shown to exist in a sustained ($A_{OFF\text{-}S}$) and a transient responding type ($A_{OFF\text{-}T}$) (van Wyk *et al.*, 2009). It should be noted here that $A_{OFF\text{-}T}$ and $A_{OFF\text{-}S}$ cells stratify in slightly different strata of the IPL, according to findings that transient responding cells branch in the centre, whereas sustained or

[2] An important exception is formed by outer-stratifying melanopsin expressing ganglion cells. Similar to dopaminergic amacrine cells, the dendrites of these ganglion cells branch at the outer border of the IPL (OFF-layer), but respond to the onset of light (Dacey *et al.*, 2005).

tonic responding cells branch closer to the borders of the IPL (van Wyk *et al.*, 2009; Baden *et al.*, 2013).

In addition to this broad subdivision of ganglion cell types, ganglion cells, which are dedicated to specific functions, such as the processing of movement direction (direction-selective ganglion cells (DSGCs)), colour (e.g. small bistratified ganglion cells of the primate retina) or contrast, are described and match in many cases to morphologically classified cells. Therefore, many ganglion cells provide good examples for the correlation of structure and function in neurons. Further, the diversity of ganglion cells shows that the information of a light stimulus is processed in several parallel pathways dedicated to specific features.

Melanopsin ganglion cells

Special cases of ganglion cell are the intrinsically-photosensitive ganglion cells (ipRGCs), which express the photopigment melanopsin (Berson *et al.*, 2002; Hattar *et al.*, 2002; Provencio *et al.*, 1998). The expression of melanopsin renders these ganglion cells intrinsically photosensitive even in the absence of synaptic input derived from the classical photoreceptors (reviewed by Pickard & Sollars, 2012), which was demonstrated in sophisticated physiological experiments on retinae with ablated photoreceptors and chemical blockage of synaptic transmission. In contrast to the conventional photoreceptors, rods and cones, ipRGCs depolarise in response to the onset of light independent of the depth of stratification of their dendrites within the IPL. In addition to their intrinsic photosensitivity, ipRGCs are also integrated in the retinal circuits and receive synaptic input from amacrine and bipolar cells (*anatomy:* Belenky *et al.*, 2003; Jusuf *et al.*, 2007; Viney *et al.*, 2007; *physiology:* Dacey *et al.*, 2005; Perez-Leon *et al.*, 2006; Viney *et al.*, 2007; Wong *et al.*, 2007; reviewed by Pickard & Sollars, 2012). Interestingly, it was demonstrated, that also outer-stratifying ipRGCs receive synaptic input from ON-bipolar cells within the OFF-layer of the IPL (Dumitrescu *et al.*, 2009; Hoshi *et al.*, 2009; Grünert *et al.*, 2011). However, ipRGCs in the primate retina were also shown to exhibit colour opponent responses, showing OFF-responses to short-wavelegth and ON-reponses to light of longer wavelengths (S-OFF/yellow ON responses) (Dacey *et al.*, 2005).

Before further prominent examples of ganglion cells types and the retinal circuits they rely on are discussed in more detail, different types of synapses of the retina are depicted.

1.2 Triads, dyads and conventional synapses of the retina

The glutamatergic neurotransmission in the retina from photoreceptors and bipolar cell is mediated by specialised synapses, called **ribbon synapses** (Fig. 1.3). The vesicles containing the neurotransmitter are tethered to a protein band (synaptic ribbon) at the presynaptic site. The ribbon is thought to facilitate the transport of the vesicles to the presynaptic membrane and the constant release of glutamate. Ribbon synapses can be labelled using antibodies against the C-terminal binding protein 2 (CtBP2; see Fig. 1.3 F and H, cyan tag). In light microscopy, the CtBP2 labelling results in a punctate staining within the IPL whereas ribbon synapses in the OPL appear punctate at cone pedicles and horseshoe-shaped at rod spherules (Tom Dieck *et al.*, 2005). Such differences of the staining are based on the difference of the synapses of the OPL and IPL. **Rod spherules** contain typically only one large bent ribbon resulting in the horseshoe-shaped staining in light microscopy. Using electron microscopy it was demonstrated that on the post-synaptic site, apposed to the synaptic ribbon, is a complex of two lateral elements formed by horizontal cell processes and a central element formed by the invaginating dendrite of a rod bipolar cell (Fig. 1.3 B). This synaptic entity composed of the presynaptic ribbon, two lateral elements and an invaginating bipolar cell process, is called synaptic **triad** (Dowling & Boycott, 1966; Kolb, 1970; Boycott & Kolb, 1973a,b).

Cone pedicles by contrast contain multiple synaptic ribbons and form multiple synaptic triads (Figs. 1.3 C–F). Like in rod spherules, the lateral elements of triads of cone pedicles are also formed by horizontal cell processes, whereas the central elements are formed by invaginating dendrites of cone bipolar cells. These bipolar cells possess axon terminals branching in the inner part of the IPL (ON-layer) and are, hence, presumably ON-bipolar cells (Famiglietti & Kolb, 1976). The invaginations at cone pedicles are immuno-

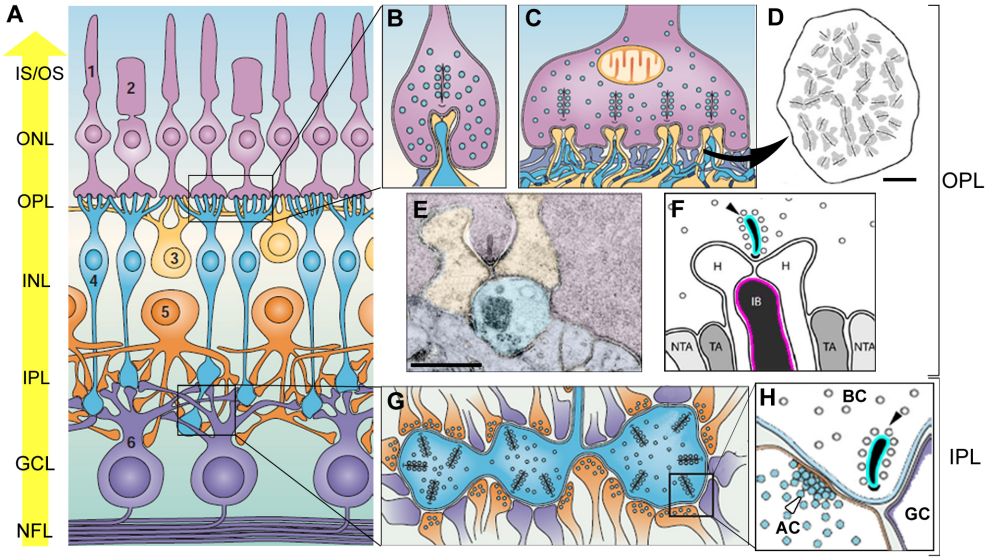

Figure 1.3: Ribbon synapses of the mammalian retina - dyads and triads. (A) Scheme of a mammalian retina depicting the neuronal cell classes (photoreceptors (1, 2), horizontal- (3), bipolar- (4), amacrine- (5) and ganglion cells (6)) and the retinal layers (left). Arrow depicts the light path through retinal layers (legend see Fig 1.1 A). **(B – F)** Synaptic triads of the OPL. **(B)** Scheme of a rod spherule. One synaptic ribbon is apposed to two horizontal cell processes (yellow) and a central invaginating dendrite of rod bipolar cells. **(C)** Scheme of a cone pedicle. Cone pedicles harbour multiple ribbons, each building a synaptic triad with two lateral processes of horizontal cells and a central element formed by invaginating cone ON-bipolar cells (blue). The cone pedicle base is contacted by dendritic tips of OFF-bipolar cells (purple) at flat contacts. **(D)** Drawing of a horizontal view through a cone pedicle (synaptic ribbons: black lines; invaginating horizontal and bipolar cell processes: dark and light grey). **(E)** Electron microscopic image of a cone pedicle triad. The overlaid colouration follows the colour scheme in A – C. **(F)** Drawing of a cone pedicle triad. The arrowhead points to the synaptic ribbon (cyan: labelling pattern of CtBP2 antibodies; magenta staining pattern of peanut agglutinin (PNA)). Basal (flat) contacts are divided in triad associated (TA) and non triad associated (NTA) contacts. **(G – H)** Synaptic dyads of the IPL. **(G)** Scheme of a bipolar cell terminal (blue) within the IPL. The synaptic ribbons of cone bipolar cells apposed to ganglion cell dendrites (lilac) and amacrine cell processes (orange) forming synaptic dyads. **(H)** Drawing of a synaptic dyad. The synaptic ribbon (arrowhead, cyan: CtBP2 staining) of bipolar cells (blue outline). The dendrites of a ganglion cell (GC, lilac outline) are identifiable in electron micrographs by their lack of synaptic vesicles. Amacrine cell (AC, orange) possesses synaptic vesicles and forms a conventional feedback synapse (open arrowhead) onto the bipolar cell terminal. Scale bars: 2 µm (D) and 0.5 µm (E). (Modified from Wässle, 2004 (A – C, G and H), Haverkamp *et al.*, 2000 (D and E) and Puller *et al.*, 2007 (F)).

histochemically identifiable using the lectin peanut agglutinin (PNA), coupled to a fluorophore (Blanks & Johnson, 1984; Haverkamp *et al.*, 2001; see also Fig. 1.3 F, pink marking). Hence, PNA is a suitable marker for synaptic sites at cone pedicles.

In addition to invaginating contacts, cone pedicles are also massively decorated with flat or basal contacts, formed by putative OFF-bipolar cells on their base. In primate retina these basal contacts are further divided in triad associated (TA) and non-triad associated (NTA) contacts depending on the distance to the next triad (Fig. 1.3 F). Midget bipolar cells (flat midget bipolar cells, FMBs) mostly harbour the TA contacts, while diffuse bipolar cells form NTA contacts in most cases (Hopkins & Boycott, 1997)[3].

Whithin the IPL, terminals of bipolar cells also form ribbon synapses. In contrast to the synaptic triads at the photoreceptors, the ribbons of bipolar cells are apposed to only two postsynaptic elements, forming an entity called **synaptic dyad** (Dowling & Boycott, 1966). Generally an amacrine cell process and a ganglion cell dendrite form the postsynaptic elements of the dyad (Fig. 1.3 G, and H).

Amacrine cells in the IPL make **conventional synapses**, which are identifiable by electron microscopy as close appositions of the membrane of the presynaptic amacrine cell and the postsynaptic cell and the accumulation of neurotransmitter vesicles at the presynaptic membrane (Fig. 1.3 H, open arrowhead). With light microscopy and immunohistochemistry conventional synapses can be revealed by using specific antibodies against synaptic proteins, for instance against receptors of the neurotransmitter on the postsynaptic site (section 1.3).

Synaptic contacts between neurons can also be formed via **gap junctions** or electrical synapses. With this type of synapse neurons are electrically coupled to each other, allowing a transmission of the electrical potential between the coupled cells without a neurotransmitter. The intracellular space of the cells is directly connected with connexons, or hemichannels, which allow the diffusion of ions and small molecules. Thereby gap junctions allow the transmission of

[3]The authors reported 76 TA and 20 NTA contacts on 41 synaptic ribbons, formed by an FMB, whereas a previous study reported 32 TA and no NTA contacts of an FMB in vervet monkey retina.

the electric potential of the cells (reviewed by Söhl *et al.*, 2005 and Cook & Becker, 1995).

1.3 GABA and Glycine Receptors

GABA and glycine are the major inhibitory neurotransmitters of the central nervous system. Within the retina horizontal cells and wide-field ACs were found to contain GABA, whereas glycine was found in amacrine and some ON-bipolar cells. However, only the amacrine cells use glycine as their neurotransmitter. Bipolar cells, by contrast, are glutamatergic neurons and thought to contain glycine because of extensive coupling to glycinergic amacrine cells (Vaney *et al.*, 1998). Both inhibitory neurotransmitters, glycine and GABA, act on ionotropic or metabotropic receptors expressed by the postsynaptic cells.

Only little is known about **metabotropic GABA ($\mathbf{GABA_B}$)** and **glycine receptors (GlyRs)** in the retina. The G-protein coupled $GABA_B$ receptors form dimers assembled from two distinct seven-transmembrane subunits. They are localised at amacrine and ganglion cells, however their existence on bipolar cells remains controversial (Benke *et al.*, 2002; Koulen *et al.*, 1998; Song & Slaughter, 2010). Only one study found physiological evidence for metabotropic GlyRs in salamander retina (Hou *et al.*, 2008).

1.3.1 Ionotropic Receptors

Ionotropic $GABA_A$ and glycine receptors are ligand gated ion channels, which are assembled from 5 subunits. Upon ligand binding, the channel opens, leading to a conductance of chloride ions through the cell membrane. In the mature retina this conductance leads to an influx of chloride ions, hyperpolarising the postsynaptic cell. In the developing retina, in contrast, GABA acts as excitatory neurotransmitter, because of an elevated intracellular chloride ion concentration in cells expressing the ionotropic receptors (Ben-Ari, 2007; Ben-Ari *et al.*, 2007).

Two classes of ionotropic GABA receptors, the so-called **$\mathbf{GABA_A}$** and **$\mathbf{GABA_C}$** receptors exist in the central nervous system. $GABA_C$ receptors are assembled from ρ-subunits. Five different subunits ($\rho 1 - \rho 5$) exist, but

only subunits $\rho 1-\rho 3$ were documented in the retina until now (reviewed by Zhang & McCall, 2012). For $GABA_A$ receptors subunits $\alpha 1-\alpha 6$, $\beta 1-\beta 3$, $\gamma 1-\gamma 3$, δ, ϵ, θ and π were described. Commonly, $GABA_A$ receptors in retina are composed of two α, two β and one γ subunit (Wässle *et al.*, 1998). Ionotropic **glycine receptors** are composed of three β and two α subunits (Grudzinska *et al.*, 2005; reviewed by Betz & Laube, 2006 and Lynch, 2009). The β subunit is necessary to bind to the anchoring protein gephyrin, which forms a scaffold clustering the receptors at postsynaptic sites (Fritschy *et al.*, 2008). The α subunits, by contrast, contain the ligand- and agonist-binding sites. Whereas only one β subunit exists, four different α subunits ($\alpha 1-\alpha 4$) encoded by different genes are described (*human:* GlyRs $\alpha 1$ and $\alpha 2$: Grenningloh *et al.*, 1990, $\alpha 3$: Nikolic *et al.*, 1998; *mouse:* GlyRs $\alpha 1$: Ryan *et al.*, 1994, $\alpha 2$: Derry & Barnard, 1991, $\alpha 3$: Kingsmore *et al.*, 1994 and $\alpha 4$: Matzenbach *et al.*, 1994; Harvey *et al.*, 2000; reviewed by Becker, 1995). It should be noted that the gene encoding for the $\alpha 4$ subunit is likely to be a pseudogene in humans, the same may hold true in other primate species (Lynch, 2014). The different α subunits convey different kinetic properties to the receptors. GlyRs equipped with the $\alpha 1$ subunit exhibit fast ($\tau_{\text{(bipolar cells)}}$ 5.9 ms), receptors containing the $\alpha 2$ or $\alpha 3$ subunits medium ($\alpha 2$: $\tau_{\text{(small-field amacrine cells)}}$ 27 ms; $\alpha 3$: $\tau_{\text{(AII amacrine cells)}}$ 11 ms) and those containing the $\alpha 4$ subunit slow decay time constants ($\tau_{\text{(starburst amacrine cells)}}$ 70 ms) (*bipolar cells:* Ivanova *et al.*, 2006, *small-field amacrine cells:* Weiss *et al.*, 2008, *wide-field amacrine cells:* Majumdar *et al.*, 2009). Physiological studies, primarily on mouse retinae, in which one or more subunits are eliminated, have shown that certain receptor types are associated with retinal cells and pathways. Also the localisation of the different receptor subtypes varies.

Localisation of Receptor subunits

A precious tool to analyse the localisation of the receptor subunits and gain insight into their involvement in distinct retinal pathways are subunit-specific antibodies. The processing of retinal tissue with such markers results in a punctate staining pattern within the synaptic layers of the retina. Electron microscopy confirmed, that the punctate staining seen with the light microscope represents labelled clusters of receptors containing the marked subunit

at postsynaptic membranes (*primate:* Grünert & Wässle, 1996; Jusuf *et al.*, 2005; *rat:* Sassoe-Pognetto *et al.*, 1994). The reliability of the receptor staining was further corroborated in double-immunolabelling experiments, which demonstrated a colocalisation of the receptor stainings with other synaptic markers such as gephyrin or bassoon (Sassoè-Pognetto *et al.*, 1995; Dick *et al.*, 2003).

Because of their pentameric composition, ionotropic receptors could be assembled from different α subunit types (such as a combination of a GlyRα1 and a GlyRsα2 subunit in the same receptor). Many double-immunolabelling experiments of different receptor subunits demonstrated, that most α subunits do not colocalise within the same postsynaptic clusters, indicating that they are located at different synapses and involved in different pathways. Further, it suggests that most glycine receptors are assembled of only one kind of α subunit.

However, about a third of the GlyRα2 subunit colocalises with GlyRα3 in primate (Jusuf *et al.*, 2005) or with GlyRα3 or GlyRα4 in mouse retina (Haverkamp *et al.*, 2004; Heinze *et al.*, 2007; reviewed by Wässle *et al.*, 2009b). Since the GlyRα2 with GlyRα3 and GlyRα4 clusters were not in perfect register, it was suggested that receptors containing only the α2 or α3 subunits are both located at the same synaptic sites, rather than GlyRs containing one α2 and one α3 subunit.

For $GABA_A$ receptors different staining patterns were found for the different subunits. In rodent retina $GABA_A$ subunits were found accumulated in different strata of the IPL, indicating to their involvement in distinct retinal circuits (Greferath *et al.*, 1995). The clusters of $GABA_A\alpha2$ subunit, for example, are accumulated in the same sublaminae, where the dendrites of cholinergic starburst amacrine cells stratify and are involved in the circuitry of DSGCs (Auferkorte *et al.*, 2012; Brandstätter *et al.*, 1995). In primate retina, however, the α subunits of the $GABA_A$ receptors analysed until now, were distributed more homogeneous (Neumann *et al.*, 2011) and are shown in detail in subsection 3.2.1.

1.4 Specialisations of the primate retina and implications for colour vision

1.4.1 Topography

The primate retina contains a specialised area dedicated to high acuity vision, the fovea. Objects and visual scenes of interest detected by the peripheral retina are brought in register with the fovea by targeted movements of the head or the eyes for closer analysis. The fovea and central area is marked by certain specialisations in their anatomy and connectivity of cells.

The fovea is marked by the highest cone density, but contains only very small numbers of S-cones or is even S-cone free (Ahnelt *et al.*, 1987; Curcio *et al.*, 1991; reviewed by Ahnelt, 1998; Hunt & Peichl, 2013). The fovea also lacks rod photoreceptors, rendering the individual night blind within this retinal spot (Wikler *et al.*, 1990; Curcio *et al.*, 1990; Ahnelt, 1998). Schematic topography maps of the distribution of rod, M-/L-cone and S-cone photoreceptors in human retina are shown in Figure 1.4 A. At the foveal center inner retinal layers are absent creating a depression known as foveal pit. The foveal cones connect to the downstream neuron, which are shifted to the surrounding area via the so-called fibers of Henle (Hendrickson & Kupfer, 1976; Hendrickson, 1992; reviewed by Hendrickson, 1994; Provis *et al.*, 2013; see also Fig. 1.1 B and Fig. 3.11 A). The area surrounding the foveal pit is known as foveal slope and is characterised by high ganglion cell densities, observable as multiple layers of ganglion cells within the GCL (Hendrickson, 1992; compare Fig. 1.1 B and Fig. 3.11 A).

The cell density within the retina changes considerably, also outside of the foveal centre. The maximal density of rods was found in an area dorsal to the fovea (Figure 1.4 A, left). The S-cone density is also highest outside the fovea within an annulus surrounding the fovea, and decreases towards the periphery (Figure 1.4 A, right). Generally the cell density increases from the periphery towards the fovea, however, the ratio is not similar for all cell types. Ganglion cells, for instance, were shown to exhibit the steepest gradient, whereas the number of cone photoreceptors increases to a lesser amount, implying changes in the connectivity (Fig. 1.4 B and C; Wässle & Boycott, 1991). The change in

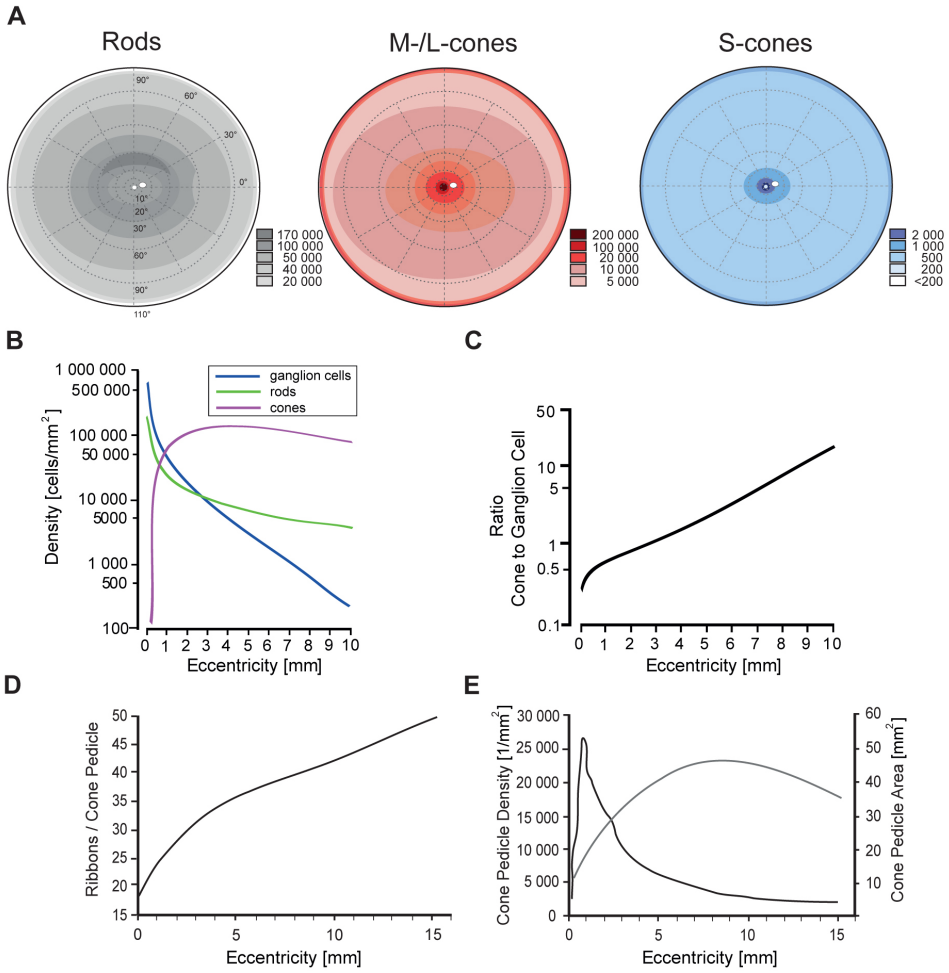

Figure 1.4: Topography of photoreceptors in primate retina. (A) Schematic topography maps of rod (left) and M-/L- (middle) and S-cone (right) photoreceptors in human retina. The papilla is indicated as small white circle next to the fovea. Areas of high cell density are marked by intense, those of low densities by pale colours. Examples of the densities corresponding to the colour intensities are shown in the colour code legends. Visual angles are indicated by circles, meridian angles by radiate lines. **(B – E)** Graphs of topographical data in primate retina. **(B)** Density of photoreceptor types (rods and cones) and ganglion cells and cone to ganglion cell ratio **(C)** in macaque. The number of ganglion cells falls steeply with eccentricity, the number of rods only moderatly. Cone density is highest in the centre and slowly decreases with eccentricity resulting in an increase of the convergence of cones onto ganglion cells with eccentricity. The number of ribbons per cone pedicle increases with eccentricity **(D)**. The number of cone pedicles is maximal in the foveal region and decreases with eccentricity. The area occupied by the pedicles increases but declines in the far periphery ($>$ 10 mm). (Modified from Ahnelt, 1998 (A), Wässle & Boycott, 1991 (B, C) and Haverkamp *et al.*, 2001 (D, E).)

the cell density is inversely mirrored by changes in the cells size, meaning that cues like the dendritic field sizes of the cells increase in the periphery, while their density decreases, to ensure a full coverage of the retina (Dacey, 1993). Such changes are also observable in the cone photoreceptors, which change the size of the cone pedicle area and the number ribbons they contain from the central to the peripheral retina (Fig 1.4 D and E; Haverkamp *et al.*, 2001).

1.4.2 Colour processing in primate retina – the midget pathway

Probably the most striking result of the high cell density in the primate central retina is the midget system, serving high acuity and colour vision. Due to the high cell density, a single cone is connected to a single midget bipolar cell, which in turn signals to a single midget ganglion cell, reaching the anatomical limitation for visual resolution. A side effect of this high acuity system is its colour selectivity. Since only one cone type is contacted, its spectral sensitivity is transposed to the downstream cells, for instance a midget ganglion cell, receiving synaptic input from a midget bipolar cell sampling from an M-cone, will respond to green light, while those sampling from L-cones will be responsive to red light in their receptive field centre (Fig. 1.5 A; discussion section 4.3 and Kolb, 1970).

This input is further compared to the antagonistic surround, which is likely formed by several cone types. Colour opponency for L- and M- signals in the midget system is well established for both the OFF- and the ON-system. Connections of the midget system to S-cones, by contrast, are discussed controversially (Klug *et al.*, 2003; Lee *et al.*, 2005). A consensus of physiological as well as anatomical studies exists, that in central retina the ON-midget system is not connected to S-cones (Field *et al.*, 2010; Herr *et al.*, 2003). An anatomical study, however, has shown connections from S-cones onto FMBs, which are presumably OFF-cells (Klug *et al.*, 2003) in the central macaque retina. A physiological study using multi electrode arrays (MEAs) demonstrated, that OFF-midget ganglion cells, in contrast to ON-midget or parasol ganglion cells, receive substancial input deriving from S-cones (colour coded ganglion cell soma in Fig. 1.4 B; Field *et al.*, 2010).

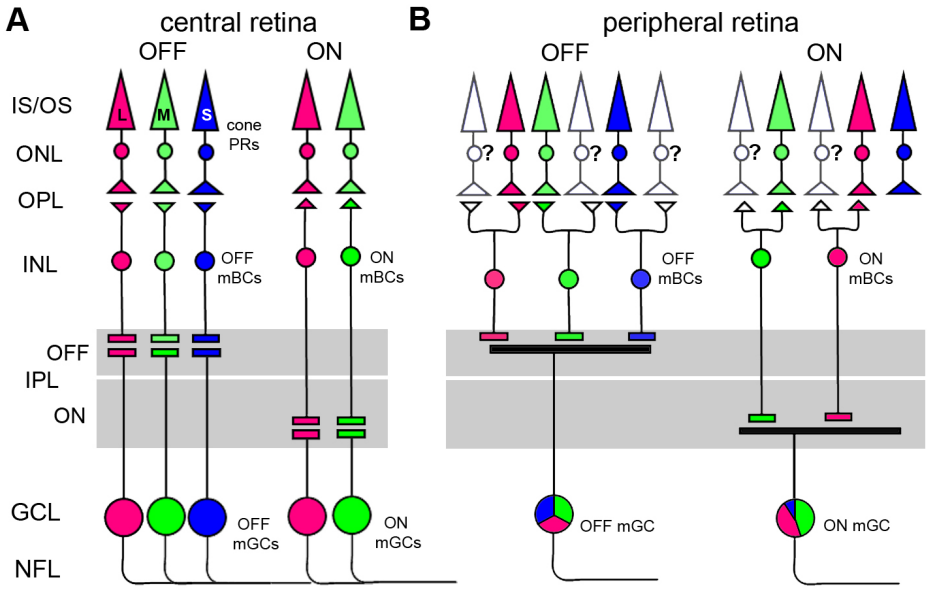

Figure 1.5: Scheme of neuronal circuits in the primate retina – the midget system. (A) Within the central primate retina, the midget system builts a one-to-one connection from a single cone to a single midget bipolar cell (mBC) onto a single midget ganglion cell (mGC). S-cones are contacted by OFF- but not ON-mBCs. **(B)** In peripheral retina signals of multiple cones converge onto mBCs in turn converging onto a mGC. It is not yet known if these mBCs contact only cones of the same (e.g. two M-cones) or if they contact cones of different spectral tuning (e.g. an M- and an L-cone), indicated by clear cones with a question mark. Whereas OFF-mGCs receive significant S-cone input, ON-mGCs receive only minor if any input from S-cones (colour area code indicates the fraction of S-, M-, and L-cone input (adapted from Field *et al.*, 2010)).

Following the density gradient of cells described above, the ratio of cones per ganglion cell, and thereby per midget ganglion cell, changes in the periphery. Whereas one midget ganglion cell samples from a single cone in its receptive field centre in the central retina, signals of multiple cones converge onto the receptive field centre of a midget ganglion cell (Fig. 1.5 B). Multiple cones (up to 4 in macaque retina) are contacted by a midget bipolar cell, and in turn multiple midget bipolar cells synapse onto a midget ganglion cell. Whereas it is not shown if peripheral midget bipolar cells sample from cones of the same spectral sensitivity or if they receive a mixed input, it was physiologically demonstrated that peripheral midget ganglion cells receive mixed input from cones. The input in the receptive field centre, however, is often dominated by either M- or L-cones supporting colour opponency against an antagonising

surround. If the antagonising surround of peripheral midget ganglion cells is formed by a mixed input of several cone types or by selective input from the cone type antagonistic to the cone type providing the dominant input in the receptive field centre, is still on debate (Field *et al.*, 2010; Reid & Shapley, 2002).

1.4.3 Colour processing in primate retina – blue yellow opponency

The classical pathway processing S-cone signals appears to be evolutionary ancient and seems to be conserved in many mammalian species. In the following section the **classical S-cone pathway** in trichromatic primate retina is depicted, since it was studied in most detail in the past. In the primate the S-cone signals are processed by small bistratified ganglion cells, which display a blue (S-) ON/yellow (M + L) OFF antagonism (Dacey & Lee, 1994). These cells receive their driving input from S-ON bipolar cells onto their inner dendritic tree. On their outer dendritic tree small-bistratified ganglion cells receive input from OFF-bipolar cells non-selectively contacting L- and M-cones (Fig. 1.6 A). The classical pathway contrasting S-ON signals to either green (M) or yellow (M + L) OFF signals is regarded as evolutionary conserved since S-ON bipolar cells were described in many mammalian species (Famiglietti, 2008; Haverkamp *et al.*, 2005; Kouyama & Marshak, 1992; Li & DeVries, 2006; MacNeil & Gaul, 2008).

This classical pathway, however, lacks an explanation for the existence of S-OFF signals, which were demonstrated in ganglion cells in primates and dichromatic mammals, in higher brain areas, such as the LGN, and in psychophysical experiments (Ekesten & Gouras, 2005; Chen & Li, 2012; Sher & DeVries, 2012; reviewed by: Dacey *et al.*, 2003, 2005, 2013; *psychophysics:* Shinomori & Werner, 2008; *LGN:* Valberg *et al.*, 1986). Recently the evidence for the processing of S-OFF signals in the retina by several distinct pathways is growing. One possible pathway to transfer S-cone signals onto ganglion cells would be directly via an OFF-bipolar cell selectively contacting S-cones. Such bipolar cells were described in the rabbit retina, and FMBs in the central primate retina would be good candidates (*macaque:* Klug *et al.*, 2003; *rabbit:* Liu

& Chiao, 2007; Mills *et al.*, 2014). A hypothetical **alternative S-cone pathway** could be mediated by amacrine cells receiving input from S-ON bipolar cells and making inhibitory output-synapses, which invert the S-ON into an S-OFF signal to ganglion cells (Fig. 1.6 B). Evidence for such blue-amacrine cells were found in the ground squirrel as well as in the rabbit retina (Chen & Li, 2012; Mills *et al.*, 2014; Sher & DeVries, 2012).

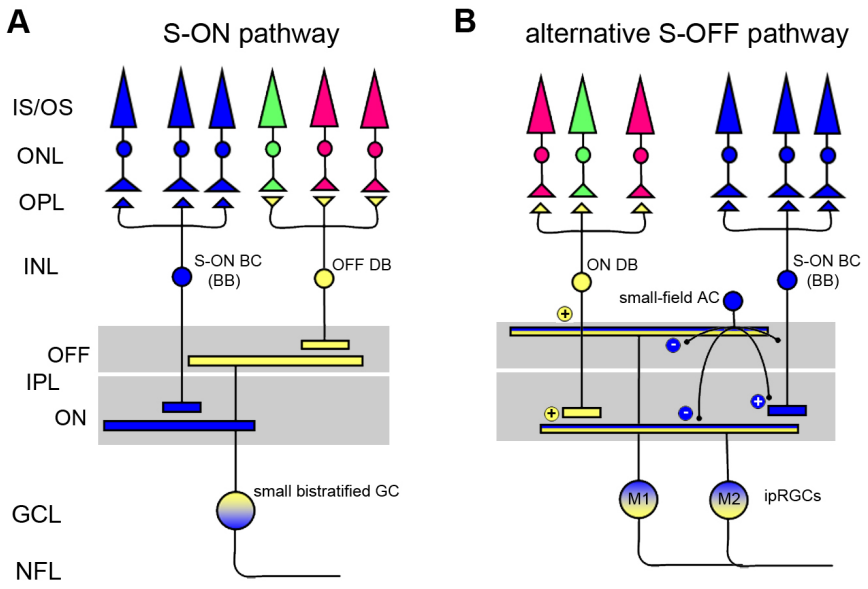

Figure 1.6: Scheme of neuronal circuits in the primate retina – S-cone pathways. **(A)** The classical blue- or S-ON pathway in primate retina. Small bistratified ganglion cells (GCs) display yellow OFF- and S-ON responses. They receive input from S-cone selective "blue" ON-bipolar cells (S-ON BCs or BB), relaying S-ON signals onto their inner dendritic tier. Diffuse OFF-bipolar cells (OFF DBs), which contact M- and L-cones, relay yellow (M + L) signals onto the outer dendritic arbour. **(B)** Alternative pathway for S-OFF signals via a hypothetical bistratified amacrine cell. In primate retina ipRGCs (M1 and M2) display S-OFF/Yellow ON-responses (Dacey *et al.*, 2005). The yellow ON-responses derive, in addition to their intrinsic ON-responses, from ON-DBs contacting L- and M-cones, which also make *en passant* synapses onto M1 ipRGCs in the OFF-layer (Grünert *et al.*, 2011). A bistratified ACs could invert S-ON signals from S-ON BCs (+) to S-OFF signals (-) via inhibitory synapses. Such blue-ACs were described in the ground squirrel and rabbit retina (see subsection 1.4.3).

1.5 Aim of the thesis

The main questions of this thesis were how distinct functions of ganglion cell types are implemented by their wiring connections to their presynaptic partners, and to what extent specificity in these synaptic connections exists. These questions were addressed using anatomical approaches relying on a structure-function correlation of cells neuronal networks. The thesis is subdivided into three subsections according to the system investigated to resolve these questions.

First the specificity of the bipolar cell input onto distinct ganglion cells were analysed in retinae of transgenic mouse lines in which certain ganglion cell types were labelled by the expression of fluorescent proteins. In a second approach, the expression of different subunits of ionotropic inhibitory neurotransmitter receptors by ipRGCs was examined in primate retina. In a third approach, the integration of M1 ipRGCs was analysed to shed light on a potential anatomical source of their S-OFF responses.

Chapter 2

Materials and Methods

2.1 Animals

During this thesis retinae of mice and macaque monkeys were used to examine the neuronal circuitries and to elucidate synaptic connections underlying the physiogical properties found in distinct ganglion cells. All procedures concerning the use of animals described in the following were approved from the local animal care committee and were in accordance with the law for animal experiments issued by the German government (Tierschutzgesetz).

2.1.1 Mice

Two transgenic mouse lines expressing fluorescent proteins in different ganglion cell types were used, the *thy1*-GFP-O mouse line and the Jam-B (junctional adhesion molecule B) mouse line.

***Thy1*-GFP-O mice** (Feng *et al.*, 2000), abbreviated as GFP-O mice in the following, express the enhanced green fluorescent protein (GFP) under the control of neuron-specific regulatory regions of the thy1-gene. The thy1-gene codes for an immunoglobulin expressed by cells of the nervous system as well as other non-nervous tissues, including spleen, kidneys the thymus in mice. Regulatory elements, located in introns 1 and possibly 2, of the thy1-gene determine the tissue-specific expression of Thy1 (Vidal *et al.*, 1990). The vector controlling the expression of GFP in GFP-O mice contains the promotor region of the thy1-gene and extends to the end of exon 4. The insertion of

the transgene and the following deletion make the construct devoid of the thy1 coding sequence and sequences directing the expression to thymus tissue, while sequences responsible for the expression in nervous tissue remains intact (Vidal *et al.*, 1990; Caroni, 1997; Feng *et al.*, 2000). The colony of GFP-O mice was breaded within the animal house of the Max-Planck-Institute for Brain Research. The expression of GFP in the mice was determined by technical staff of the animal house by a non-invasive, visual examination. Positive animals were used for breeding to maintain the colony, or used for experiments. GFP-O mice express enhanced GFP in retinal ganglion and amacrine cells (Feng *et al.*, 2000; Heinze *et al.*, 2007) in a golgi-like manner[1]. The expression of GFP in the whole cell in only a few cells per retina allows the morphological identification of distinct cell types and the further investigation of their circuitries.

Mice of the **JAM-B** line, in contrast, selectively express enhanced yellow fluorescent protein (YFP) in OFF-DSGCs only (Kim *et al.*, 2008). These cells are characterised by an asymmetric branched dendritic tree in S1 of the IPL and correspond to C6 ganglion cells described in the cell catalogue by Sun *et al.* (2002). Eyes of these animals with induced YPF expression were generously provided by Dr. In-Jung Kim (Yale University, Massachusetts, USA) and their generation is summarised below. Jam-B is, similar to Thy1, a member of the superfamily of immunglobulins (Ig). In a wide screen using polymerase chain reaction (PCR) and in situ hybridisation Jam-B was found to be expressed by a subset of retinal ganglion cells. To selectively label the cells expressing Jam-B, the group of Josh Sanes established a transgenic mouse line called Jam-B mice. For this purpose, mice transgenic for a construct encoding the ligand-activated Cre-recombinase oestrogen receptor fusion protein (CreER) driven by regulatory sequences of the Jam-B gene were generated. These animals were crossed to transgenic mice carrying a construct, which codes for the fluorescent reporter YFP under the control of a 'stop' cassette (thy1-STOP-YFP). In the offspring mice (Jam-B-CreER; thy1-STOP-YFP) the application of tamoxifen,

[1]The golgi method is a classical staining method based on silver nitrate used in neuroanatomy, which was discovered by the italian scientist Camillo Golgi in the 19th century.The golgi method randomly stains only some neurons of a tissue sample in a black-brown colour, revealing the complete morphology of the cell. The spanish neuroanatomist Santiago Ramón y Cajal used and refined the golgi in his classical works on neuroanatomy (Ramón y Cajal, 1892, 1909).

the ligand of CreER, leads to an excision of the 'stop' cassette resulting in the expression of YFP. CreER is only active in a small time window after application of its ligand tamoxifen. Therefore, the CreER avoids changes in the YFP labelling due to developmental changes in the Jam-B expression and further amplifies the YFP expression (Kim *et al.*, 2008).

2.1.2 Primates

In addition to mouse retinae, eyes of two species of adult macaque monkeys, *Macaca mulatta* and *Macaca fascicularis* were used within this study. The eyes of the primates were obtained either from the animal house of the Max-Planck-Institute for Brain Research in Frankfurt a.M., from the Eberhard Karls University of Tübingen or from the Primatenzentrum in Göttingen. The animals were sacrificed in experiments unrelated to the here presented dissertation.

The animals were deeply anaesthetised and killed by an overdose of pentobarbital (60 – 100 mg/kg). Afterwards the animals were immediatedly perfused with 0.9 % saline buffer. The eyes were enucleated prior to perfusion of the animal with fixative. The eyeballs were cut open, and cornea and lens were removed, afterwards the posterior eyecups were immersion-fixed in 0.1 M phosphate buffer or 0.01 M phosphate buffered saline (PB or PBS, pH 7.4) containing 4 % paraformaldehyde (PFA) for 10 – 60 min. Short fixation times (about 10 min) were required for immunohistochemical experiments involving stainings against synaptic proteins such as labelling of post-synaptic receptor subunits. Longer fixation times, however, improved tissue preservation and were favourable for most cell marker proteins, but strongly impair the quality of receptor labelling (Greferath *et al.*, 1995). Following fixation the eyecups were transferred into PB and sent to the Max-Planck-Institute for brain research. Macaque monkeys belong to the group of old-world monkeys. Most species of this group, including humans, are capable of trichromatic vision due the presence of three cone types expressing opsins most sensitive to light of distinct wavelengths (S-, M- and L-opsin; see also subsection 1.1.1). All other mammalian species with the remarkable exception of some females of new-world monkey species (e.g. the common marmoset *Callithrix jacchus*), possess only two cone types (S- and L-cones), one type expressing an opsin most sensitive to short-wavelength light (S-opsin) and one most sensitive longer wavelengths

light (L-opsin) and are hence dichromats (for a review see: Jacobs, 2008, 2009). Their trichromacy makes macaque monkey interesting model organisms for the investigation of colour vision and the comparison of their retinal circuitry to the wiring in other dichromatic species.

2.2 Tissue preparation

2.2.1 Preparation of mouse eyes

Mice of the GFP-O line were deeply anaesthetised using the inhalational anaesthetic isofluorane (Deltaselect, Abbvie) in a narcosis chamber preventing any direct skin- or fur contact to the narcotic substance. Afterwards mice were sacrificed by decapitation or cervical dislocation and the eyes were immediately removed and transferred into PB. The cornea was pinched with a scalpel tip and the eyes were opened with a circular section along the Ora serrata followed by removal of the lens. The posterior eyecups were immersion fixed in 4 % PFA in PB for 10 – 30 min at room temperature. The fixation was stopped by a wash-out of the PFA by subsequent washing steps in PB. Following the fixation, the eyes were cryoprotected in graded sucrose solutions (10 %, 20 % sucrose in PB for one hour and 30 % sucrose in PB until the eyes descended to the bottom of the cuvette) and frozen at -21 °C.

Eyes of the Jam-B line, fixed in PFA, were kindly provided by Dr. I. J. Kim. The posterior eyecups were cryoprotected as described above.

2.2.2 Retina dissection

The retina was removed from the posterior eyecup with a fine paintbrush. This procedure also removed the pigment epithelium in most cases. The retina was pruned from the remaining vitreous with small forceps. Outlines of the primate retinae were drawn to document the eccentricity of the retinal pieces, which were cut subsequently. Pieces of primate retinae were cryoprotected (10 % , 20 % sucrose for 1 h at room temperature, 30 % sucrose overnight at 4 °C.) and frozen in -70 °C until further use. However, in some cases the freezing of primate tissue was omitted and the retinae were stored at 4 °C in PB containing 0.025 % sodium azide to avoid tissue damage caused by freezing.

2.2.3 Flat mount preparations

Frozen eyes or retinae were thawed and washed in PB (3 x 10 min). Retinae were dissected from the eyecup and pruned from vitreous. Primate retina pieces were thawed and trimmed. For use as retina flat mount preparations (primate and mouse) retinae or retinal pieces were either further processed free floating or the tissue was attached to dark nitrocellulose filter paper (Millipore).

2.2.4 Cryosections

To prepare cryosections the cryoprotected retinae were trimmed and incubated in TissueTek mounting medium (Jung) for 15 min at room temperature. The retina piece was flattened within a drop of the medium onto a microscope slide covered with parafilm (Pechiney Plastic Packaging) and frozen onto a frozen block of Tissue Tek medium in a cabin of a cryostat (Leica CM 3050 S) at a cabin temperature of -21 °C. The temperature of the specimen disc was cooled to about -35 °C to accelerate the process of freezing and attachment of the tissue to the block. For horizontal sections specimen disc was turned to get the desired orientation and the medium block was trimmed. For sectioning the specimen temperature was increased to -15 °C to -19 °C. Sections (thickness 30 – 55 µm) were collected onto adhesion microscope slides (Menzel Superfrost Plus) and stored at -21 °C. The advantage of horizontal sections over flat mount preparation is the facilitation of the antibody penetration and the better signal of antibodies producing high levels of unspecific background staining. If a tangential view showing the retinal layers was desired the tissue was cut in vertical sections. To produce vertical sections the block was trimmed and removed from the specimen disc. Afterwards the block was turned to desired orientation (about 90 °) and frozen onto the disc. The specimen temperature was increased to -15 °C – -19 °C and the retina was cut into sections of 16 – 25 µm. The vertical sections were also collected on adhesion microscope slides and stored at -21 °C.

In some cases the retina pieces were not directly flattened onto a microscope slide, but were placed into a cryomold (Sakura Finetek) filled with the mounting medium. The cryomold was placed onto a metal block cooled with

liquid nitrogen for rapid freezing. The retina block was then removed from the mold and frozen onto a specimen disc in the desired orientation. The following sectioning steps were the same as in the classical protocol described above.

2.3 Immunohistochemistry

Immunohistochemical stainings were performed using the indirect fluorescence method. For this method two subsequent steps were conducted. First primary antibodies directed against a specific antigen were applied. In a second step fluorescently labelled secondary antibodies, recognising the species-specific region of the primary antibody were used to visualise the primary antibody and hence the site of the antigen.

Table 2.1: Incubation solutions. If the room temperature exceeded 25 °C the conservant sodium azide was added in a concentration of 0.025 %.

Preparation	Solution	Ingredients
Flatmounts & Horizontal sections	Pre-incubation solution	10% NDS or NGS, 1% BSA, 1% Tx in PB
	Incubation solution	3% NDS or NGS, 1% BSA, 1% Tx in PB
Vertical cryosections	Pre-incubation solution	10% NDS or NGS, 1% BSA, 0.5% Tx in PB
	Incubation solution	3% NDS or NGS, 1% BSA, 0.5% Tx in PB
Immunolabellings with antibodies against SCGN	Incubationsolution	3% NHS, 0.5%Tx in 0.01M PBS

2.3.1 Immunostaining procedure

Flat mount preparations were thawed and subsequently the sucrose was removed from the tissue by washing in PB (4 x 15 min) in multi-well plates (Nunc). Cryosections were thawed and prior to the following staining procedure surrounded with a liquid-blocker pen (super PAP-Pen, SCI science services) to prevent leaking of incubation solutions and the dessication of the cryosections. Following the drying of the liquid blocker the slides were placed into a cuvette and the mounting medium was removed by washing steps in PB at room temperature on a shaker (3 x 10 min). For some immunolabellings, especially stainings involving antibodies against GABA- and glycine receptors, it was necessary to enhance the staining quality by conducting pre-incubation

following the washing steps. The tissue was incubated in a pre-incubation solution containing high serum concentrations (Table 2.1) to block unspecific binding sites of the primary antibodies for one (cryosections) or two hours (flat mounts).

The pre-incubation was followed by an incubation of the preparations in a mixture of primary antibodies diluted in an incubation solution overnight at room temperature (cryosections) or for 3 days in multi-well plates sealed with parafilm at 4 °C (flat mounts). Cryosections were incubated in a humid incubation chamber.

Similar to the pre-incubation solution, incubation solutions contained sera of the host species (normal goat, donkey or horse serum (NGS, NDS or NHS)) of the secondary antibody and serum proteins (bovine serum albumin (BSA)) to minimise unspecific binding of the antibodies and a detergent (Triton X-100 (Tx), Sigma-Aldrich) to facilitate the penetration of the antibodies (see also Table 2.1). After removing of the surplus primary antibody solution the preparations were again washed in PB on a shaker at room temperature (cryosections: 3 x 10 min; flat mounts: 4 x 15 min) and incubated in a solution of the secondary antibodies. Secondary antibodies were also diluted in incubation solution and applied for one (cryosections) or two (flat mounts) hours. Following the removal of the solution containing the secondary antibody and washing steps at room temperature (cryosections 3 x 10 min; flat mounts 3 – 4 x 15min) the preparations were coverslipped. Preceding the coverslipping flat mounts were flattend onto a microscope slide in a drop of PB to prevent dessication. A drop of mounting medium (Vectashield or Aqua-Polymount) was placed on the coverslip and it was gently placed upon the sections or the retinal flat mount. Aqua Polymount is a water soluble mounting medium, which hardens out after 24 hours and is supposed to retain the fluorescence of the fluorochromes attached to the secondary antibodies. Vectashield, in contrast, is an aqueous glycerol-based mounting medium which does not solidify, but is also supposed to posess anti-fading and anti-photobleaching properties. The coverslipped preparations were sealed using common nailpolish. All incubation procedures involving the secondary antibodies were conducted shielded from light, to prevent bleaching and the preparations were stored at 4 °C in a fridge.

In some cases especially for triple-stainings better results with minimised background staining were obtained when antibodies were not applied as mixtures, but in successive staining steps. Therefore, in GFP-O mice the GFP signal was enhanced by immunostaining against GFP, but preceeding the coverslipping the retinae were stained in a further step against CtBP2 and Syt2. For stainings against secretagogin (SCGN) staining quality was significantly increased when NHS in PBS was used instead of standard incubation solution (Table 2.1).

If it was needed to use a combination of primary antibodies generated in the same host species antibodies were not applied as a mixture, but as subsequent single or double stainings. Cross reactions of the secondary antibodies were minimised or even avoided by the us of the 'piggy-back´ staining method. For this method one of the primary antibodies was applied in a dilution concentrated too low to result in a detectable staining using one secondary antibody. Then a second secondary antibody directed against the species-specific region of the first secondary antibody was applied. This procedure led to the building of larger fluorochrome aggregates around the antigen and hence its visualisation. Further the complex of secondary antibodies sterically hinders the binding of further secondary antibodies to the species-specific region of the primary antibodies. The following single or doublestaining was carried out as described above. All primary and secondary antibodies used in this thesis are listed in Tables 2.2 and 2.3.

2.4 Microscopy and image aquisition

The fluorescent staining of immunohistochemically labelled preparations were analysed and documented using several microscopes. For this purpose image stacks along the z-axis were taken, meaning that photographs of the same area (x, y) were taken in different focal planes. The distance between the focal planes was selected depending on the following kind of analysis. Z-distances of $0.3-0.5\,\mu m$ within the confidence range of the microscopes were selected for the analysis of synaptic staining, whereas z-distances of $0.5-2\,\mu m$ were used to document the morphology of cell types.

2.4.1 Fluorescence microscopy

To document the morphology of cells in fluorescently labelled preparations a fluorescence microscope (Axio Imager Z.1, Zeiss) equipped with a mercury-short-arc lamp (HBO-100W, Osram) as light source for fluorochrome excitation was used. Photographs were taken with a cooled CCD (charged coupled device) camera (AxioCam MRm, Zeiss). Camera and microscope were operated using the Axio Vision v4.6 software (Zeiss). The microscope was further equipped with an oscillating grid (ApoTome, Zeiss). The integration of the oscillating ApoTome into the optical path led to a reduction of fluorescent stray light within the focal planes. In order to depict the layered structure of the retina and to reveal the stratification depth of certain cells in vertical sections, photographs of the sections using transmitted light and a DIC filter were used to illustrate the nuclear and synaptic layers of the section. Such DIC stacks were later overlaid with image stacks generated using the ApoTome, since insertion of the ApoTome prevented the acquisition of DIC pictures. For image acquisition the following objectives were used: the dry objectives Plan Apochromat 20x/0.8 and EC Plan Neofluar 40x/0.75 as well as the oil-immersion objectives Plan Apochromat 63x/1.4oil und EC Plan Neofluar 100x/1.3oil (Zeiss).

2.4.2 Confocal laser-scanning microscopy

Two laser-scanning microscopes were used to document images of fluorescently labelled preparations in high resolution. In contrast to conventional fluorescence microscopes, laser-scanning microscopes use a laser as light source for fluorochrome excitation. The used laser light restricts the excitation to the focal plane of interest reducing stray light from fluorophor excitation in other focal planes. Hence, a better signal-to-noise ratios and resolution are produced.

Preparations double-immunolabelled with the fluorochromes Alexa 488 and Cy3 or Alexa 594 were documented as image stacks using an Axioskop MOT microscope (Zeiss) equipped with a LSM5 Pascal modul (Zeiss). A helium-neon laser (emission wavelength [λ_{em}]: 543 nm) and an argon laser ([λ_{em}]: 450 – 515 nm). The controlling of the microscope was performed with the help of the LSM5 Pascal V3.2 SP2 software (Zeiss). The following objectives were used

for the image acquisition: the dry objective Plan Apochromat 20x/0.8 and the oil-immersion objectives Plan Neofluar 40x/1.3 for overview pictures depicting the cell´s morphology und the oil-immersion objective 63x/1.4 (Zeiss) for high resolution images used for the analysis and quantification of synaptic stainings. The resolution of the images was set to 1024 x 1024 pixels for overview pictures with z-distances of 0.5 – 2 µm and 1600 x 1600 or 2048 x 2048 pixels and z-distances of 0.3 – 0.5 µm for images used for analyses of synaptic stainings.

Triple-immunolabelled preparations using the fluorochromes Alexa 488, Cy3 or Alexa 594 and Cy5 or Alexa 647 were documented on a FluoView 1000 microscope (Olympus) equipped with a multi-argon laser ([λ_{em}]: 458, 488 and 515 nm), a helium-neon laser ([λ_{em}]: 543 nm) and two laser diods ([λ_{em}]: 405 nm and 635 nm). The microscope was controlled using the FV 1.7 software (Olympus). Overview images were taken with an UPlanSApo 40x/0.75 dry objective, detail pictures were captured using an UPlanSApo oil 60x/1.35 oil immersion objective. The resolution was set as described above.

2.5 Image processing and analysis

Fluorescence micrographs acquired at the microscopes described above were analysed with the help of the open source softwares ImageJ and Fiji (`http://rsbweb.nih.gov/ij/`). The pictures saved in the file formats of the microscope softwares were opened and saved as image stacks in the tagged image file (.tif) format. Where required brightness and contrast were adjusted preceding the image analysis. Further adjustments including adjustment of levels, brightness and contrast, colour composition (channel mixer) and sharpness of the pictures as well as the composition of pictures as figures were performed using Photoshop (versions CS3, CS4 and CS6, Adobe Systems). Drawings of cell structures and reconstructions were manually performed with the help of a drawing tablet (Intuos® 2 Modell XD-06-08-U, WACOM) or using the Imaris software (Bitplane).

2.5.1 Quantitative analysis of synapses onto ganglion cell dendrites

The quantitative analysis of synapses on ganglion cell dendrites was carried out on stacks of confocal micrographs of retinal flat mount preparations. Overview pictures of the cells were taken at low resolution, the quantititave analysis was carried out on high-resolution images of details of the cells. Image stacks of GFP-O tissue from a previous study on this topic were re-analysed, using the method described below to ensure the comparability of the data with the analysis of tissue newly labelled and analysed for this thesis. The data of the re-analysed image stacks were included into the statistical analysis.

In order to assess the number of synapses on the dendrites of retinal ganglion cells, the image stacks recorded on a confocal microscope were loaded in the ImageJ or Fiji software and saved as image stack in the .tif file format. The synapses were counted and documented within the image stack in the proper confocal plane with the help of the CellCounter PlugIn (Kurt De Vos, University of Sheffield, academic neurology, UK). The data was then further statistically analysed and plotted using Excel (Microsoft) and Prism 5 (GraphPad). The sort of statistical test used was dependent on the sort of experiment and is indicated in the results.

If presynaptic markers were used to identify the synaptic input onto ganglion cells (e.g. the ribbon marker CtBP2) labelled synaptic puncta were also counted if not in complete register with, but if located in direct apposition to the ganglion cell dendrite in a range of around 0.5 µm. If the number of postsynaptic receptor clusters was assessed on a ganglion cell dendrite, only such clusters were counted and marked which colocalised with the dendrite in the correct confocal plane. In case of large cells, e.g. ipRGCs, the length of the analysed dendrite was measured and the number of synaptic clusters counted was normalised to 100 µm dendritic length.

2.5.2 Quantitative analysis of contacts between cone pedicles and bipolar cells

In order to examine the contacts between dendrites of bipolar cells and cone pedicles, the size of the area of the cone pedicles was measured. Because the

staining pattern of the bipolar cell marker used in these experiments (GLT-1, to label OFF-bipolar cells) prevented the counting of single dendritic tips at the cone pedicle, the area occupied by the bipolar cell dendrites beneath the pedicles was measured instead. A similar method to circumvent this difficulty was established by Breuninger *et al.* (2011) and a modified method which was used herein is described in the following: Image stacks were loaded into the programm ImageJ. Afterwards the area of the cone pedicles identified by the CtBP2 or PNA staining was surrounded using the polygon selection tool and the area size was measured, cut out and pasted into an empty image with black background. In the following projections of maximally three confocal planes showing the fluorescence channel of the bipolar cell marker only were produced and binarised. The polygonal selection of the cone pedicle area was copied into the channel showing the bipolar cells and cut out. With the help of the magic wand selection tool the area occupied by the bipolar cell dendrites beneath the pedicle was selected and measured. The selected areas of all analysed M-/L- ($n = 60$) and S-cones ($n = 38$)and the corresponding areas labelled by GLT-1 are shown in figures A.2, A.3 and A.1 in the appendix. The further analysis including the calculation of the ratio of the area occupied by the bipolar cells dendrite per cone pedicle area was performed using Excel (Microsoft) and Prism 5 (Graphpad). Unpaired, two-tailed students t-test were performed to compare the area of the M-/L-cones and S-cones, the area occupied by GLT-1 labelled OFF-bipolar cells at the cone pedicles and the ratio of the area occupied by the bipolar cell per cone pedicle. P-values < 0.0001 are indicated as (****), those between $0.001 - 0.0001$ as (***), between $0.001 - 0.01$ as (**), $0.01 - 0.05$ as (*) and mark a significant difference between the mean values of the compared sample. P-values larger than 0.05 (ns) indicate that no statistically significant difference of the samples mean was detected.

The analysis was conducted on horizontal sections of three separate tissue samples obtained from two different animals (Mk Gö 15 (2009); Mk C07 15 and 30) and three different eccentricities. The data of the three samples as well as the pooled data of all samples are shown. Data of all analysed tissues were compared using one-way analysis of variances (ANOVA) combined with Tuckey´s multiple comparison test with the help of the software Prism 5 (Graphpad). All analysed cone pedicles as well as the GLT-1 labelling at the pedicle and

the binarised picture of the GLT-1 labelling are shown in the supplemental Figures A.1 (S-cones), A.2 and A.3 (M-/L-cones) within the Appendix (A).

2.5.3 Shift and rotation controls

To assess if the density of synaptic clusters on ganglion cell dendrites found in the immunolabellings correspond to a genuine colocalisation of the receptor cluster at the dendrite or a random superposition of the two channels **rotation controls** were performed on random samples of the analysed image stacks. For this purpose the channel showing the synaptic labelling was rotated 90 ° and re-combined with the channel showing the cell. Afterwards the quantitative analysis was repeated. The values obtained from the rotated control image stacks served as baseline for random superpositions of the synaptic and the cellular staining and were compared to the originally observed data. The comparison of the original and the control data was carried out by performing one-way analysis of variances (ANOVA) combined with Tuckey´s multiple comparison test with the help of the software Prism 5 (Graphpad).

To assess if the area of the cone pedicles contacted by bipolar cells measured was caused by selective labelling of the bipolar cells or, if it is caused by rather unspecific background staining of the antibodies not related to the antigen, **shift controls** were carried out in random samples of each analysed tissue. For this purpose the area selection of the cone pedicle was shifted to an area between cone pedicles, where no or a strongly reduced area occupied by OFF-bipolar cells was expected. Afterwards the analysis was repeated and the results were compared to the original data. Data of image stacks in which the GLT-1 labelled area in the shift control was not significantly reduced compared to the original data were excluded from the analysis.

Table 2.2: List of primary antibodies.

Antibody	Host	Working dilution	Antigen/Immunogen	Specificity Primage	Specificity Rodent	Manufacturer	Catalogue no.
Calb	ms	1:1000	Calbindin-D (28kDa)	Cones, horizontal and DB3 cells	Types of horizontal, amacrine and ganglion cells	Sigma Immunochemicals, St. Louis (MO), (USA)	C 8666 (clone CL-300)
CCK	rb	1:5000	Cholecystokinin	S-ON bipolar cells		kind gift of J. Del Valle, University of Michigan, Ann Arbor (MI), (USA)	
ChAT	gt	1:200	Human, placental cholin-acetyltransferase	Starburst ACs	Starburst ACs	Chemicon, Temecula (CA), (USA)	AB144P
CtBP2	ms (IgG)	1:10000	Peptide of AAs 361-445 of mouse CtBP2	Synaptic ribbons of glutamatergic synapses and the C-terminal binding protein-2 (CtBP2) in nuclei		BD Biosciences, Heidelberg, (Germany)	612044
	rb	1:5000	AAs 431-445 of rat ribeye protein coupled to key-hole limpet hemocyanin via N-terminal cystein			Synaptic Systems, Göttingen, (Germany)	193-003
$GABA_AR$ $\alpha1$ (bd24)	ms	1:50	α-chain of the $GABA_A$	Subunit $\alpha1$ of the $GABA_A$ receptor	Subunit $\alpha1$ of the $GABA_A$ receptor	Chemicon, Temecula (CA), (USA)	MAB 339
$GABA_AR$ $\alpha2$	gp	1:2000	Peptide of AAs 1-9 of the $\alpha2$ subunit of the $GABA_A$ receptor	Subunit $\alpha2$ of the $GABA_A$ receptor	Subunit $\alpha2$ of the $GABA_A$ receptor	kind gift of H. Möhler, J.M. Fritschy, Institut für Pharmakologie und Toxikologie, Universität Zürich (Schweiz)	
$GABA_AR$ $\alpha3$	gp	1:5000	Peptide of AAs 1-15 of the $\alpha3$ subunit of the $GABA_A$ receptor	Subunit $\alpha3$ of the $GABA_A$ receptor	Subunit $\alpha3$ of the $GABA_A$ receptor		

Table 2.2: Continued - List of primary antibodies.

Antibody	Host	Working dilution	Antigen/Immunogen	Specificity Primage	Specificity Rodent	Manufacturer	Catalogue no.
GFP	ch	1:1000	His-tagged green fluorescent protein (GFP) from *Aequorea victoria*	Endogenous native GFP and GFP fusion proteins		Chemicon, Temecula (CA), (USA)	AB 16901
	gt	1:1000	Fusion protein of glutathion-S-transferase and GFP			Rockland, Gilbertsville, (PA), (USA)	600-101-215
	rb	1:2000	GFP from *A. victoria*			MoBiTec - Molecular Probes, Goettingen, (Germany)	A-6255 (now A-6255 Life technology, Invitrogen)
GLT-1 (EAAT2)	gp	1:1000	Synthetic peptide of C-terminal AAs from rat GLT-1	OFF-bipolar cells (mostly FMBs and DB2, rarely DB1)	Heterogeneous population of OFF- and ON- bipolar cells in mouse retina, different in rat and rabbit	Biozol Diagnostica (LSBio), Eching, (Germany)	LS-C15448/46190
	rb	1:1000	KLH conjugated peptide of C-terminal AAs 564-573 of rat precursor glutamate transporter GLT-1 with cystein added at N-terminus			Tocris bioscience, Bristol, (UK)	2063 Batch 1
GlyRα1 (mAb 2b)	ms	1:100-1:1000	10 N-terminal AAs of the α1 subunit of the glycine receptor	Subunit α1 of the glycine receptor	Subunit α1 of the glycine receptor	kind gift of H. Betz, MPI für Hirnforschung, Frankfurt a.M. (Deutschland)	
GlyRα2 (GlyRa2[N18])	gt	1:300	Peptide of the 18 N-terminal AAs of the GlyRα2 subunit	Subunit α2 of the glycine receptor	Subunit α2 of the glycine receptor	Santa Cruz Biotechnology, Santa Cruz (CA), (USA)	sc-17279
GlyRα3 (GlyRa2[C15])	gt	1:300	Peptide of the 15 C-terminal AAs of the GlyRα3 subunit	Subunit α3 of the glycine receptor	Subunit α3 of the glycine receptor		sc-17279

Table 2.2: Continued - List of primary antibodies.

Antibody	Host	Working dilution	Antigen/Immunogen	Specificity Primage	Specificity Rodent	Manufacturer	Catalogue no.
hNA (melanopsin)	rb	1:500-1:1000	Peptide of 18 N-terminal AAs of human melanopsin, (batch A, B and C respectively)	M1 and M2 ipRGCs also in human retina, M1 cells are more intense labeled and often displaced	not analysed	kind gift of K.-W. Yau, Johns Hopkins University, Baltimore (MD), (USA)	
hNB	rb	1:100-1:1000					
hNC	rb	1:100-1:1000					
Recoverin (Rec)	rat	1:200	Purified recoverin	Photoreceptors and flat midget bipolar cells (FMBs) in macaque and human retina but not in marmoset	Photoreceptors and two (rat) or one (mouse) type of bipolar cell	G. Adamus, Casey Eye Institute, Portland (OR), (USA)	
	rb	1:1000	Recombinant human protein			Chemicon, Temecula (CA), (USA)	AB 5583
S-opsin (OPN1SW[N20])	gt	1:300-1:1000	Peptide (EFYLFKNISSVGP-WDGPQYH) in first 50 AAs at the N-terminus of human short wavelength sensitiv opsin (S-opsin)	S-cones	S-cones	Santa Cruz Biotechnology, Santa Cruz (CA), (USA)	sc-14363
S-opsin (JH455)	rb	1:100-1:1000	C-terminal peptide of human S-opsin			kind gift of J. Nathans, Johns Hopkins University School of medicine, Baltimore (MD), (USA)	

Table 2.2: Continued - List of primary antibodies.

Antibody	Host	Working dilution	Antigen/Immunogen	Specificity Primage	Specificity Rodent	Manufacturer	Catalogue no.
Secretagogin (SCGN)	sh	1:2000	Full length (276 AAs) of recombinant human SCGN with 10 additional AAs and His-tag	Diffuse bipolar cell 1 (DB1)	Bipolar cell types 2, 3, 4, 5, 6 and maybe 8	Biovendor R&D, Candler (NC), (USA)	RD 184 120 100
Synaptotagmin-2 (znp1)	ms (IgG2a)	1:1000-1:2000	Synaptotagmin-2 (Syt2) of 1-day zebrafish embryo	A8 amacrine cells	Type 2 bipolar cells, terminals of Type 6 bipolar cells	Zebrafish International Resource Center (ZIRC) Eugene (OR), (USA)	ZNP-1
Synaptotagmin-2	rb	1:1000	synthetic peptide of AAs 406-422 of rat Syt2 coupled to key hole limpet hemocyanin			Synaptic Systems, Göttingen, (Germany)	105123

Table 2.3: List of secondary antibodies and lectins.

Conjugate	Antibody form	Host and antigen	Working dilution	Vendor	Filter sets for Epifluorescence microscopy
Alexa Fluor **488** [λ_{abs} = 496 nm] [λ_{em} = 519 nm]	whole IgG	dk α gp	1:500	JacksonIR/Dianova, Hamburg, (Germany)	No. 10 (Zeiss)
		dk α gt		Life Technologies - Invitrogen, Karlsruhe, (Germany)	
		dk α ms		JacksonIR/Dianova, Hamburg, (Germany)	
		dk α rat			
		dk α rb			
		dk α sh			
		gt α ch		Life Technologies - Invitrogen, Karlsruhe, (Germany)	
		gt α gp			
		gt α ms			
		gt α rb		MoBiTec, Goettingen, (Germany) (no longer available)	
		gt α rat		JacksonIR/Dianova, Hamburg, (Germany)	
	IgG F(ab)$_2$	dk α rb			
Alexa Fluor **594** [λ_{abs} = 591 nm] [λ_{em} = 614 nm]	whole IgG	dk α sh	1:500	MoBiTec - Molecular Probes, Goettingen, (Germany)	No. 31 and/or No. 26 (Zeiss)
		PNA		Life technologies - Molecular Probes, Eugene (OR), (USA)	
Cy3 [λ_{abs} = 550 nm] [λ_{em} = 570 nm]	whole IgG	dk α gp	1:500	JacksonIR/Dianova, Hamburg, (Germany)	No. 31 (Zeiss)
		dk α gt			
		dk α ms			
		dk α rb			
		gt α ms			
		gt α rat			
	IgG F(ab)$_2$	dk α gt			
		dk α ms			
		dk α rb			
		gt α rb			
Cy5 [λ_{abs} = 652 nm] [λ_{em} = 670 nm]	whole IgG	dk α gp	1:200	JacksonIR/Dianova, Hamburg, (Germany)	No. 26 (Zeiss)
		dk α gt			
		dk α ms			
		dk α rb			

Table 2.3: Continued - List of secondary antibodies and lectins.

Conjugate	Antibody form	Host and antigen	Working dilution	Manufacturer	Filter sets for Epifluorescence microscopy
Alexa Fluor **647** [λ_{abs} = 650 nm] [λ_{em} = 665 nm]	whole IgG	dk α ms	1:200	Invitrogen, Karlsruhe, (Germany)	No. 26 (Zeiss)
		dk α rb		JacksonIR/Dianova, Hamburg, (Germany)	
		gt α gp gt α ms		MoBiTec - Molecular Probes, Goettingen, (Germany)	
		PNA	1:500	Life technologies - Molecular Probes, Eugene (OR), (USA)	

Table 2.4: Applied buffers and solutions.

Buffers/Solutions	Composition
Antibody incubation and pre-incubation solutions	Please refer to table 2.1
Paraformaldehyde Solution (PFA; 4%)	4 g PFA were dissolved in 100 ml PB by stirred heating to 60 - 65 °C. If necessary NaOH was added to facilitate the dissolving of the PFA until the solution cleared. After cooling to room temperature the solution was filtered and stored at -21 °C.
Phophate buffer (0.2 M stock solution, pH 7.4)	43,42 g $Na_2HPO_4 \cdot 7H_2O$ and 5.24 g $NaHPO_4 \cdot H_2O$ diluted in 1 l Aqua dest.
Phosphate buffer (PB; 0.1 M, pH 7.4)	21.71 g $Na_2HPO_4 \cdot 7H_2O$ and 2.62 g $NaHPO_4 \cdot H_2O$ diluted in 1 l Aqua dest., or dilution of 0.2 M stock solution (1:1)
Phosphate buffered saline (PBS; 0.01 M, pH 7.4)	8.67 g $NaCl$ and 0.2 g KCl dissolved in 50 ml 0.2 M PB filled up to 1 l with Aqua dest.
Sucrose solution, 20% and 10% (w/v)	Dilution of 30% sucrose in PB or PBS respectively (10%: ratio 1:2; 20%: ratio 2:1)
Sucrose solution, 30% (w/v)	30 g sucrose dissolved in 100 ml PB or PBS
Triton X-100 (10% stock solution)	1 ml Triton X-100 was diluted in 9 ml PB or PBS

Table 2.5: Chemicals and Reagents used for this thesis.

Chemical / Reagent	Abbreviation / Additivity Formula	Manufacturer
Aqua Polymount		Polysciences Europe, Eppelheim, (Germany)
Bovine Serum Albumin fraction V	BSA	Merck, Darmstadt, (Germany)
di-Sodium Hydrogen Phosphate Heptahydrate	$Na_2HPO_4 \cdot 7H_2O$	Carl-Roth, Karlsruhe, (Germany)
Florene (Isofluran)	$C_3H_2ClF_5O$	Abbvie, Ludwigshafen, (Germany)
Hydrochloric Acid	HCL	Merck, Darmstadt, (Germany)
Isofluran	$C_3H_2ClF_5O$	DeltaSelect, München, (Germany)
Nail polish		e.g. by essence, purchased in local drugstores
Normal Donkey Serum Normal Goat Serum Normal Horse Serum	NDS NGS NHS	Sigma-Aldrich, Steinheim, (Germany)
Paraformaldehyd	PFA; $OH(CH_2-O)_nH$ (n=8-100)	Merck, Darmstadt, (Germany)
Sodium azide Sodium chloride	NaN_3 $NaCl$	Sigma-Aldrich, Steinheim, (Germany)
Sodium Hydrogen Phosphate Monohydrate	$NaHPO_4 \cdot H_2O$	Merck, Darmstadt, (Germany)
Sodium Hydroxid Solution	$NaOH$	KMF, Lohmar, (Germany)
Sucrose (D+)	$C_{12}H_{22}O_{11}$	Sigma-Aldrich, Steinheim, (Germany)
TissueTek Mounting Medium	TFM	Reichert-Jung, Bensheim, (Germany)
Triton X-100	Tx	Sigma-Aldrich, Steinheim, (Germany)
Vectashield mounting medium		Biozol Diagnostica, Eching, (Germany)

Table 2.6: Auxiliary tools and devices used within this thesis.

Tools and Devices	Vendor/Manufacturer
Adobe Illustrator Adobe Photoshop (CS3-6)	Adobe Systems, Neu-Isenburg, (Germany)
Axio Imager Z.1 (Fluorescence microscope) AxioCam MRm CCD camera Axioskop MOT and Pascal LSM5 module (laser scan microscope) Axiovision release 4.6 software	Zeiss, Oberkochen, (Germany)
Binocular equipped with external halogen lamp	Wild, Heerbruck (Switzerland), Zeiss, Oberkochen and Schott, Mainz (Germany)
Centrifuge Hereaus™ Biofuge pico	Thermo Fisher Scientific, Langenselbold, (Germany)
CM 3050S Cryostat	Leica, Nussloch, (Germany)
Cover slips: 18x18mm; 24x24mm; 24x40mm	Menzel Gläser, Braunschweig, (Germany), Carl Roth, Karlsruhe, (Germany)
Coverslips (precision): 18x18x0.17mm	Carl Roth, Karlsruhe, (Germany)
Cryomold® Biopsy (10mm x10mm x5mm)	Sakura Finetek Europe, Zoeterwoude, Netherlands (www.laborversand.de)
Dissecting sets	Fine Science Tools, Heidelberg, (Germany)
FluoViewer 1000 equipped with multi-argon and helium-neon lasers (laser scan microscope) FV 1.7 software	Olympus, Hamburg, (Germany)
ImageJ v 1.38 / FiJi	National Institutes of Health, Bethesda, (USA)
Imaris software	Bitplane AG, Zürich, (Switzerland)
Intuos® 2 XD-06-08-U (drawing tablet)	WACOM Europe, Krefeld, (Germany)
Laboratory shaker	Heidolph, Schwalbach, (Germany) and IKA Werke, Staufen (Germany)
LSM5 Pascal V3.2 SP2 software	Zeiss, Oberkochen, (Germany)
Magnetic stirrer with contact thermometer	IKA Werke, Staufen, (Germany)
Microscope objectives (Olympus): UPlanSApo 40x/0.75, UPlanSApo oil 60x/1.35	Olympus, Hamburg, (Germany)
Microscope objectives (Zeiss): Apochromat 20x/0.8, Plan Apochromat 20x/0.8, Plan Neofluar 40x/1.3, EC Plan Neofluar 40x/0.75, Plan Apochromat 63x/1.4;, Apochromat 63x/1.4oil, EC-Plan-Neofluar100x/1.3oil	Zeiss, Oberkochen, (Germany)
Microsoft Office software (Excel, Word, Power Point)	Microsoft, Unterschleißheim, (Germany)

Table 2.6: Continued - Auxiliary tools and devices used within this thesis.

Tools and Devices	Vendor/Manufacturer
MultiWell plates	Nunc, Langenselbold, (Germany)
Nitrocellulose filter membranes	Millipore, Schwalbach, (Germany)
PAP-Pen	SCI science services, München, (Germany)
Parafilm M Laboratory Film	Pechiney Plastic Packaging, Chicago (IL), USA
pH meter	WTW, Weilheim, (Germany)
Precision balance	Sartorius, Göttingen, (Germany)
Prism version 5 software	Graphpad Software, La Jolla (CA), USA
SuperFrost Plus microscope slides	Menzel Gläser, Braunschweig, (Germany)
Vortex	Heidolph, Schwalbach, (Germany) and IKA Werke, Staufen (Germany)
MilliQ Academic (Water purification system)	Millipore, Schwalbach, (Germany)

Chapter 3

Results

3.1 Synaptic input onto OFF-ganglion cells in the mouse retina

3.1.1 Classification of ganglion cell types

Two transgenic mouse lines were used to investigate the specificity of the bipolar cell input onto OFF-ganglion cell types in sublamina 1 (S1) of the IPL.

In retinae of the **Jam-B** mouse line enhanced GFP is selectively expressed in OFF-DSGCs, which are characterised by an asymmetric dendritic tree and respond to upward motion (Kim *et al.*, 2008, see also Fig. 3.1 A and the Material and Methods subsection 2.1.1). These cells correspond to C6 ganglion cells described by Sun *et al.* (2002). In retinae of **GFP-O mice**, in contrast, various amacrine and ganglion cell types express GFP in a random, golgi-like manner (Feng *et al.*, 2000; Majumdar *et al.*, 2007, and Fig. 3.1 B – F). In retinae of this mouse line, ganglion cells, which co-stratified with type 2 bipolar cells in S1 of the IPL were selected for further analysis. In addition to distinct types of monostratified ganglion cells, bistratified cells, corresponding to D2 cells described by Sun *et al.* (2002), whose outer plexus branches within the OFF layer of the IPL were found and analysed.

All **monostratified ganglion cells** included in the analysis of their bipolar cell input were reconstructed in order to reveal and compare their morphological properties (Fig. 3.2). The size of dendritic trees was previously

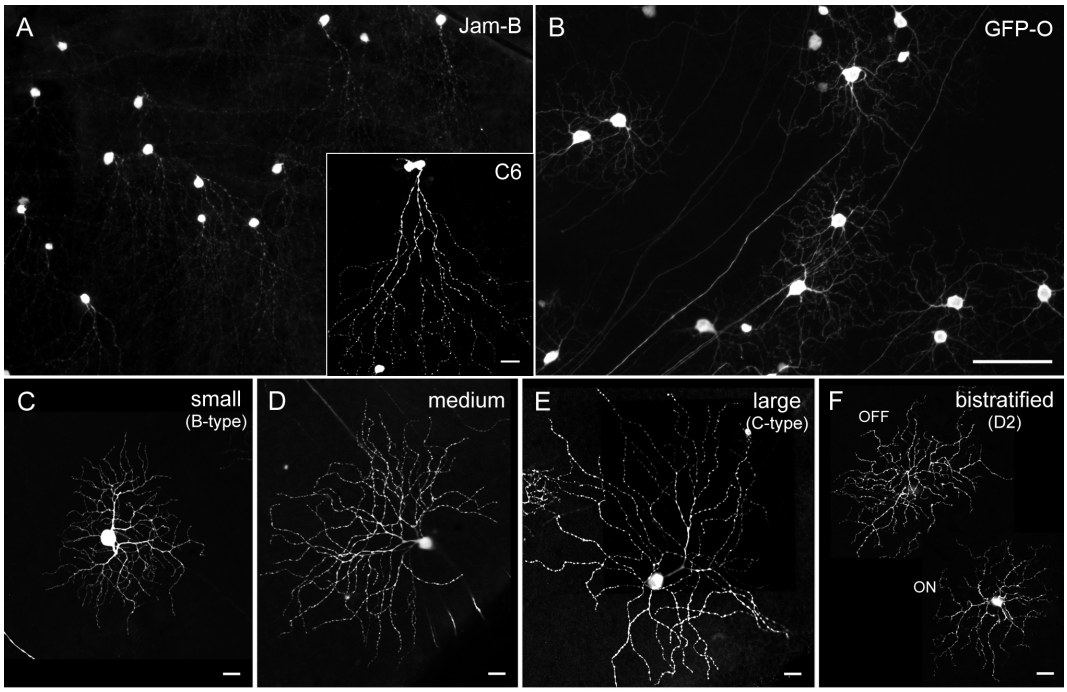

Figure 3.1: Ganglion cell characterisation – GFP-O and Jam-B retinae.
(**A and B**) Low power micrographs of retinal flat mount preparations of (**A**) Jam-B and (**B**) GFP-O mice. The **inset in (A**) shows a high resolution image of a C6 ganglion cell from a Jam-B mouse retina. Examples for ganglion cell types in S1 of the GFP-O mouse line are shown in **C** – **D**. Monostratified cells with of different dendritic tree sizes were found. Cells with small dendritic trees (**C**) showed complex dendritic branching pattern, whereas cells with large (**D**) and most cells with medium (**E**) sized dendritic trees had sparsely branched dendrites. Additionally bistratified ganglion cells were found (**F**). Potential correlates of cell types in Sun *et al.* (2002) are shown in brackets.
Scalebars: B (applies also to A): 100 µm; A_{inset} and C – F: 20 µm.

described as one of the morphologically most important parameters to characterise ganglion cells in the mouse retina (Hong *et al.*, 2011; Kong *et al.*, 2005). Therefore, the monostratified ganglion cells were classified according to their dendritic tree size, which was measured as the mean feret diameter of, and as the area covered by the dendritic tree of the cell (Table 3.1) in a first approach. However, a recent study had shown evidence that some ganglion cells change their tree sizes along a nasal-to-temporal gradient (Bleckert *et al.*, 2014). Therefore the ganglion cells were re-classified based on the complexity of the dendritic tree, measured as number of dendritic tips as dominant parameter, (subsection 3.1.3). All morphological measurements and the resulting

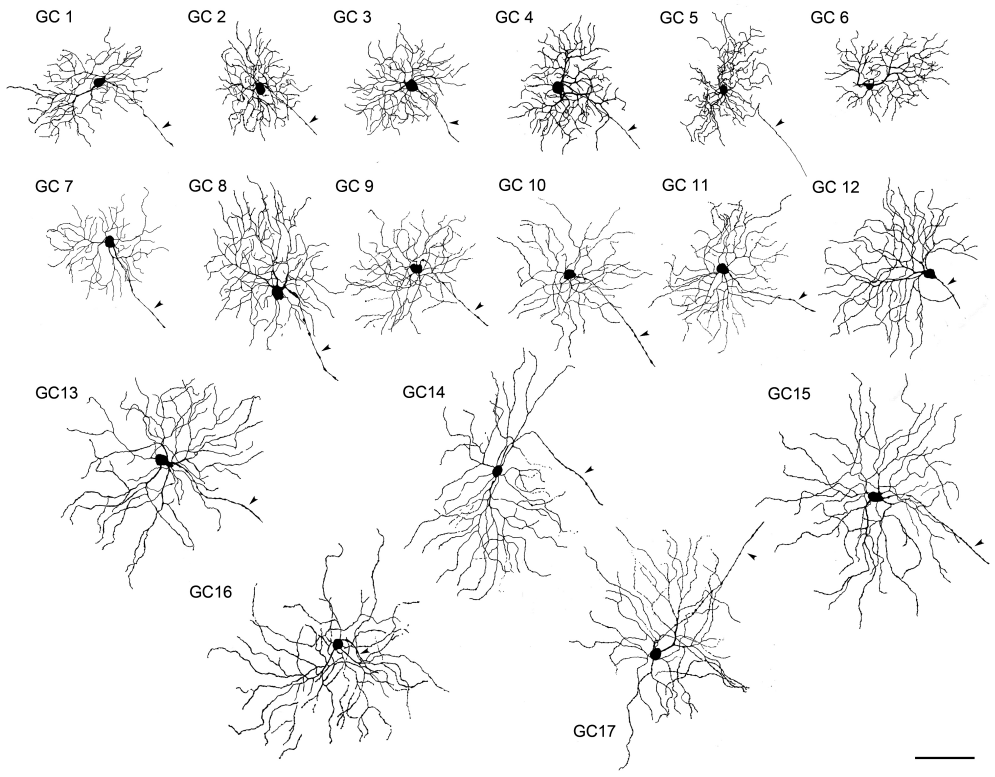

Figure 3.2: Summary of monostratified ganglion cells in S1 of GFP-O mouse retinae. According to their dendritic tree size, ganglion cells (GC) 1 – 7 have been classified as "small" (B-type like), GCs 8 – 12 as "medium size" and GCs 13 – 17 as "large" C-type like) ganglion cells. Compared to all other small-type GCs, GC7 showed a sparser dendritic arborisation. GC8 displayed a denser arborisation than GC7 and GC9 – 17. Axons are marked by arrowheads. All ganglionc cells shown were used for the quantitative analysis of the type 2 bipolar cell input. Scale bar: 100 µm.

cell classifications of both classification methods are summarised in Table 3.1 and the results of both classification schemes are described in detail below (subsections 3.1.2 and 3.1.3).

3.1.2 Classification based on dendritic tree size

Using a classification based on the size of their dendritic trees, three distinct groups of monostratified ganglion cells emerged (Fig. 3.1 C – E, Fig. 3.3 A and Table 3.1).

The first group comprised of cells possessing small complex dendritic trees with highly branched dendrites (76.9 ± 3.7 dendritic tips/cell (mean $\pm$ SEM))

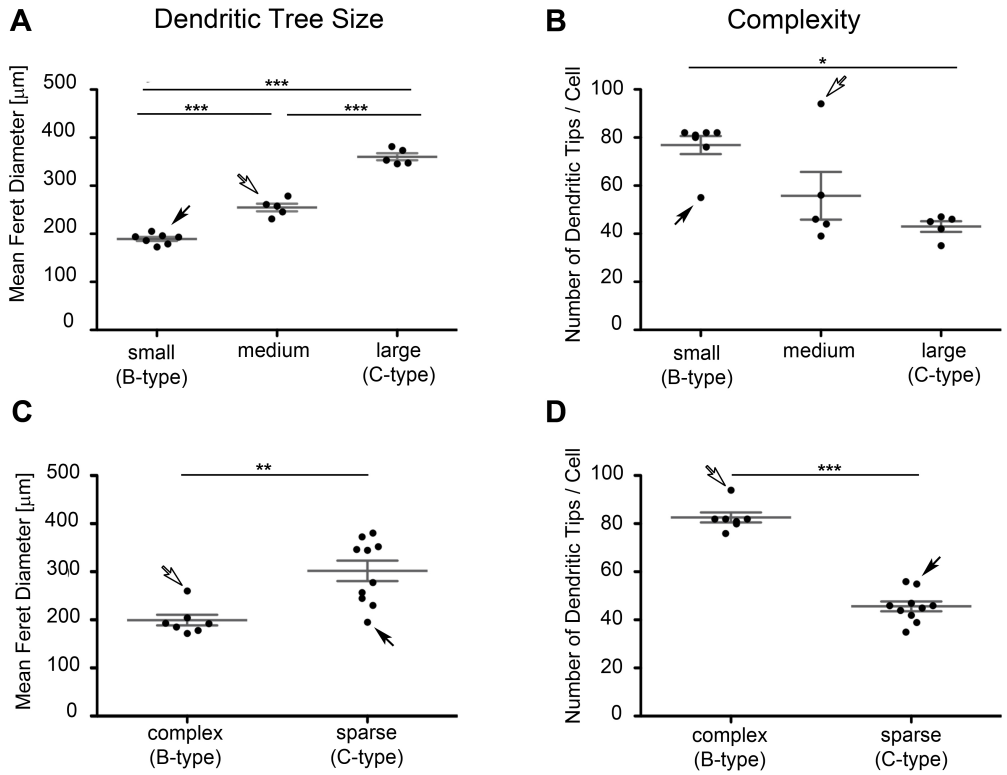

Figure 3.3: Morphological characterisation of monostratified ganglion cells in retinae of GFP-O mice. Scatter plots showing morphological properties of the monostratified ganglion cells. The dendritic tree size, measured as mean feret diameter is shown in (**A**) and (**C**), the complexity of the dendritic branching, measured as the number of dendritic tips in (**B**) and (**D**). Each symbol represents the value (the diameter, or the complexity of its dendritic tree) of a single cell, large bars depict the arithmetic mean of all cells in a gr oup, error bars the standard error of the mean (SEM). Cells were first classified as three cell types according to their dendritic tree size (**A and B**), but the analysis of the complexity of their dendritic trees indicated that some (arrows; GC7 and GC8 in Fig. 3.2) cells displayed morphological deviations from other cells within the group. A "small" cell had a sparser dendritic arborisation than the other small cells (arrow) resembling cells in the groups of "medium" and "large" cells. A "medium" cell possessed a dendritic arborisation similar to cells within the group of "small" cells. (open arrow). Since it was demonstrated that certain ganglion cell types change their size with eccentricity (Bleckert *et al.*, 2014), cells were reclassified using the complexity of their dendritic tree as dominant parameter and two rather than three groups of cells emerged (**A and B**). (GC7 and GC8 in Fig. 3.2).
Groups were compared using one-way ANOVA and Tuckey´s multiple comparison test (significance: not significant (ns) $P > 0.05$; (*) $P < 0.05$; (**) $P < 0.01$; (***) $P < 0.001$; (****) $P < 0.0001$.

and diameters of 189 ± 4 µm (mean ± SEM) (GC 1 – 7 in Fig. 3.2 and Fig. 3.3 A and B). These cells were classified as **"small" ganglion cells** ($n = 7$). One cell of this group (GC 7 of Fig. 3.2; Fig. 3.3, black arrows), however, had a sparser dendritic arborisation than the remaining cells within this group. The morphology of all other type small ganglion cells was largely similar to B1 and B3 type ganglion cells described by Sun *et al.* (2002).

Ganglion cells of the second group had dendritic tree diameters of 255 ± 8 µm and were classified as **"medium" ganglion cells** ($n = 5$, Fig. 3.1 D; Fig. 3.2 (GC 8 – 12)). Most of the medium sized ganglion cells had a sparser dendritic arborisation (55.8 ± 9.9 dendritic tips/cell, Fig. 3.3) than the small ganglion cells and resembled C2 ganglion cells described in Sun *et al.* (2002). One medium size ganglion cell (GC 8 in Fig. 3.2, Fig. 3.3 open arrows), however, possessed a denser and more complex dendritic arborisation than the remaining ganglion cells within this group. The third group comprised of ganglion cells which possess a rather sparse dendritic arborisation (43.0 ± 2.1 tips/cell) resembling also C2 ganglion cells described in Sun *et al.* (2002), but were significantly larger (360 ± 7 µm) than cells within the groups of small and medium ganglion cells (Fig 3.3 A). Such cells were classified as **"large" ganglion cells** ($n = 5$; Fig. 3.1 E; Fig. 3.2 (GC 13 – 17) and Fig. 3.3 A). In summary medium and large ganglion cells, most likely correspond to alpha-type or A-type ganglion cells described in previous studies.

3.1.3 Classification based on the complexity of dendritic branching

It had been a largely accepted assumption that, unlike in primates and some predatory animals, the ganglion cells size and distribution does not change significantly across the retina in rodents (Sun *et al.*, 2002). However, as mentioned before, there is recent evidence that at least sustained and transient A-type ganglion cells, namely the $A_{ON\text{-}S}$ and $A_{OFF\text{-}T}$ ganglion cells, undergo drastic changes in their dendritic field size depending on their location within the retina (Bleckert *et al.*, 2014). Therefore, the ganglion cells were re-classified using an alternative classification system based on the complexity of their dendritic tree rather than dendritic field size. According to this classification two

Table 3.1: Summary of monostratified ganglion cells of the GFP-O mouse retina.

Ganglion Cell	Soma Diameter [µm]	Dendritic Tree Diameter [µm]	Dendritic Tree Area [mm^2]	Complexity [# of dendritic tips per cell]	Cell type according to size	Cell type according to complexity
GC1	19	194	27065.1	76	small (B-type)	complex (B-type)
GC2	19	173	21325.4	72	small (B-type)	complex (B-type)
GC3	20	186	25852.2	80	small (B-type)	complex (B-type)
GC4	19	205	29965.6	81	small (B-type)	complex (B-type)
GC5	15	179	22923.9	82	small (B-type)	complex (B-type)
GC6	18	193	26692.6	82	small (B-type)	complex (B-type)
GC7	18	196	27905.4	55	small (B-type)	sparse (C-type)
GC8	25	261	52833.6	94	medium	complex (B-type)
GC9	20	231	39091.4	47	medium	sparse (C-type)
GC10	19	278	55933.5	39	medium	sparse (C-type)
GC11	21	258	47989.6	54	medium	sparse (C-type)
GC12	15	272	58348.6	44	medium	sparse (C-type)
GC13	21	346	81775.3	46	large (C-type)	sparse (C-type)
GC14	18	353	90108.9	42	large (C-type)	sparse (C-type)
GC15	22	374	106120.9	45	large (C-type)	sparse (C-type)
GC16	19	382	107182.1	47	large (C-type)	sparse (C-type)
GC17	21	374	85236.8	35	large (C-type)	sparse (C-type)

groups of ganglion cells emerged, **"complex" and "sparse" type** ganglion cells (Fig. 3.3 C and D). Whereas the group of complex cells was mostly derived from ganglion cells with small dendritic tree diameters, most medium to large ganglion cells were merged in the group of sparse cells (compare Table 3.1). Hence, the group of complex cells resembled the small, B-type cells, whereas the group of sparse cells most likely corresponded to the larger, C2 cells in the catalogue of Sun *et al.* (2002), which also correspond to $A_{OFF\text{-}S}$ cells described in van Wyk *et al.* (2009) and Bleckert *et al.* (2014).

It was also attempted to use the soma size of the ganglion cells for their classification (Table 3.1, second column), but no significant differences between the soma sizes of the different ganglion cell types were detected (data not shown). Therefore, the soma size was not used to classify the different ganglion cells.

In addition to monostratified ganglion cells, cells with a **bistratified** dendritic arborisation ($n = 5$, Fig. 3.1 F) were also found within the retinae of GFP-O mice and were classified as D-type cells according to the catalogue of Sun *et al.* (2002). D-type cells had small dendritic trees (OFF-plexus: 195.4 ± 9.0 µm; ON-plexus: 155.5 ± 6.6 µm) with dendrites which often changed their direction in a nearly perpendicular manner. The bistratified cells strongly resembled D2 ganglion cells in Sun *et al.* (2002) which likely correspond to ON/OFF-DSGCs. However, in contrast to D2 cells in Sun *et al.* (2002), the outer plexus of bistratified cells found during this study in retinae of GFP-O mice co-stratified with type 2 bipolar cell terminals at the border of S1 and S2 in the IPL. Therefore these cells were included in the analysis of the specificity of bipolar cell input.

Specificity of bipolar cell input

After determining the ganglion cell types the question, whether some of these ganglion cell types receive specific input from a certain bipolar cell type only, or if they sample their bipolar cell input non-selectively from all bipolar cell types stratifying within the area of their dendritic field arose. To address this question, retinae of both mouse lines were triple-immunolabeled for GFP to visualize the ganglion cells, CtBP2 to mark all ribbon synapses and Syt2 to mark the axon terminals of type 2 bipolar cells (Fig. 3.4).

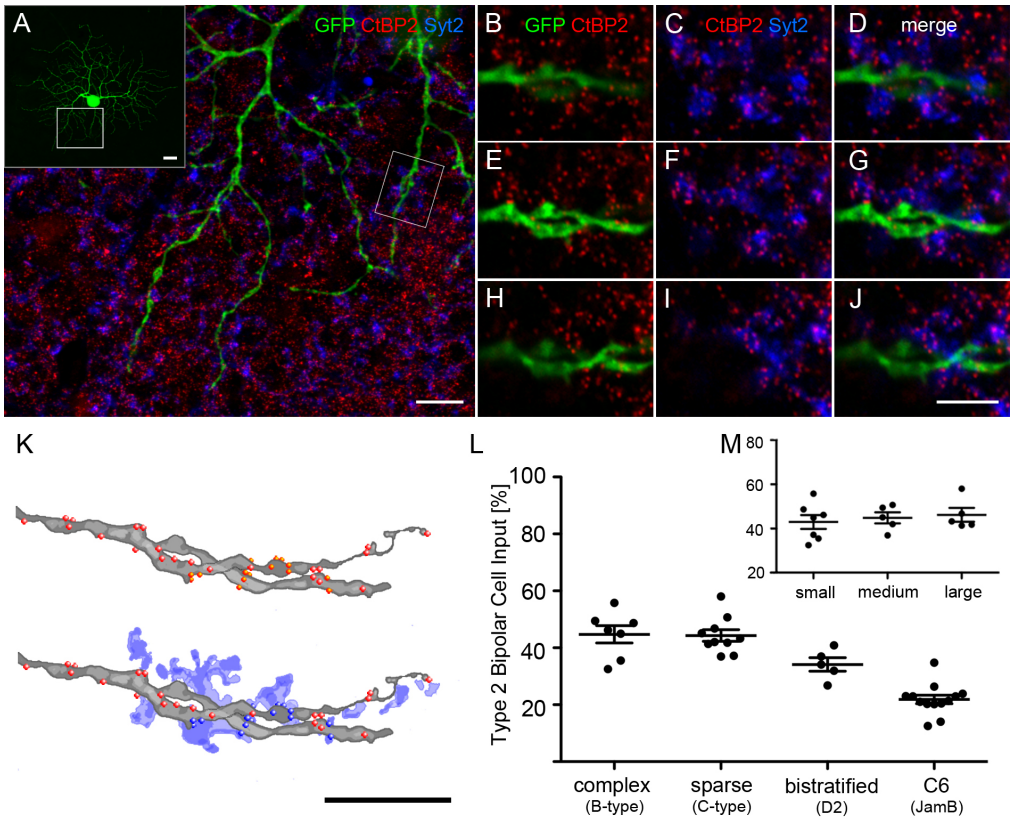

Figure 3.4: Type 2 bipolar cell input onto ganglion cells. (**A**–**J**): Confocal micrographs of a retinal flat mount of GFP-O mouse immunostained against GFP, CtBP2 and Syt2 showing a representative small, complex ganglion cell. An overview of the cells morphology is shown in **inset of A**. The framed region is shown in high resolution in (**A**). The image shows the GFP labelled dendrites of the ganglion cell, the punctate staining of CtBP2 and the axon terminals of Syt2 labelled type 2 bipolar cells. The framed area is shown in higher magnification in three consecutive planes of an image stack in (**B**–**J**). CtBP2 staining combined with GFP labelling (**B, E and H**) and with Syt2 labelling (**C, F and I**). Merges of all three channels are shown in (**D, G and J**). (**K**) Reconstruction of the dendrite in B–J with input synapses from bipolar cells (red dots, upper picture) and combined with reconstructed type 2 bipolar cell terminals (blue, lower picture). Input synapses from type 2 bipolar cells are shown as blue dots. Scale bars: A and K: 10 µm, A_{inset}: 20 µm; J (applies to B–J): 5 µm). (**L and M**): Scatter plots showing the percentage of type 2 bipolar cell input onto different ganglion cells. Symbols represent the percentage of type 2 bipolar cell input of individual ganglion cells, long bars depict the mean of the percentage of the type 2 input onto all ganglion cells within a group, small bars show the SEM. (**L**) shows percentage of type 2 bipolar cell input onto all analysed cells types, when cells were classified according to the the complexity of the dendritic tree. (**M**): Percentage of type 2 bipolar cell input onto monostratified ganglion cells classified according to their dendritic tree size in (**M**). The annotation of the y-axis in L applies to the y-axis in M. The range shown on the Y-axis in M was shortened for better visibility (20–80 % instead of 0–100 %).

Depending on the size of the dendritic tree, image stacks of the whole cell or of parts of the dendritic tree were imaged at high resolution. All synaptic ribbons in direct apposition of the dendrites of the labelled ganglion cells were counted within the image stack to assess the total number of bipolar cell input to the ganglion cell in a 3D space (Fig. 3.4 B, E and H).

Afterwards, it was analysed how many of these ribbons are located within the terminals of type 2 bipolar cells, in order to assess the proportion of the type 2 bipolar cell input to the ganglion cell (Fig. 3.4 C, F and I). Figure 3.4 K shows a 3D reconstruction of the dendrite of the small, complex ganglion cell shown in Figure 3.4 A – J (see also GC 4 in Fig. 3.2 and Table 3.1). The total bipolar cell input (upper panel, red puncta) as well as the input from type 2 bipolar cells to the dendrite (lower panel, blue puncta) is shown.

The amount of type 2 bipolar cell input onto the monostratified ganglion cells was similar for both classification methods used (Fig. 3.4 L and M). Complex type, as well as sparse type ganglion cells received similar proportions of bipolar cell input from type 2 bipolar cells (complex type ($n = 7$): $45 \pm 3\,\%$; sparse type ($n = 10$): $44 \pm 2\,\%$ (mean $\pm$ SEM), Fig. 3.4 L), whereas the remaining input is provided by other bipolar cells stratifying within this area of the IPL, e.g. type 1 or 4 bipolar cells. Also, when the monostratified cells were subdivided into three types S-, M- and L-ganglion cells, according to their dendritic tree sizes, no significant differences in the proportion of type 2 bipolar cell input between the three ganglion cell types were detected (S: $43 \pm 3\,\%$ ($n = 7$); M: $45 \pm 3\,\%$ ($n = 5$); L: $46 \pm 3\,\%$ ($n = 5$); (mean $\pm$ SEM); Fig. 3.4 M).

The bistratified D-type ganglion cells ($n = 5$) received a slightly smaller amount of bipolar cell input from type 2 bipolar cells ($34 \pm 2\,\%$ (mean $\pm$ SEM)) onto their outer plexus than the monostratified cells. Asymmetric C6 ganglion cells in the Jam-B mouse line ($n = 13$), in contrast, received only $22 \pm 2\,\%$ (mean $\pm$ SEM) of their bipolar cell input from type 2 bipolar cells (Fig. 3.4 L). The proportions of type 2 bipolar cell input for each individual ganglion cell analysed in this study are shown in Table 3.2.

Table 3.2: Type 2 bipolar cell input to ganglion cells in retinae of GFP-O and Jam-B mice.

GFO-O mice						Jam-B mice		
Monostratified ganglion cells			Bistratified ganglion cells			C6 ganglion cells		
Cell	Input synapses [total]	Type 2 BC input [%]	Cell	Input synapses [total]	Type 2 BC input [%]	Cell	Input synapses [total]	Type 2 BC input [%]
GC 1	212	43	D2 1	463	36.98	1	377	20.2
GC 2	221	33	D2 2	711	31.97	2	599	21.35
GC 3	226	49	D2 3	625	34.10	3	292	14.07
GC 4	1006	45	D2 4	590	40.85	4	263	21.07
GC 5	264	36	D2 5	396	26.80	5	476	26.41
GC 6	549	56				6	439	23.06
GC 7	333	37				7	88	12.50
GC 8	663	49				8	191	20.42
GC 9	311	42				9	900	34.78
GC 10	432	45				10	514	22.96
GC 11	221	37				11	133	20.30
GC 12	626	51				12	1131	23.89
GC 13	203	41				13	283	22.97
GC 14	212	58						
GC 15	206	42						
GC 16	217	43						
GC 17	169	47						
SUM	**6071**			**2785**			**5686**	

3.2 Synaptic inhibition of intrinsically photosensitive ganglion cells[1]

3.2.1 Distribution of glycine and $GABA_A$ receptor subunits in the macaque retina

Electron microscopic studies have found glycine and $GABA_A$ receptors clustered at postsynaptic sites, which can be visualised as punctate staining using light microscopy (for a review see (Wässle *et al.*, 2009b; Zhang & McCall, 2012). In this thesis subunits $\alpha 1$, $\alpha 2$ and $\alpha 3$ of glycine (GlyR$\alpha 1-\alpha 3$) and

[1]Parts of the data and results described in the following chapter have been published as research article in *Neuroscience* titled: "Intrinsically Photosensitive Ganglion Cells of the Primate Retina express distinct Combinations of Inhibitory Neurotransmitter Receptors" in 2011 (Neumann *et al.*, 2011).

$GABA_A$ receptors ($GABA_A$ ($\alpha1-\alpha3$)) were immmunohistochemically labelled to investigate their distribution in the primate retina as well as their involvement in certain retinal circuits.

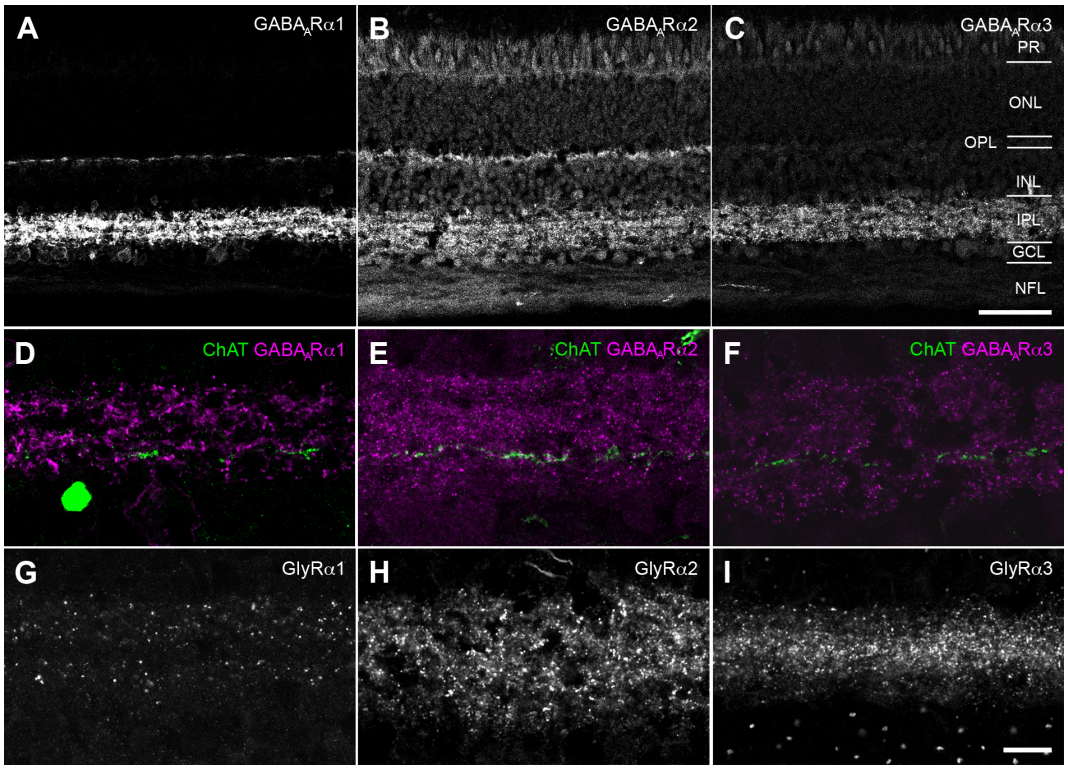

Figure 3.5: Distribution of $GABA_A$ and glycine receptor subunits in macaque retina. Low power micrographs of vertical retina sections labelled against $GABA_A$ receptor subunits $\alpha1$, $\alpha2$ and $\alpha3$ (**A**$-$**C**). All subunits were evenly distributed as punctate staining across the IPL. However, a subtle layering in the staining pattern was observed in some cases. $GABA_A\alpha1$ and $\alpha2$, but not $\alpha3$, were also localised in the OPL. (**D**$-$**F**)**:** Higher magnifications of retina sections double-labelled for ChAT and $GABA_A\alpha1-\alpha3$ showing the distribution of immunoreactive puncta throughout the IPL. Sublamina 3/4 is marked by the ON-ChAT band of starburst amacrine cells.(**G**$-$**I**)**:** High power micrographs of vertical retina sections immunolabelled for GlyR$\alpha1$, $\alpha2$ and $\alpha3$.
Scalebars: C (applies to A$-$C) 50 µm; I (applies to D$-$I): 10 µm. All images of the figure show single confocal planes.

Low power micrographs of vertical sections through macaque retina were processed with antibodies against $GABA_A\alpha1$, $\alpha2$ and $\alpha3$ (Fig. 3.5 A$-$C). All subunits were evenly distributed within the IPL, and only a subtle layering of denser accumulated clusters of $GABA_A$ receptors were found, which contrasts the laminated expression of these receptors in the rodent retina (reviewed by

Grünert, 2000; Zhang & McCall, 2012). Figure 3.5 D – F shows high power micrographs of the IPL of vertical sections double-immunolabelled for $GABA_A\alpha1$, $\alpha2$ or $\alpha3$ with choline acetyl transferase (ChAT). ChAT is expressed by starburst amacrine cells, which stratify in S2 and S3/4 of the IPL, in most species. In the macaque retina, the OFF-ChAT band in S2 was only weakly stained or absent (Fig. 3.5 D – F, green). Only the staining of the ON-ChAT band in S3/4 was sufficient to be used as marker for a subdivision of the IPL into sublaminae. This pattern of ChAT staining was consistent with previous studies of the primate retina (Mariani & Hersh, 1988; Majumdar *et al.*, 2009).

$GABA_A\alpha1$ labelling (Fig. 3.5 A, D) was found as evenly distributed punctate staining within the IPL reflecting receptor clusters containing this subunit at postsynaptic sites. In some cases an accumulation of synaptic puncta in two bands of slightly higher density was observed within the IPL. Additionally to the synaptic staining in the IPL some somata within the GCL were also immunoreactive for $GABA_A\alpha1$. In summary the staining pattern of $GABA_A\alpha1$ was similar to $GABA_A\alpha1$ staining previously shown in primate retina (Mariani *et al.*, 1987). **$GABA_A\alpha2$** labelling (Fig. 3.5 B, E) also appeared as punctate staining of postsynaptic receptor clusters in the IPL, which in some cases appeared accumulated in 4 – 5 subtle bands. An accumulation of the synaptic puncta in two bands of higher density in layers occupied by starburst amacrine cells as described for the rodent retina by Greferath *et al.* (1995) was not observed. Additionally, some somata within the GCL and INL were also labelled, likely reflecting cell bodies of amacrine and ganglion cells expressing this subunit. Synaptic clusters containing the **$GABA_A\alpha3$** subunit were also evenly distributed throughout the IPL (Fig. 3.5 C, F). Within the other synaptic layer of the retina, the OPL, structures were also recognised by antibodies against $GABA_A\alpha1$ and $\alpha2$, but not $GABA_A\alpha3$ (Fig. 3.5 A – C). The $GABA_A\alpha1$ labelling in the OPL was localised close to the cone pedicle base, whereas the $GABA_A\alpha2$ appeared more diffusely distributed (Fig. 3.5 A, B). Consistent with previous studies of the primate retina (Grünert & Ghosh, 1999; Jusuf *et al.*, 2005; Lin *et al.*, 2000) immunostainings with antibodies against **GlyR$\alpha1$, $\alpha2$, and $\alpha3$** resulted in punctate labelling of synaptic clusters in the IPL (Fig. 3.5 G – I). GlyR$\alpha1$ clusters were located in a broad band in the outer and a less dense band in the inner IPL. Between the bands and close to

the GCL only few synaptic puncta were found (Fig. 3.5 G). GlyRα2 and α3, in contrast, were more homogeneously distributed throughout the IPL. However, in the very inner IPL GlyRα2 clusters were slightly reduced compared to more outer layers (Fig. 3.5 H). Synaptic clusters containing GlyRα3 appeared to accumulate within the centre of the IPL and a probably unspecific staining occurred within the cell bodies in the GCL (Fig. 3.5 I).

3.2.2 Intrinsically photosensitive ganglion cells (ipRGCs) in the macaque retina

Two types of ipRGCs, which express the photopigment melanopsin rendering them photosensitive, have been described in the primate retina until today, the outer stratifying M1 and the inner stratifying M2 cells (Dacey *et al.*, 2005; Jusuf *et al.*, 2007; Hannibal *et al.*, 2014; Neumann *et al.*, 2011).

To identify ipRGCs, retinal flat mount preparations were labelled with antibodies against their photopigment melanopsin (Fig. 3.6). Both ipRGC types, M1 and M2 cells, were recognised by the antibody. Figure 3.6 A shows a projection of an image stack through the full width of the IPL. In the full projection a M1 (upper left) and a M2 cell (lower right) are seen. Projections of images of only the outer (Fig. 3.6 B) and only the inner part (Fig. 3.6 C) of the IPL show the outer-stratifying M1 and the inner-stratifying M2 cell, respectively. Both ipRGC types were characterised by large and sparsely branched dendritic trees. However, compared to M2 cells the immunolabelling of M1 cells was generally more intense. Another difference between the two types was the location of their cell bodies. Whereas the somata of M2 cells were always located within the GCL, cell bodies of M1 cells were in most cases displaced in the INL. The stratification of the dendrites and soma location is also depicted in the schematic shown in Figure 3.6 D. In summary, the immunolabelling with antibodies against the marker melanopsin was consistent with previous studies describing ipRGCs in primate retina (Dacey *et al.*, 2005, 2006; Jusuf *et al.*, 2007).

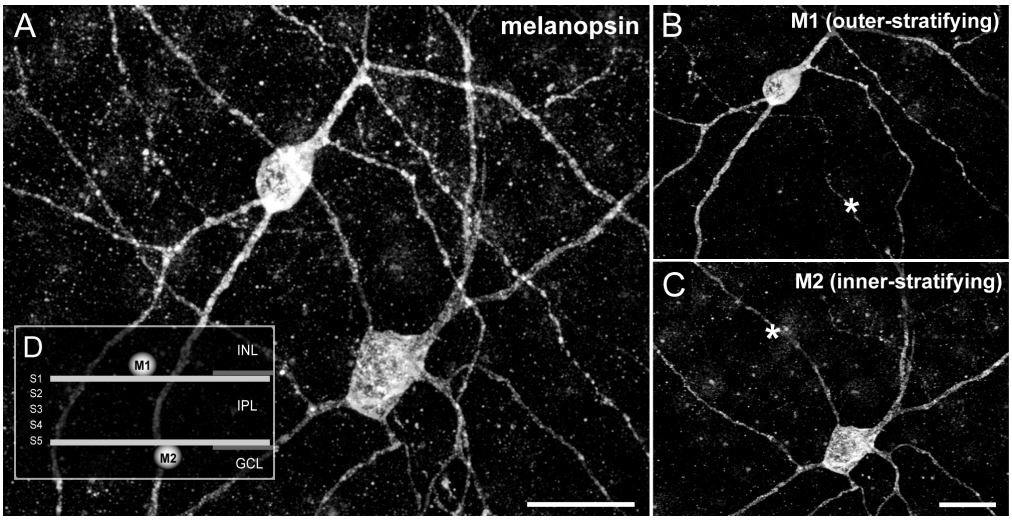

Figure 3.6: Melanopsin containing ganglion cells in macaque retina. (**A**) Projected image stack (z1 – 9) of flat mounted macaque retina processed with antibodies against the photopigment melanopsin. The picture shows an M1 and an M2 type ganglion cell. (**B and C**) Projected images focused on different stratification depths of the IPL. Asterisks depict location of the M1 (C) and M2 (B) cells in the other layer of the IPL. (**B**) Projection of the outer part of the IPL showing the M1 cell, only. (**C**) Projection of the inner part of the IPL showing the M2 cell. (**D**) Scheme demonstrating the stratification of M1 and M2 ganglion cells in the IPL: M1 cells frequently have their somata displaced in the INL and their dendrites stratify at the outer border of the IPL, M2 cell dendrites occupy the very inner stratum of the IPL with their somata placed in the GCL.
Scalebars: A: 50 µm, C (applies also to B): 10 µm.

3.2.3 Quantitative analysis of glycine and $GABA_A$ receptor subunits on ipRGC dendrites

Retinal flat mount preparations were double-immunostained for melanopsin and subunits $\alpha 1$, $\alpha 2$ or $\alpha 3$ of glycine and $GABA_A\alpha$ receptors, in order to analyse the distribution of different receptor types on ipRGCs. First, the overall morphology of the analysed ipRGCs was documented and the subtype, M1 or M2, was identified based on the soma location and stratification of their dendrites (Fig. 3.7 A, inset). Afterwards, high-resolution images along a dendritic process were taken, the number of colocalised synaptic receptor clusters was counted and normalised to 100 µm dendritic length. An example of a retina labelled for melanopsin and $GABA_A\alpha 3$ is shown in (Fig. 3.7 A – C). The outlines of the dendritic process are overlaid to the receptor staining and

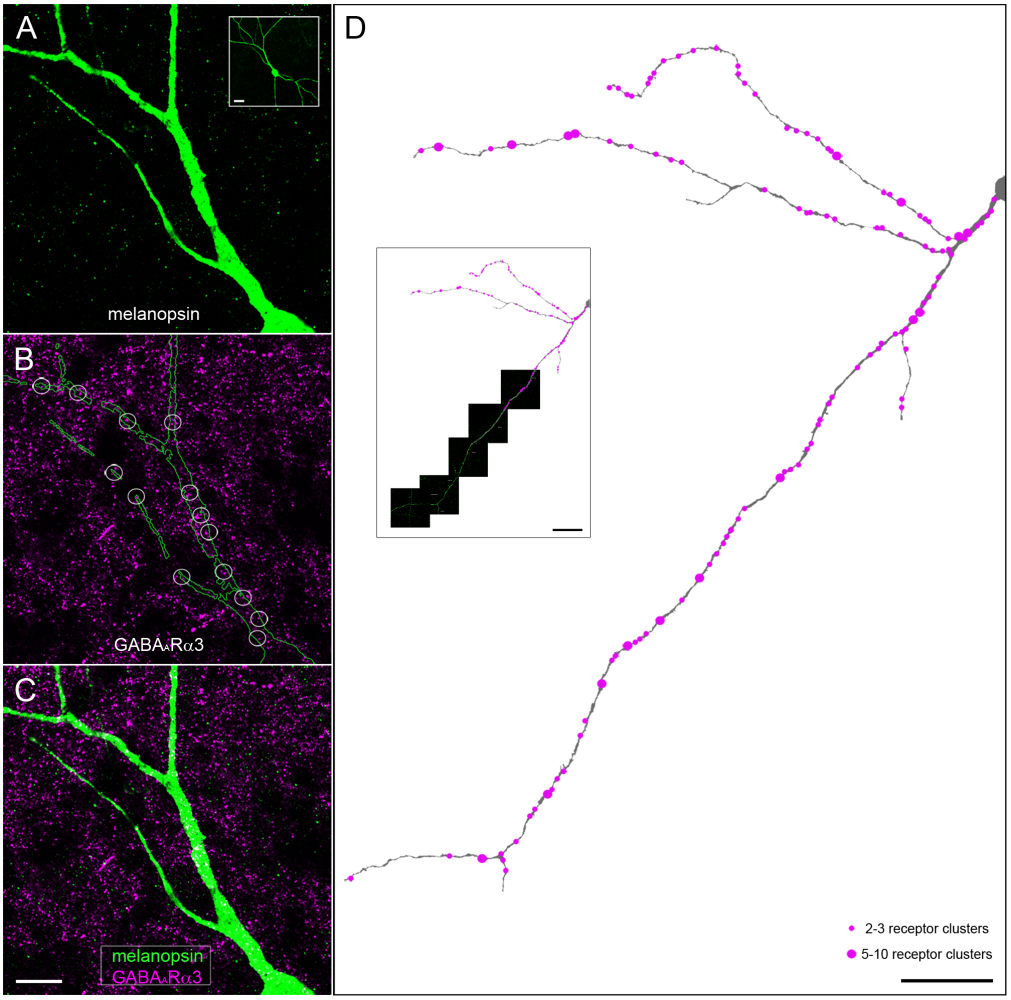

Figure 3.7: Analysis of inhibitory neurotransmitter receptors on ipRGCs. (**A** – **C**): Micrographs of flat mounted macaque retina immunolabelled for melanopsin and $GABA_A\alpha3$. An overview of the M1 cell in low magnification is shown in the (**inset of A**). Parts of the dendrites of the M1 cell are shown in (**A**), the $GABA_A\alpha3$ immunostaining in the same confocal plane as the dendrite in A is shown in (**B**) with an outline of the M1 dendrite. Circles mark clusters of $GABA_A\alpha3$ colocalised with the dendrite. The merge of both channels is shown in (**C**).(**D**) Partial reconstruction of an M1 cell from a flat mounted macaque retina immunolabelled for melanopsin and GlyRα2. Small dots indicate aggregations of 2 – 3, large dots aggregations of 5 – 10 synaptic GlyRα2 clusters. (**D inset**) depicts the method how the cell was reconstructed from individual high resolution stacks along the dendrite. Scale bars: A_{inset}: 20 µm; C (applies to A – C): 10 µm; D and D_{inset}: 50 µm. A – C show single confocal planes.

circles mark the colocalised receptor clusters (Fig. 3.7 B). The merge of the melanopsin and GABA$_A\alpha$3 labelling is shown in Figure 3.7 C. Figure 3.7 D shows a partial reconstruction of a representative M1 cell and the distribution of colocalised GlyRα2 receptor clusters (magenta dots). The inset shows how the reconstruction was generated from stacks of high-resolution images along the M1 cell dendrites which were used for the quantitative analysis. As shown on the reconstruction, dendrites of the ipRGCs were decorated with receptor clusters, however segments of the dendrites bare of any receptor clusters were also frequently observed.

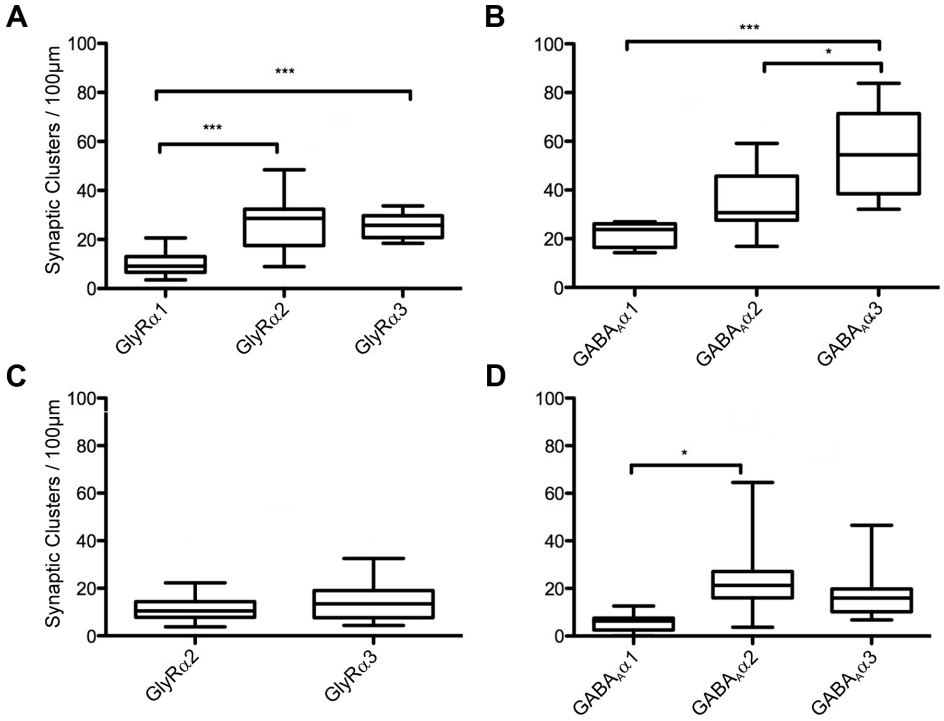

Figure 3.8: Density of glycine and GABA$_A$ receptors on ipRGCs in macaque retina. Box plots showing the linear density of glycine and GABA$_A$ receptors (synaptic clusters per 100 µm dendritic length) on M1 (**A, B**) and M2 cells (**C, D**). The analysis of the GlyRα1 density on M2 cells was omitted because of the low density of GlyRα1 in the stratification depth of M2 ipRGCs. Whiskers show the minimum to maximum range of all analysed image stacks, boxes the interquartil range, line indicates the median value. Statistical analysis: One-way ANOVA with Tuckey´s multiple comparison test (significance: not significant (ns) $P > 0.05$; significant (*) $P < 0.05$, (**) $P < 0.01$, (***) $P < 0.001$).

The quantitative analysis of the linear **density of glycine and GABA$_A$ receptor subunits** on ipRGC dendrites revealed differences in the abundance

of certain receptor subunits as well as differences in the expression of these subunits between M1 and M2 cells. The data of the quantitative analysis is summarised in Figure 3.8. Since the receptor clusters were not homogeneously distributed along the dendrites (compare Fig. 3.7 D), median values, which are less susceptible to outliers, are shown instead of arithmetic means in the following description of the data. Densities of different subunits were compared using one-way analysis of variance (ANOVA), followed by Tuckey´s Multiple Comparison Tests (see also Material and Methods). On **M1** cell dendrites it was found that GlyRα2 clusters were most abundant (median: 28.6; range: 9.0 – 48.5 clusters/ 100 µm; Fig. 3.8 A). However, no statistically significant difference was found compared to the density of GlyRα3 clusters (median: 25.8; range: 18.5 – 33.7 clusters / 100 µm; $P\alpha2-\alpha3 > 0.05$). The linear density of GlyRα1 on the M1 dendrites, in contrast, was with 9.1 clusters / 100 µm (range: 3.5 – 20.6 clusters / 100 µm) substantially lower ($P_{\alpha1-\alpha2} < 0.001$; $P_{\alpha1-\alpha3} < 0.001$).

To estimate if the colocalisation of the receptor clusters with the dendrites resulted from a random superposition of the channel showing the melanopsin and the one showing the receptor staining, rotation controls were performed. In brief, one of the channels of the image stacks was rotated 90 ° from its original orientation and the quantitative analysis was repeated (see also Material and Methods). Only for GlyRα2 a difference in the density of the receptor clusters on M1 cells between the rotation control and the original data was found (data previously published in Neumann *et al.*, 2011, Fig. 3). This suggests that M1 cells express glycine receptors containing the α2 subunit. However, an additional expression of GlyRα3 cannot be excluded. GlyRα1 appears to be an unlikely candidate to be responsible for the glycinergic modulation of M1 cells, due to its low abundance on the dendrites, which did not differ significantly from density found in the rotation control (median: 11.0; range: 6.4 – 20.7 clusters / 100 µm; $P_{\alpha1-\alpha1\ ctr} > 0.05$). The most abundant $GABA_A$ receptor subunit found on M1 cells was α3 (median: 54.4; range: 32.1 – 20.7 clusters / 100 µm) (Fig. 3.8 B). Its density was significantly higher compared to the density of $GABA_A\alpha1$ (median: 14.3; range: 32.1 – 20.7 clusters / 100 µm; $P_{\alpha1-\alpha3} < 0.001$) and α2 (median: 30.7; range: 16.9 – 59.1 clusters / 100 µm; $P_{\alpha1-\alpha3} < 0.05$). However, only for $GABA_A\alpha3$ a significant reduction of the

density of receptor clusters on the M1 dendrites was observed (median: 31.7; range: 16.8 – 48.7 clusters / 100 µm; $P_{\alpha 3-\alpha 3\ ctr} < 0.001$). This data suggests that M1 cells are modulated from GABAergic amacrine cells via receptors containing the $GABA_A\alpha 3$ subunit, whereas receptors containing subunits $\alpha 1$ and $\alpha 2$ seem to play minor roles.

The density of $GABA_A\alpha 3$ clusters on M1 cell dendrites was significantly higher than the density of all GlyRα subunits ($P_{GlyR\alpha 1,\alpha 2,\alpha 3-GABA_A\alpha 3} < 0.001$). This result supports a strong modulation of M1 cells from GABAergic amacrine cells which have been shown to be in contact with axon-like processes of wide-field amacrine cells which co-express dopamine and GABA as neurotransmitter (Dacey *et al.*, 2006; Vugler *et al.*, 2007). However, it also indicates a fine tuning through glycinergic amacrine cells. An amacrine cell candidate providing glycinergic synaptic input to M1 cells will be provided in the section below. Figures 3.8 C and D show the density of glycine and $GABA_A$ receptor subunits on inner-stratifying M2 ipRGCs. The analysis of GlyRα1 on M2 cells was omitted because of the scarcity of this subunit at the inner IPL border occupied by the M2 dendrite (compare Fig. 3.5 G). The densities of GlyRα2 and α3 on M2 dendrites were also very low ($median_{(GlyR\alpha 2)}$: 10.5; range: 3.8 – 22.3 clusters / 100 µm; $_{(GlyR\alpha 3)}$: 13.4; range: 4.4 – 32.5 clusters / 100 µm). Only the density of $GABA_A\alpha 2$ subunit clusters on M2 cell dendrites was slightly elevated compared to the other receptor subtypes investigated ($median_{(GABA_A\alpha 2)}$: 30.7; range: 3.7 – 64.5 clusters / 100µm; Fig. 3.8 D). However, only the density of $GABA_A\alpha 1$ was significantly lower ($median_{GABA_A\alpha 1}$: 6.3; range 0 – 12.6 clusters / 100 µm; $P_{GABA_A\alpha 1-GABA_A\alpha 2} < 0.05$). No statistically convincing differences were found between the densities of other receptor subunits or the respective rotation controls found (data previously published in Neumann *et al.*, 2011, Fig. 3 C, D). In summary, the data show that M2 cells receive less glycinergic and GABAergic inhibition than M1 cells. Whereas receptors subunits GlyRα2 and α3, as well as the $GABA_A\alpha 3$ are found at higher densities on M1 cells, only $GABA_A\alpha 2$ was found at higher densities on M2 cell dendrites compared to the other analysed receptor subunits.

It should be noted that the linear densities for receptor subunits on ipRGC dendrites described here exceeded those described in a previous study by Jusuf *et al.* (2007) in marmoset retina. In their study the linear density of gephyrin

clusters, a protein which anchors glycine and GABA receptors to postsynaptic sites, were analysed on ipRGCs. In order to examine if the high densities of the receptor subunits found in our study is merely an oversampling, our analysis was repeated for M1 cells using gephyrin, the same synaptic marker used in the study of Jusuf *et al.* (2007). Gephyrin is supposed to label the majority of glycine and $GABA_A$ receptors. Also for this antibody a higher linear density than described in marmoset was found (mean density: 40 ± 4 gephyrin clusters / 100 µm (mean ± SEM; range: 22 – 51 clusters / 100 µm; n = 9 quadrants). However, the density of gephyrin clusters on M1 dendrites did not reach the total density of the sum of all receptors subunits (sum of the densities of all glycine and all $GABA_A$ receptor subunits analysed) which would hypothetically reach over 100 clusters per 100 µm dendritic length. This discrepancy is likely due the localisation of different GlyRα subunits on the same synapse. Further, antibodies against gephyrin do not recognise all inhibitory postsynaptic sites. These possible explanations will be discussed in detail later (chapter 4). In summary, the data obtained from the analysis of the gephyrin density on M1 cells argues against an oversampling of the densities of receptor subunits on ipRGC dendrites described above.

3.2.4 A8 amacrine cells provide synaptic input to M1 ipRGCs – a potential source of S-OFF signals?

Since M1 cells appear to receive a glycinergic input via GlyRα2, it was further investigated which amacrine cell may be a presynaptic partner of M1 cells. In macaque retina A8 amacrine cells, a type of bistratified small-field amacrine cell, are recognised by antibodies against the protein synaptotagmin-2 (Neumann & Haverkamp, 2013). They possess a dense dendritic plexus within S1 and a less dense plexus in S4 of the IPL. Their dendrites were highly decorated with GlyRα2 clusters (Neumann, 2010) making A8 amacrine cells a good candidate as presynaptic partner of M1 cells. To assess, if A8 amacrine cells are indeed presynaptically to M1 cells, retinal flat mount preparations were triple-immunolabelled with antibodies against synaptotagmin-2, melanopsin and GlyRα2 (Fig. 3.9). The dendrites of M1 cells were found in close contact with dendrites of the outer plexus of A8 dendrites. Furthermore, almost all

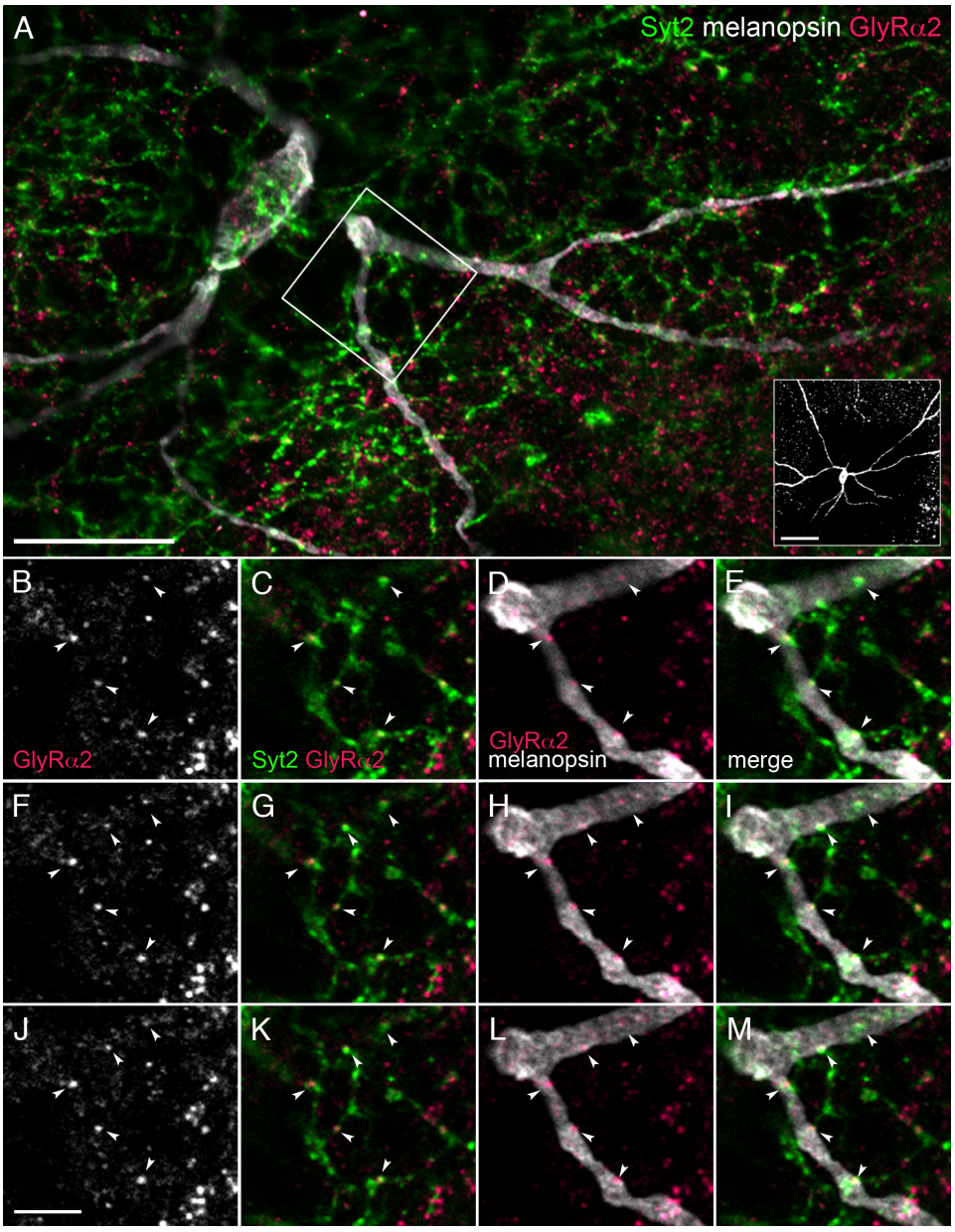

Figure 3.9: A8 amacrine cells provide input to M1 ipRGCs. Micrographs of a flat mounted macaque retina processed with antibodies against synaptotagmin-2 (Syt2), melanopsin and GlyRα2. The **inset in A** shows an overview of the M1 cell shown in A. The dendrites of A8 amacrines are decorated with GlyRα2 clusters. The majority of GlyRα2 clusters on M1 dendrites are apposed to A8 amacrine cell dendrites. The framed area in A is shown in higher magnification and three subsequent confocal planes in (**B – M**). The GlyRα2 staining is shown as monochrome image (**B, F and J**), as composit image with the Syt2 labelling (**C, G and K**) and the melanopsin staining (**D, H and L**). Merges of all three channels are shown in (**E, I and M**). Arrowheads point to GlyRα2 clusters on the M1 cell dendrite apposed to dendrites of A8 amacrine cells.
Scalebars: A: 20 µm, A_{inset}: 50 µm; J (applies to B – M): 5 µm. A and A_{inset}: Projection of 6 and 4 confocal planes, B – M: Single confocal planes.

synaptic GlyRα2 clusters located on the dendrites of M1 cells were also associated with dendrites of A8 cells. A representative photomicrograph is shown in Figure 3.9 A, the inset shows the M1 cell in low magnification to reveal the morphology. The framed area in A is shown in high resolution in three subsequent confocal planes in Figures 3.9 B – M displaying the GlyRα2 labelling alone (Fig. 3.9 B, F and J), in combination with the A8 plexus (Fig. 3.9 C, G and K), the M1 dendrite (Fig. 3.9 D, H and L) and as superposition of all three channels (Fig. 3.9 E, I and M). The arrowheads point to examples of GlyRα2 clusters located on the M1 dendrite. All these clusters were found in opposition to dendrites of A8 amacrine cells labelled by antibodies against synaptotagmin-2 (Fig. 3.9 C, G and K). In a few cases, GlyRα2 clusters on M1 dendrites not directly associated with A8 cells were observed (data not shown). These, however, appeared only in rare cases.

M1 cells in primate retina have been shown to respond to blue-OFF stimuli (Dacey *et al.*, 2005). Such a blue- or S-OFF response can be mediated via bistratified amacrine cells receiving excitatory blue-ON input from S-ON bipolar cells and invert this signal via an inhibitory synapse as shown in ground squirrel and rabbit retina (Fig. **??** D) (Chen & Li, 2012; Mills *et al.*, 2014; Sher & DeVries, 2012). In the following it was analysed if bistratified A8 amacrine cells may be postsynaptic to S-ON bipolar cells and transfer a blue-OFF signal via an inhibitory synapse to M1 cells. To study the connection of A8 amacrine cells with S-ON bipolar cells vertical sections of macaque retina were double-immunolabeled with antibodies against synaptotagmin-2 and cholecystokinin (CCK), a marker for S-ON bipolar cells (Fig. 3.10). The labelling pattern with antibodies against CCK in macaque retina is shown in Figure 3.10 A. Two S-ON bipolar cells, with characteristically long dendrites connecting to S-cones are seen. Figure 3.10 B shows a S-ON bipolar cell axon in higher magnification (arrows). No convincing contacts between S-ON bipolar cell axons and A8 amacrine dendrites were found. A terminal of an A8 dendrite close to but not in contact with the bipolar cells axon is marked with a box. Taken together, the data indicate that outer-stratifying M1 cells receive their glycinergic inhibition via glycine receptors containing the α2 subunit from A8 amacrine cells. But A8 amacrine cells are unlikely to serve as source for blue-OFF responses in M1 ipRGCs. Therefore it was investigated if synaptic input from OFF-bipolar

cells, particularly from FMBs might be the source of S-OFF signals in M1 ipRGCs. Furthermore it was analysed how frequently S-cones are contacted by FMBs.

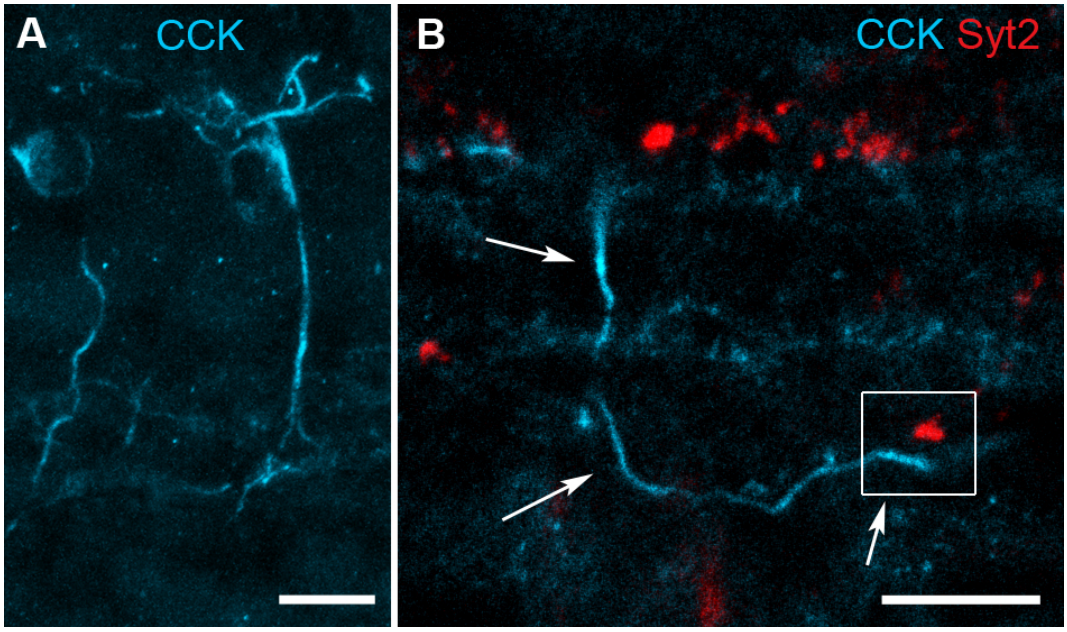

Figure 3.10: S-ON bipolar cells do not contact A8 amacrine cells in the macaque retina. Vertical section of macaque retina processed with antibodies against cholecystokinin (CCK) and synaptotagmin (Syt2). (**A**): Low power micrograph depicting CCK labelled S-ON bipolar cells. The somata are located at the outer border of the INL. Several dendrites emerge from the soma which make contacts putative S-cones. The axon submerge vertically into the inner part of the IPL. (**B**): High power micrograph of the IPL showing an CCK-labelled axon (arrows). No contacts between the axon and nearby located Syt2 labelled A8 dendrite in the ON-layer were found (framed region).
Scale bars: A and B: 10 µm. Projection of 30 (A) and of 3 (B) confocal planes.

3.3 S-cones feed into the OFF-pathway in the macaque retina

3.3.1 The OFF-bipolar cell markers recoverin and glutamate transporter-1 (GLT-1) in macaque retina

Antibodies against the protein recoverin (Rec) label the classical photoreceptors and FMBs in human and macaque retina (Milam *et al.*, 1993; Wässle *et al.*, 1994; Haverkamp *et al.*, 2003a). Fig. 3.11 A shows a collage of 6 individual fluorescence micrographs taken along a vertical section through the fovea of a macaque retina immunolabelled for Rec. Within the foveal pit inner retinal layers beneath the photoreceptors, INL, IPL and GCL of the retina are absent and emerge adjacent to the fovea. Second order neurons are connected to the terminals of the photoreceptors via the Henle fibers. Consistent with previous studies photoreceptors are vigorously labelled by antibodies against Rec and partially outshine structures in the OPL. In addition to photoreceptors a subpopulation of bipolar cells, the FMBs are labelled. The central area exhibits the highest density of FMBs across the retina (Wässle *et al.*, 1994). FMBs possess a single apical dendrite ascending vertically from the soma to the OPL. The dendrite ends in a characteristic bouquet of dendritic tips contacting a single cone pedicle in central, or multiple cones (up to 4 in the far periphery (Wässle *et al.*, 1994)) in the periphery. Due to the dense arrangement of cells around the fovea, FMBs appeared slightly oblique with their dendrites directed closer to the centre and their terminals located at more peripheral regions. Their somata were located in the middle of the INL, with axons descending into S1 of the IPL, where they end in varicose terminals (Fig. 3.11). In frequent cases small protrusions of the terminals towards inner layers of the IPL (S2) are seen (Fig. 3.11 B). The terminals of FMBs tile the area S1 of the IPL without gaps. However, in some preparations, the intensity of the staining of dendrites and terminals of FMBs (compare Fig. 3.11 B and G) was too low to analyse their connectivity to other cells in the OPL or IPL. If immunolabelled with Rec, dendrites of FMBs were in most cases weakly stained, with the tips concealed by the strong photoreceptor labelling. Antibodies against GLT1, in contrast, recognise multiple subpopulations of OFF-bipolar cells in the macaque and

human retina (Grünert *et al.*, 1994; Haverkamp *et al.*, 2003a). In macaque retina, GLT-1 labelled OFF-bipolar cells including FMBs, and diffuse bipolar cells type 1 (DB1) and 2 (DB2) (Grünert *et al.*, 1994; Puthussery *et al.*, 2011). Representative examples of the dendritic trees of all three bipolar cell types labelled by GLT-1 are shown in Figures 3.11 D – F.

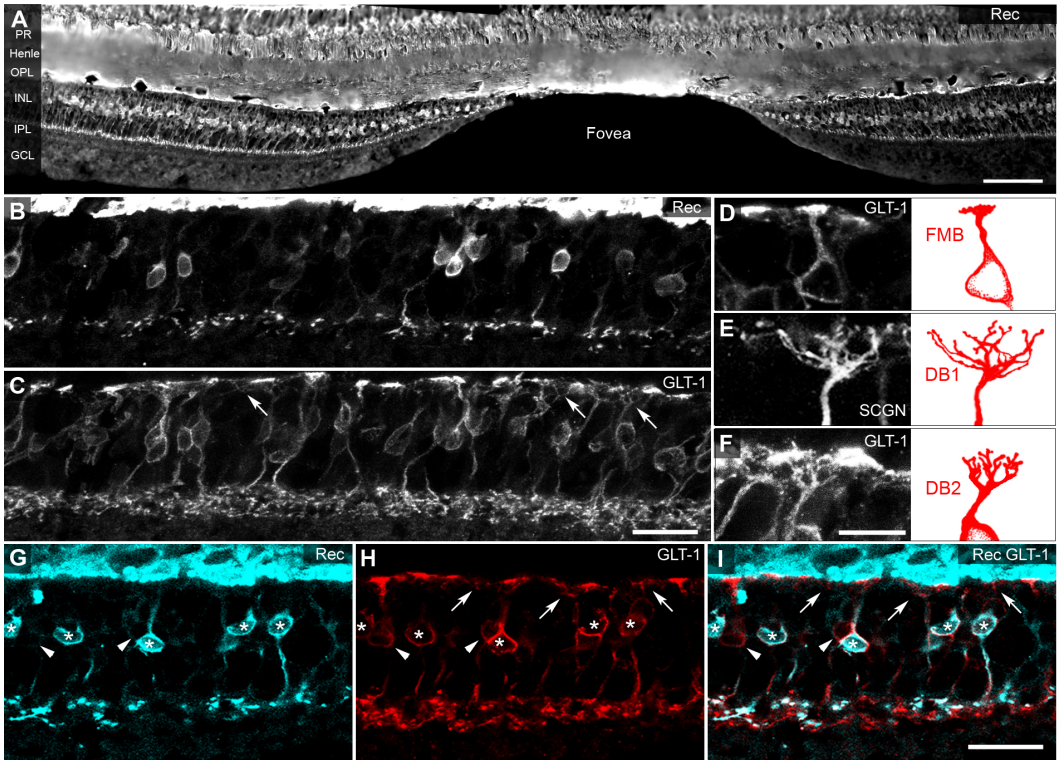

Figure 3.11: OFF-bipolar cell marker in macaque retina. (**A**): Collage of images of a sections through the fovea of macaque retina immunostained for recoverin (Rec). (**B and C**): Macaque retina double-immunolabelled for Rec and GLT-1 shown as single channels (B: Rec, C: GLT-1). (**D – F**): High resolution confocal images of dendritic terminals of the three types of OFF-bipolar cells immunoresponsive for GLT-1. Drawings of the representative dendritic terminals of each type are shown on the right side. The dendritic terminal from the DB1 cell (E) was taken from a section processed with antibodies against secretagogin (SCGN) instead of GLT-1 to improve the visibility of the DB1 dendrites. (**G – I**): Vertical section of macaque retina double-labelled for Rec and GLT-1. Asterisks mark cell bodies of Rec labelled FMBs, arrowheads point to cells immunoreactive to GLT-1 only. Cells labelled by Rec were also GLT-1 positive. Arrows point to dendritic terminals of GLT-1 labelled bipolar cells which do not end in plateau- or bouquet-like terminals.
Scale bars: A: 100 µm, C (applies also to B): 20 µm; F (applies to D – F): 10 µm; I (applies to G – I): 20 µm. A: Collage of fluorescence micrographs, B – D and F projections of 2 (D) and 3 (B and F) confocal planes, E and G – I single confocal planes.

The majority of the GLT-1 labelled cells was characterised by a single apical dendrite, ending in a plateau-like head of dendritic tips, which cannot be resolved in single tips using conventional fluorescent microscopy (Fig. 3.11 C, D and H – I). In some cases cells were found whose dendritic branches gave rise to more than one plateau-like structure (see also the cell reconstructed from a horizontal section in Fig. 3.13 D. These cells strongly resembled FMBs. In addition to these FMB-like cells, other OFF-bipolar cells with apical dendrites ending in more branched dendritic trees, which resembled DB1 and DB2 cells, were found to be GLT-1 immunoreactive (Fig. 3.11 G – I, arrowheads). These bipolar cells were in most cases weaker labelled than the FMB-like cells and the extent of their dendritic tips was often concealed by the dense plateau-like tips Fig. 3.11 C, F, H and I). The axon terminals of GLT-1 labelled cells were located in the OFF-sublamina of the IPL. However compared to the Rec staining the axon terminals occupied a broader layer in the IPL than the FMBs terminals labelled by Rec alone (Fig. 3.11 B, C, H and I).

To distinguish between different types of OFF-bipolar cells labelled by GLT-1, typical dendritic trees of OFF-bipolar cells were imaged in high magnification and reconstructed (Fig. 3.11 D – F). Since the dense labelling of the plateau-like structures often hampered the identification of other OFF-bipolar cells and concealed the extent of the dendritic trees, the tree of a DB1 cell was drawn from a section labelled for secretagogin (SCGN)(Fig. 3.11 E). The extent of the DB2 cells dendritic tree is likely to be underestimated because of the dense labelling of FMBs and the limits of the retina section. It is notable that DB1-like OFF-bipolar cells were found only in rare cases in GLT-1 labelled material. In summary, FMBs were most frequently labelled with GLT-1 and were readily distinguishable from the GLT-1 labelled DB1 and DB2 cells by the morphology of their dendritic trees.

To unambigously identify FMBs in the population of GLT-1 labelled bipolar cells, retinal sections were double labelled with Rec and GLT-1 (Fig. 3.11 B, C and G – I). GLT-1 immunoreactive bipolar cells with dendrites ending in plateau-like structures were co-labelled with Rec, proving that these cells are indeed FMBs and that the plateau-like dendritic endings correspond to the bouquet of dendritic tips of FMBs at a cone's pedicle (Fig. 3.11 G – I, asterisks). Cells with branched dendritic trees (DBs), in contrast, were not labelled by Rec

and belong to the group of diffuse bipolar cells (arrowheads). Most dendritic trees of the DB cells had a more sturdy appearance than the dendrites of DB1 cells (compare Fig. 3.11 F and E). This is in agreement with previous studies, which estimated that nearly one third of the GLT-1 immunoreactive bipolar cells in the macaque retina correspond to DB2 cells and the other two thirds correspond to FMBs, whereas DB1 cells are only faintly labelled (Grünert *et al.*, 1994; Puthussery *et al.*, 2011). The characteristic morphology of FMBs allows their identification in the population of GLT-1 labelled OFF-bipolar cells. Further, GLT-1 lacks the disadvantage of the strong labelling of photoreceptors as occurs in Rec labelling, qualifying GLT-1 as a suitable marker for the analysis of synaptic connections of FMBs within the OPL.

3.3.2 S-OFF midget bipolar cells

Many physiological and behavioural studies demonstrated the existence of blue-OFF signals in the retina and higher brain areas (reviewed by Dacey *et al.*, 2014). However, until now only one study reported FMBs that received synaptic input from S-cones using electron microscopy, restricting this study to small sample sizes. Therefore it was of major interest to investigate if FMBs are frequently connected to S-cones and if they are a possible source of S-OFF signals in primate retina and possibly for M1 ipRGCs.

S-cones contact FMBs

In order to analyse if FMBs connect to S-cones retinal sections were double-immunolabelled for Rec and S-opsin (Fig. 3.12). Photoreceptors were vigorously labelled by Rec. However, Rec did not label the whole FMB population within this preparation, indicated by the incomplete tiling of the IPL by the FMB terminals in S1. Furthermore, the intensity of the Rec immunoreactivity of individual FMBs varied massively from absent to very strong and saturated staining (Fig. 3.12 D). To enhance its visibility, the Rec staining of a retinal section is illustrated as monochrome photograph in Figure 3.12 D. The position of S-cones within the shown area is indicated by an overlay reconstructed from the S-opsin channel. Three S-cones were located within the area. Whereas no FMBs were labelled beneath the pedicles of the S-cone at the left, and at the

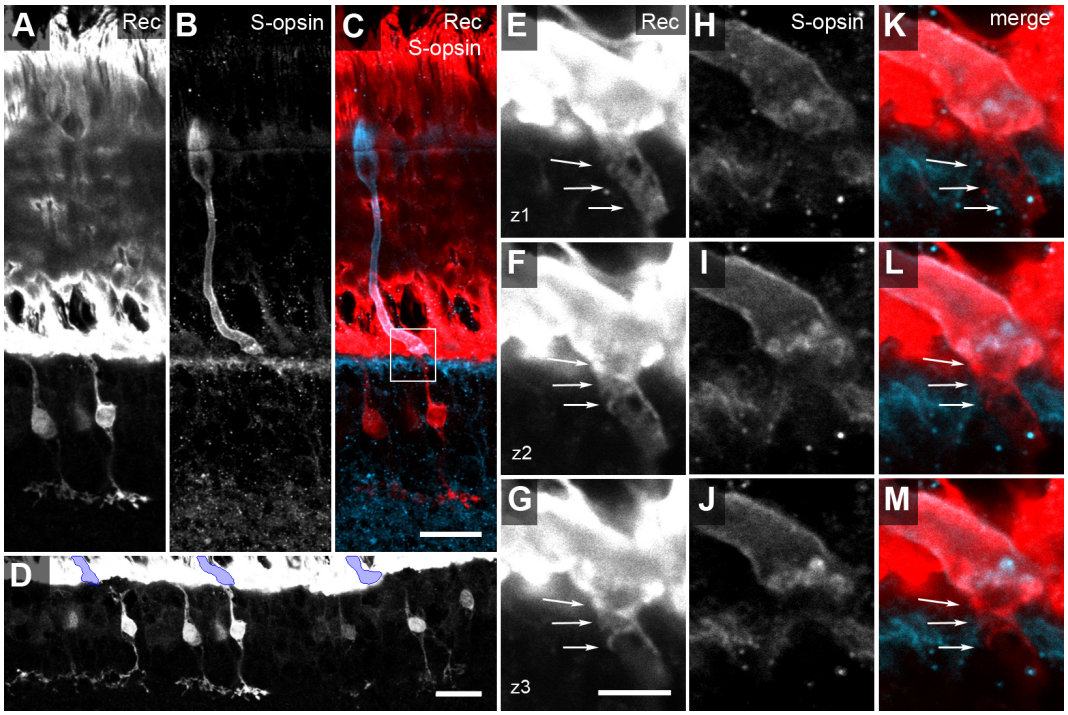

Figure 3.12: S-OFF midget bipolar cell.
(**A**–**C**): Vertical section of macaque retina processed with antibodies against recoverin (Rec) and S-opsin. The channel showing the Rec and the S-opsin labelling are shown as monochromatic images for better visibility in (**A**) and (**B**), respectively.The merge of both channels is shown in (**C**). A Rec labelled bipolar cell which contacts an S-opsin positive cone pedicle with its apical dendrite is shown. (**D**): Rec staining of the same section showing a larger area of the section. Schematic drawings of the S-cones are overlayed. (**E**–**M**): Enlarged images of the framed region in C showing the contact between the dendrite of the flat midget bipolar cell (arrows) and the S-cone pedicle in three consecutive confocal planes (z1–3). The Rec labelling is shown as monocrome images in (**E, F and G**), the S-opsin labelling in **(H, I and J**); the corresponding composit images of both channels are displayed (**K, L and M**).
Scale bars: C (applies to A–C) and D: 20 µm; G (applies to E–M): 5 µm. A–D: Projections of 5 confocal planes, E–M: single confocal planes.

right side, a strongly labelled FMB was located beneath the S-cone pedicle in the middle of the micrograph. This S-cone and the contacted FMB are shown in higher magnification as monochromatic images of each channel (A and B) as well as a composite picture of both channels (C). The framed area in Figure 3.12 C is shown in high resolution in three subsequent confocal planes (z1–z3) in Figures 3.12 E–M. It is notable that the contacted S-cone pedicle is

also seen in the Rec channel, since Rec labels photoreceptors, but the outline of the S-cone is depicted by the S-opsin labelling. The arrows in Figures 3.12 E – M point to the dendrite of the FMB, which contacts the S-cone pedicle. The incomplete staining of FMBs with Rec antibodies in this preparation (a more complete Rec labelling of the FMB population is shown in Fig. 3.11 A) rather than the lack of FMBs contacting S-cones might explain the absence of FMBs beneath the other S-cone pedicles. In summary, the data shown here confirm the finding from Klug and colleagues (2003) that at least some S-cones feed their signal onto FMBs. The unreliability of Rec labelling of FMBs in some tissues as well as the intense staining of photoreceptors, however, made it necessary to use GLT-1 as marker to further analyse if all S-cones or only some are contacted by OFF-bipolar cells particularly by FMBs.

3.3.3 S-cones provide synaptic input to the OFF-channel similar to M-/L-cones

The finding that S-cones are indeed frequently contacted by FMBs, raised the question if all S-cones transmit their signal into the OFF-bipolar channel via FMBs. Therefore, horizontal sections of macaque retinae were triple-immunolabelled against GLT-1, S-opsin and CtBP2 or with the lectin peanut agglutinin (PNA coupled to a fluorophore) to mark synaptic sites at cone pedicles (Fig. 3.13).

Horizontal sections labelled for S-opsin, GLT-1 and CtBP2

In the OPL of retinal horizontal sections, CtBP2 labelling was found as nest-like aggregations of multiple elongated synaptic ribbons within cone pedicles and as a horseshoe-shaped synaptic ribbon in each rod photoreceptor (Fig. 3.13 A). PNA in contrast, labels synaptic invaginations in cone pedicles only (Blanks & Johnson, 1984; Haverkamp *et al.*, 2001, see also introduction). Compared to M- and L-cone pedicles the area labelled by CtBP2 and PNA at S-cone pedicles was smaller, consistent with smaller sizes of S-cone pedicles. The more intense labelling at the S-cone pedicle observed in preparations labelled with PNA, was not observed in stainings with CtBP2. Hence, S- and M-/L-cones were readily distinguished by their size. However, to unambigu-

ously identify S-cones antibodies against S-opsin were applied (Fig. 3.13 A – C, blue circles). The GLT-1 labelling, corresponding to the dendritic plateau-like or bouquets of dendritic tips of OFF-bipolar cells was concentrated beneath the cone pedicles. Figures 3.13 D – F show a 3D-reconstruction of the GLT-1 labelled bipolar cell. The primary dendrite of the bipolar cell bifurcates to contact two cone pedicles identified by nest-like aggregated ribbons labelled by CtBP2 (Fig. 3.13 F). One of the cone pedicles was immunoreactive for S-opsin. The morphology of the reconstructed bipolar cell strongly resembled double-head FMBs occurring in mid-peripheral macaque retina sampling from two cones of different spectral sensitivities.

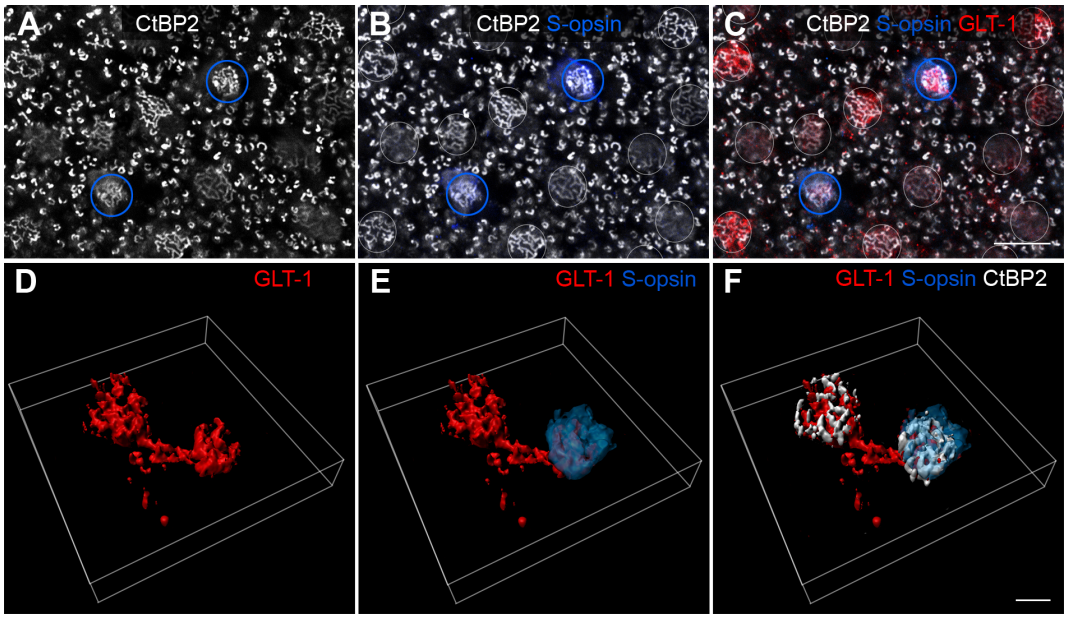

Figure 3.13: S-cones contact OFF-bipolar cells in macaque retina. (**A-C**): Horizontal sections of the macaque OPL immunolabelled against CtBP2, S-opsin and GLT-1. (**A**) shows the staining pattern of CtBP2 only, (**B**) combined with S-opsin and (**C**) as merge of all three channels. S-cones labelled by S-opsin are marked with blue circles. 3D-reconstructions of a GLT-1 labelled OFF-bipolar cell with two bouquet-like dendritic trees are shown in (**D – F**). (**D**): Reconstruction of the bipolar cell only. Reconstructed bipolar cell with the reconstructed S-opsin labelled S-cone pedicle (**E**) and with the reconstructed S-cone pedicle and the reconstructed CtBP2 labelled synaptic ribbons (**F**).
Scale bars: C (applies to A – C): 10 µm, F (applies to D – F): 3 µm. A – C: Single confocal planes.

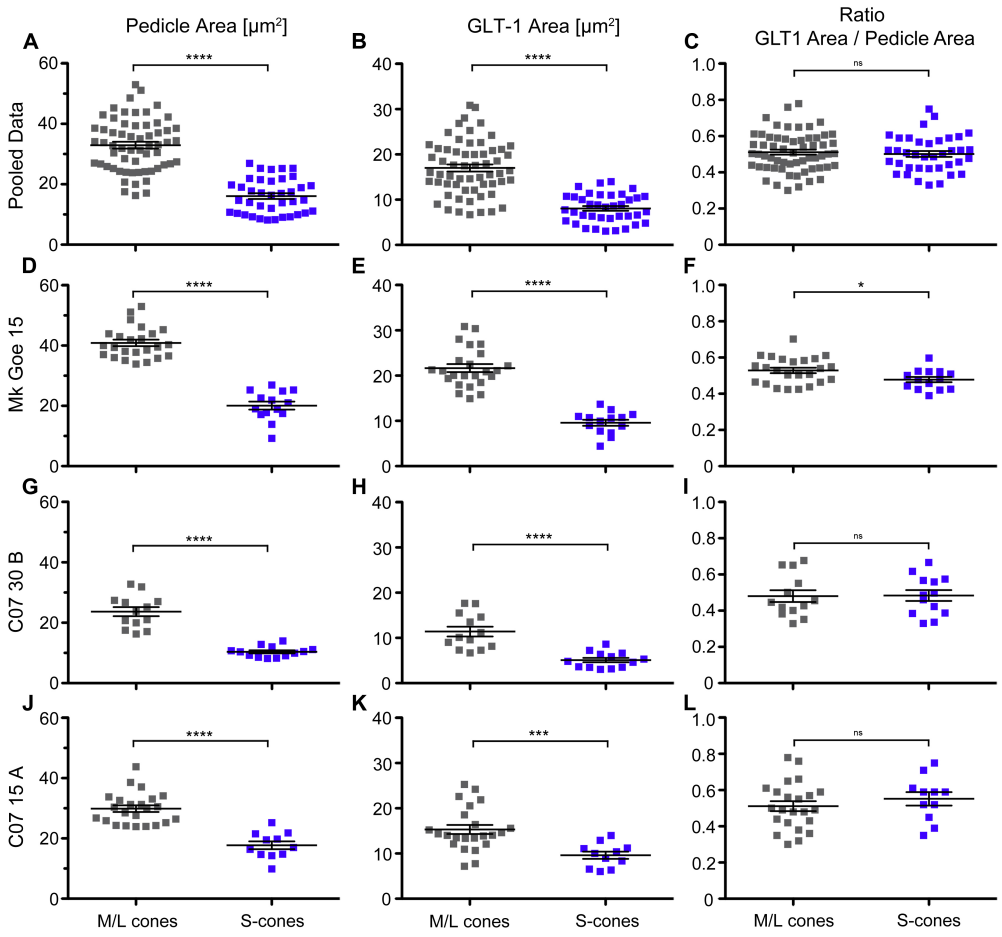

Figure 3.14: Quantification of contacts between OFF-bipolar cell and cone pedicles. Scatter plots comparing the pedicle size [µm^2], the area of the pedicles occupied by GLT-1 labelled OFF-bipolar cells [µm^2], and the ratio of the GLT-1 labelled area per cone pedicle are at M-/L- (grey symbols) and at S-cones (blue symbols). Each dot represents the value of a single cone pedicle (pooled data: M-/L-cones n = 60; S-cones: n = 38), lines show the arithmetic mean error bars the standard error of the mean (SEM). (**A** − **C**) show the pooled data of all tissue samples, (**D** − **F**): of the far peripheral sample, (**G** − **I**) of the sample collected at an eccentricity of 6-12 mm and (**J** − **L**) of 4 − 6 mm. The con pedicle area was measured by surrounding CtBP2 or PNA labelled synaptic ribbons at cone pedicles. In all of the three analysed tissues M-/L- cone pedicles occupied significantly larger areas than S-cones (D, G and J) Second column: In all samples, larger areas at L-/M-cone pedicles were occupied by GLT-1 labelled dendrites than at S-cone pedicles. The proportion of the pedicle area occupied by GLT1 dendrites, was similar for M/L and S-cones at all eccentricities. Only in the far peripheral sample a difference in this ratio M-/L-cones and S-cones was observed. The data shown here is also summarised in Table 3.3.Statistical analysis: One-way ANOVA with Tuckey-Kramer multiple comparison test (not significant (ns) $P > 0.05$, significant: (*) $P < 0.05$, (**) $P < 0.01$, (***) $P < 0.001$), (****) $P < 0.0001$).

Quantitative analysis of contacts between S-cones and OFF-bipolar cells

Preceding the quantification and the comparison of the amount of contacts to OFF-bipolar cells the **size of the pedicles** of M-/L-cones and S-cones was measured and marked as the area occupied by synaptic ribbons or invaginations. The cone pedicle area of S-cones (pooled data from all analysed tissues: $16.08 \pm 0.93\,\mu m^2$ (mean $\pm$ SEM); n = 38) was significantly smaller than the area of M- and L-cone pedicles in all tissues analysed (pooled data: $32.94 \pm 1.1\,\mu m^2$ (mean $\pm$ SEM); n = 60)) (values for each analysed tissue and the pooled values are displayed in Fig. 3.14, first column, and in Table 3.3). The size of each analysed S-cone pedicle in three tissue samples of different eccentricities is shown in the supplemental Figure A.1 within the Appendix).

The area of both, S-cone as well as M-/L-cone pedicles, were larger at higher eccentricities (Table 3.3). However, whereas the area of M-/L-cone pedicles were significantly different at all analysed eccentricities, the area of S-cone pedicles differed only slightly between the two tissue samples of higher eccentricities ($17.71 \pm 1.31\,\mu m^2$in far peripheral tissue and $20.10 \pm 1{,}7\,\mu m^2$ at 6 – 12 mm; compare Table 3.3, Fig. 3.14 and the supplemental Figs. A.1, A.2 and A.3). The data suggest that the size of the S-cone pedicles increases less steep than the size of M-/L-cones in far peripheral areas.

To assess the amount of OFF-bipolar cell contacts at M-/L- and S-cone pedicles the area labelled with GLT-1 at the marked cone pedicle areas were measured (see also chapter 2), since the staining pattern of GLT-1 did not allow the counting of single dendritic tips. Briefly, the area of the cone pedicle was marked and measured, afterwards the GLT-1 labelled area within this marked cone pedicle area was documented as binary pictures and measured.

In all analysed tissues significantly larger GLT-1 labelled areas (P value $< 0.0001 - 0.001$) were found at the base of M-/L-cone pedicles (pooled data: $17.01 \pm 0.78\,\mu m^2$ (mean $\pm$ SEM)) compared to S-cone pedicles (pooled data: $8.06 \pm 0.51\,\mu m^2$ (mean $\pm$ SEM)) (Fig. 3.14, second row and Table 3.3). However, at both, M-/L-cones and S-cones, about half of the pedicle area was occupied by GLT-1 labelled dendrites from OFF-bipolar cells (Table 3.3) indicating that all types of cones feed their signal into the OFF-pathway. Since most of the GLT-1 labelled cells are in fact FMBs (Grünert *et al.*, 1994, Fig. 4)

the data strongly suggest that S-cones feed their signal into the OFF-midget pathway.

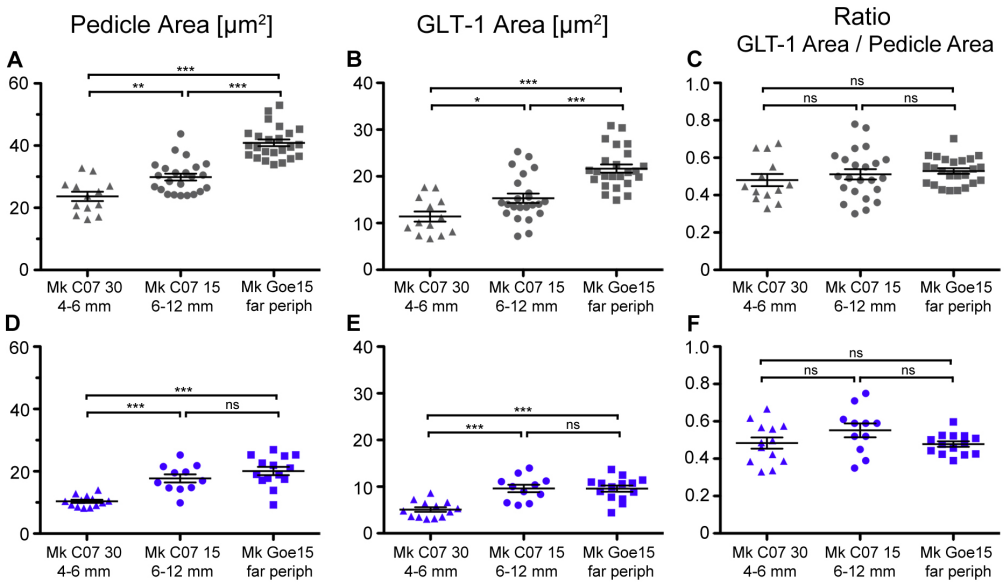

Figure 3.15: Quantification of contacts between OFF-bipolar cells and cone pedicles – Comparison at different excentricities. Scatter dot plots comparing the cone pedicle area, the area of the cone pedicles occupied by GLT-1 labelled bipolar cell dendrites and the ratio of the GLT-1 labelled area per cone pedicle in different tissue samples of different eccentricities for M-/L- (**A** – **C** and S-cones (**D** – **F**). For M-/L-cones the cone pedicle area and the area occupied by GLT-1 increased with eccentricity (**A, B**), whereas the ratio of the GLT-1 labelled area and the pedicle area remained stable (**C**). The area of S-cone pedicles and the area occupied by OFF-bipolar cells the increased from the most central tissue sample, but remained stable in the periphery (**D, E**). The ratio of the GLT-1 labelled area and the pedicle area was similar at all eccentricities (**F**).
Statistical analysis: One-way ANOVA with Tuckey-Kramer multiple comparison test (not significant (ns) $P > 0.05$, significant: (*) $P < 0.05$, (**) $P < 0.01$, (***) $P < 0.001$).

To further assess if the smaller area occupied by GLT-1 labelled dendrites beneath S-cone pedicles might be caused by the overall smaller size of S-cone pedicles, the area occupied by GLT-1 was normalised to the size of the cone pedicles as ratio of the GLT-1 labelled area per cone pedicle area (Fig. 3.14, third column). When normalised to the area size of the respective cone pedicle, no significant differences were detected in the proportion of the pedicle area occupied by GLT-1 between S- and M-/L-cones (ratio: $0.50 \pm 0{,}02$ (S-cones); 0.51 ± 0.01 (M-/L-cones) (mean $\pm$ SEM), see Table 3.3 and Fig. 3.14) in the

data pooled from all tissue samples.

Only in the far peripheral tissue sample (Mk Goe 15, Fig. 3.14 F) a small difference between the ratio of GLT-1 area at M-/L-cones and S-cones pedicles was observed (ratio GLT-1 per M-/L-cones: 0.53 ± 0.01, GLT-1 per S-cone: 0.48 ± 0.01; difference: 0.05 ± 0.02 (mean $\pm$ SEM); $P = 0.0331$). In neither of the other analysed tissues nor when data of all tissues were pooled a statistical significant difference was detected in the ratio of the area occupied by GLT-1 beneath M-/L-cones and S-cones (difference between the ratio of GLT-1 labelling per M-/L- and S-cones: tissue sample: Mk C07 15 (eccentricity $6-12$ mm): 0.04 ± 0.04; tissue sample: Mk C07 30 (eccentricity $4-6$ mm): 0.003 ± 0.044; pooled data: 0.01 ± 0.02 (mean $\pm$ SEM)) see also Fig. 3.14 C, F, I and L, and Table 3.3).

According to the change of the pedicle sizes at the different eccentricities, the size of the area occupied by GLT-1 at the cone pedicle also changed. The GLT-1 labelled area at M-/L-cones increased at larger eccentricities. The increase of the GLT-1 labelled area at the S-cone pedicles stagnated at higher eccentricities mirroring the stagnation of the increase of the S-cone pedicle size (Fig. 3.15 B and E). Hence, the ratio of the GLT-1 labelled area at cone pedicles remained stable at all analysed eccentricities for both S- and M/L-cone pedicles (Fig. 3.15 C and F).

Shift controls

In order to ensure that the GLT-1 labelled area beneath the cone pedicles represents selective staining of OFF-bipolar cell dendrites rather than unselective background-staining shift controls were performed at random samples (Fig. 3.16). Briefly the area of the cone pedicles were marked and measured, but the marking was shifted into the area between cone pedicles, where no labelling of OFF-cone bipolar cell dendrites would be expected.

Thereafter, the area labelled with GLT-1 within the marking was measured and compared to the values observed when the marking was not shifted. To confirm that the shift controls were compared to the coresponding observed values, the cone pedicles sizes between the observed and shifted data were compared (Fig. 3.16 A and D). No differences in the pedicle area in the analysis (observed data) and the shift control occurred, confirming that the GLT-1

area was measured at the same marking. The GLT-1 labelling was significantly reduced in areas between the cone pedicles for both M-/L- and S-cones. Accordingly, the ratio of the GLT-1 area at the marking area/cone pedicle area was also reduced. Samples with high background staining of GLT-1 where such a difference was not found were excluded from the analysis.

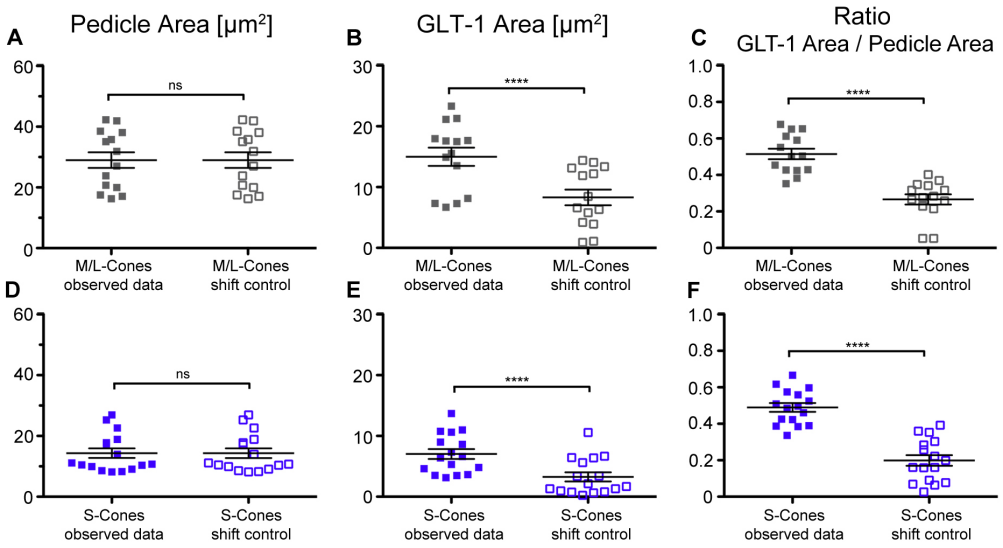

Figure 3.16: Quantification of contacts between OFF-bipolar cells and cone pedicles – Shift controls. Scatter plots comparing the cone pedicle area, the area of the cone pedicles occupied by GLT-1 labelled bipolar cell dendrites and the ratio of the GLT-1 labelled area per cone pedicle between the original observed data (full symbols) and the data when the analysed are was shifted between the cone pedicles (open symbols). Shift controls were carried out for L-/M- (**A** – **C**, n = 14) and S-cones (**D** – **F**; n = 16). Since the pedicle area was shifted the area size remained the same in the observed and shifted data (**A, D**). The area occupied by GLT-1 labelled OFF-bipolar cells was significantly reduced in when the analysed area was shifted between the cone pedicles (**B, E**), which was mirrored by a reduced ratio of the GLT-1 labelled area per cone pedicle in the shift controls (**C, F**). Statistical analysis: unpaired (A, D), and paired (B, C, E and F) two-tailed t-test (not significant (ns) $P > 0.05$, significant: (*) $P < 0.05$, (**) $P < 0.01$, (***) $P < 0.001$, (****) $P < 0.0001$)). Scatter symbols indicate values of individual cone pedicles, large line show the arithmetic mean of the group, errorbars the SEM. Please mind the different scaling of the Y-axes in the three columns.

In summary, it appears that the smaller area occupied by OFF-bipolar cell dendrites at S-cone pedicles compared to the area at M-/L-cone pedicles arises from the smaller size of the S-cone pedicles, rather than a lack of contacts

to OFF-bipolar cells. The similarity of the ratio of GLT-1 labelled area per cone pedicles for M-/L-cones and S-cones further supports the conclusion that both, M-/L- and S-cones feed their signal into the OFF-midget pathway. This similarity appears to be stable across retinal eccentricities. GLT-1 labels predominantly FMBs, indicating that most if not all S-cones are contacted by FMBs. Hence, FMBs contacting S-cones are likely candidates to provide S-OFF signals to outer-stratifying M1 ipRGCs.

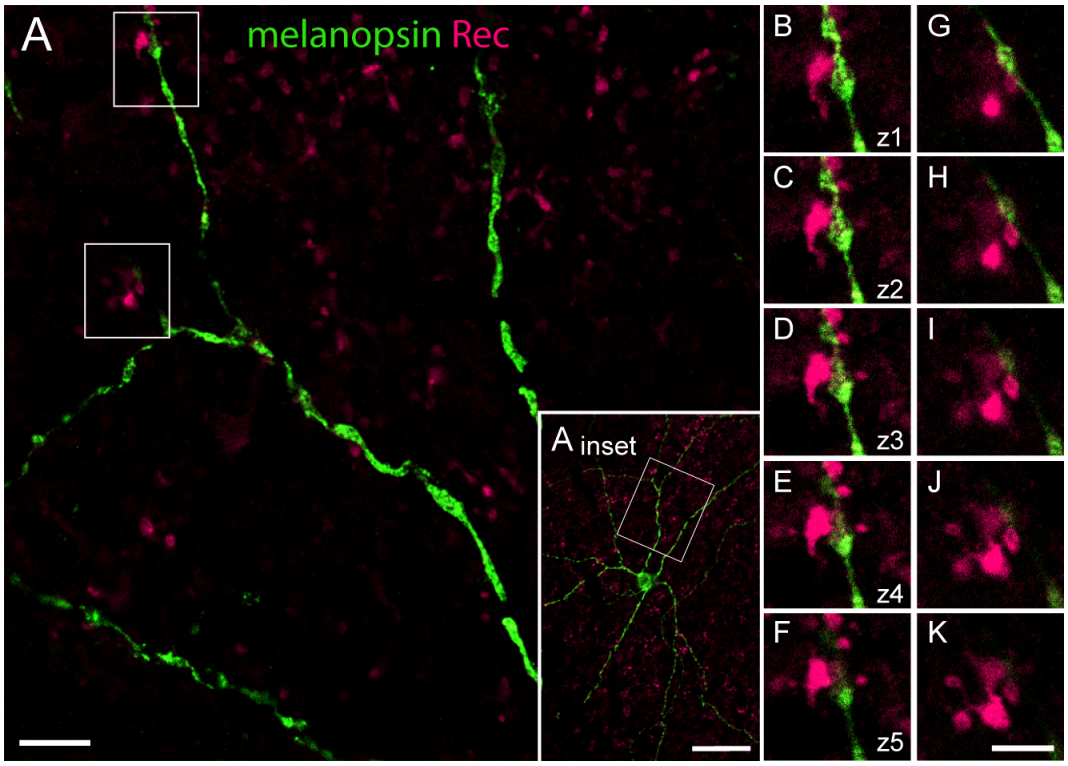

Figure 3.17: OFF-midget bipolar cells contact M1 ipRGCs. Horizontal sections of macaque retina double-immunolabelled for melanopsin and recoverin (Rec). ($\mathbf{A_{inset}}$) shows the morphology of an M1 ipRGC and the staining pattern of Rec. The framed is shown as summed projection of two confocal planes in higher magnification in (**A**). Two examples of contact sites between FMB terminals and M1 cell dendrites (framed area in (A)) are shown enlarged as 5 single confocal planes of an image stack (z1−5) in (**B**−**F**) and (**G**−**K**), respectively.
Scale bars: A: 10 µm; A_{inset}: 50 µm; K (applies to B−K) 5 µm.

3.3.4 FMBs provide synaptic input to M1 cells

A8 amacrine cells are likely to provide the majority of glycinergic input to M1 cells but do not convey an S-OFF signal (Figs. 3.9 and 3.10). Hence, S-OFF signals in M1 cells are likely to derive directly from OFF-bipolar cells which contact S-cones, for example S-OFF FMBs. Therefore, it was investigated if M1 cells receive synaptic input from FMBs. For this purpose retinal horizontal sections were double-immunolabelled for melanopsin and recoverin (Fig. 3.17). The ganglion cell dendrites contacted frequently terminals of FMBs, possibly at synaptic sites. However, it appeared that not all FMB terminals along the dendrites were contacted by M1 cells. To confirm this observation in better vertical resolution and to assess if the contact sites found in double-immunostained flat mount tissue are indeed synaptic sites, vertical sections of macaque retina were triple-immunolabelled for melanopsin, recoverin and CtBP2 (Fig. 3.18). It occurred that the M1 cell dendrites stratified closer to INL than the terminals of FMBs. In some cases, however, contacts between the dendrites of the ganglion cell and FMBs were found (Fig. 3.18 A). These contacts were confirmed as synaptic sites by the presence of CtBP2 labelled synaptic ribbons. Figures 3.18 B – M show a representative example of an FMB terminal providing three input synapses onto an M1 cell dendrite. The image is shown in three consecutive confocal planes (z1: B – E; z2: F – I and z3: J – M) to allow the tracking of the synapses through the depth of the retina section. To facilitate the visualisation a channel showing the CtBP2 staining is displayed as monochrome (B, F and J), combined with the melanopsin (C, G and K) or recoverin (D, H and L). Merge pictures of all three channels are displayed in (E, I and M). In conclusion, M1 ipRGCs appear to receive occasional bipolar cell input from some but not all FMBs. Hence M1 cells are likely to also receive blue-OFF signals from FMBs contacting S-cones.

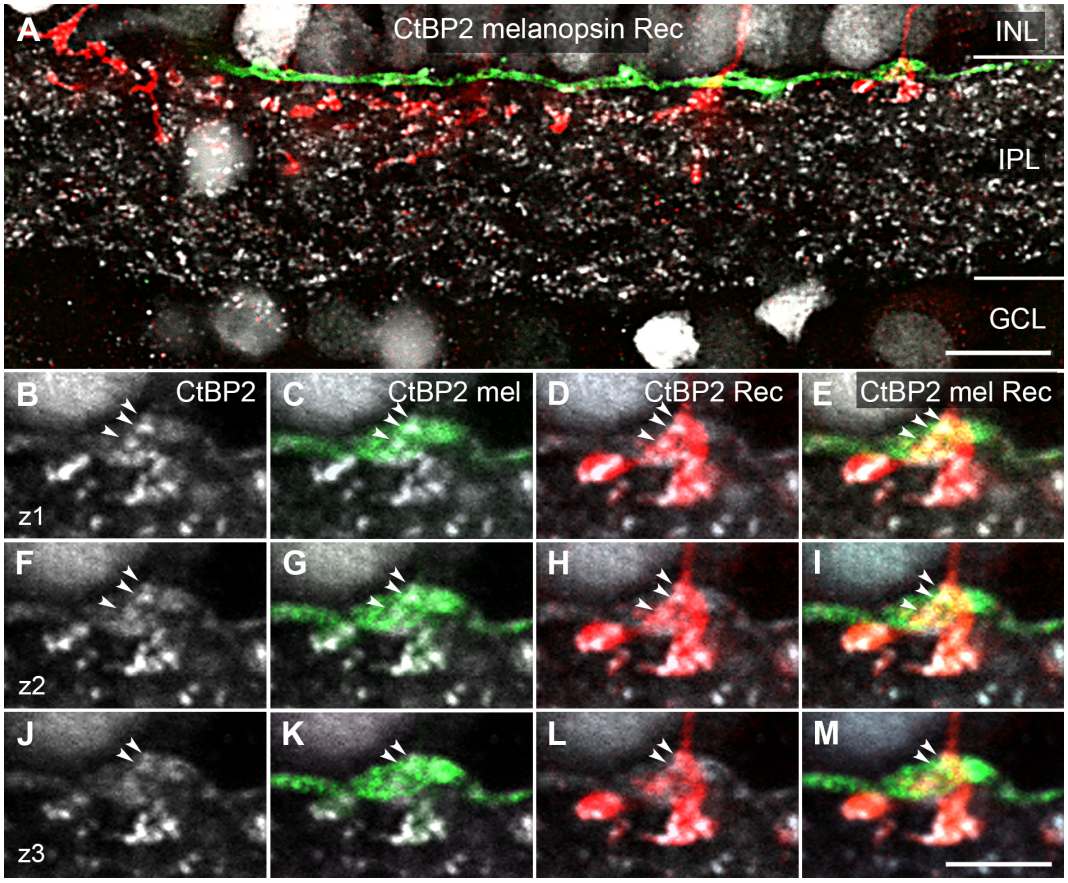

Figure 3.18: M1 ipRGCs receive occasional synaptic input from FMBs. Vertical section of macaque retina triple-immunolabelled against recoverin (Rec, red), melanopsin (mel, green) and CtBP2 (white). (**A**): Sum projection of 8 confocal planes. The M1 cell dendrite stratified at the outermost boarder of the IPL, slightly above the stratification depth of the FMB terminals. In some cases contacts between both cell types occured. One of these contact sites is shown in high resolution in three subsequent confocal planes (z1 – 3) in ((**B** – **E**), z1), ((**F** – **I**), z2) and ((**J** – **M**), z3). Arrowheads point to three synaptic ribbons of an FMB terminal apposed to the M1 dendrite. The CtBP2 labelling is displayed as monochrome image (**C, F, and J**), as composite image with the mel staining (**C, G, and K**), and the Rec staining (**D, H and L**) for better visibility. Merges of all three channels are shown in (**A, E, I and M**).
INL: inner nuclear layer; IPL: inner plexiform layer; GCL: ganglion cell layer. Scale bars: A: 10 µm; M (applies to B – M): 5 µm.

Table 3.3: Cone contacts to OFF bipolar cells.

Tissue	Eccentricity	Cone pedicle area [µm²] (mean ± SEM)				Cone pedicle area occupied by GLT-1⁺ dendrites [µm²] (mean ± SEM)				Ratio (GLT-1⁺ area / cone pedicle)				n	
		M/L-cones	S-cones	diff.	P-value	M/L-cones	S-cones	diff.	P-value	M/L-cones	S-cones	diff.	P-value	M/L-cones	S-cones
Mk Gö15	far periphery	40.90 ± 1.059	20.10 ± 1.315	20.80 ± 1.713	< 0.0001 (****)	21.67 ± 0.8941	9.590 ± 0.6679	12.08 ± 1.281	< 0.0001 (****)	0.5285 ± 0.01492	0.4783 ± 0.01488	0.05017 ± 0.02264	0.0331 (*)	24	14
Mk C07 15 A	6 - 12 mm from Fovea	29.90 ± 1.096	17.71 ± 1.1311	12.18 ± 1.829	< 0.0001 (****)	15.32 ± 1.010	9.621 ± 0.8013	5.695 ± 1.570	0.0010 (***)	0.5113 ± 0.02723	0.5518 ± 0.03709	0.04051 ± 0.04703	0.3954 (ns)	23	11
Mk C07 30 B	4 - 6 mm from Fovea	23.66 ± 1.505	10.36 ± 0.4924	13.29 ± 1.583	< 0.0001 (****)	11.40 ± 1.093	5.099 ± 0.4888	6.305 ± 1.197	< 0.0001 (****)	0.4806 ± 0.03272	0.4836 ± 0.03008	0.003204 ± 0.04445	0.9431 (ns)	13	13
Pooled Data	**4 - 12 mm**	**32.94 ± 1.119**	**16.08 ± 0.9323**	**16.87 ± 1.591**	**< 0.0001 (****)**	**17.01 ± 0.7773**	**8.063 ± 0.5079**	**8.946 ± 1.058**	**< 0.0001 (****)**	**0.5115 ± 0.01391**	**0.5013 ± 0.01626**	**0.01017 ± 0.02175**	**0.6411 (ns)**	**60**	**38**

Chapter 4

Discussion

4.1 Synaptic connectivity of ganglion cells in the mouse retina

4.1.1 OFF-ganglion cell types of the mouse retina: a comparison of functional and morphological types

Many distinct ganglion cell types were described in the mouse retina, as well as in retinae of other vertebrate species (e.g. turtle, ox, rabbit, cat, dog and wolf, monkey, or human) (Ramón y Cajal, 1892; Kolb *et al.*, 1981, 1992; Peichl, 1992; Ammermüller & Kolb, 1995; Rockhill *et al.*, 2002; Dacey *et al.*, 2003). In some cases it was possible to directly link a certain morphological cell type to a functional type, for example the ON/OFF-DSGCs and local edge detectors in rabbit and mouse retina or OFF-DSGCs in mice (Levick, 1967; Amthor *et al.*, 1984; Kim *et al.*, 2008; Huberman *et al.*, 2009; Zhang *et al.*, 2012). In other cases, however, a clear functional identification, based on morphological cues, is more subtle. Good examples for this case are provided by $A_{OFF\text{-}S}$ and $A_{OFF\text{-}T}$ ganglion cells. The dendritic trees of both cell types appear morphologically very similar, but ramify in slightly different strata of the OFF-layer and display sustained or transient responses to proper stimulation, respectively (van Wyk *et al.*, 2009). For other ganglion cell types such a matching of the functional and morphological cell type is not possible yet, e.g. because the physiology of a cell is not yet described, or the morphology of a functionally described cell

is not yet known.

Table 4.1: Cell types.

Ganglion Cells in this study	Small & Complex	Medium - Large & Sparse	Bistratified GCs	Asymetrical monostratified GCs
Physiological Type		$A_{OFF\text{-}S}$ (van Wyk *et al.*, 2009)	ON/OFF-DSGC (Huberman *et al.*, 2009)	OFF-DSGC (Kim *et al.*, 2008)
Sun *et al.* 2002	B1	$C2_{outer}$ $B3_{outer}$ (large version)	D2	C6
Badea & Nathans 2004	Cluster 3	Cluster 7	bi1/2	Cluster 6
Kong *et al.* 2005	3	10 (large 6)		Cluster 6 cell in Fig. 17
Coombs *et al.* 2006	$M3_{OFF}$	M9	M12 / M13	M5a
Völgyi *et al.* 2009	G4, G14 or G7	G11	G16 / G17	G15
Hong *et al.* 2011	X2	X3	X11	X1
Farrow *et al.* 2013	PV6		PV0	PV7
Bleckert *et al.* 2014		$A_{OFF\text{-}S}$		

The first question addressed within this dissertation was wether the glutamatergic input onto different ganglion cell types in S1 of the IPL is dominated by a single bipolar cell type, or if these ganglion cells sample their input non-selectively from all bipolar cell types stratifying in the area of their dendritic tree. Both cases would influence the function of the respective ganglion cell, since the bipolar cell types differ in their connectivity to cones and their kinetic response properties (reviewed by Euler *et al.*, 2014).

A lot of effort was invested in the past to classify ganglion cells in the mouse retina (Sun *et al.*, 2002; Kong *et al.*, 2005; Coombs *et al.*, 2006; Hong *et al.*, 2011), which is a model system of growing importance in retinal research. Nevertheless, the morphological classification of the ganglion cell types found in S1 of GFP-O retinae and the identification of their potential functional counterparts was rather challenging. Three groups of monostratified ganglion cells, which differed significantly in the size of their dendritic trees (small, medium and large), were found. However, most of the medium and large ganglion cells possessed rather sparse dendritic arborisations, whereas most

small cells displayed more complex arborisations. Therefore the cells were newly grouped into a group of "complex" type ganglion cells, comprising mainly of cells with small dendritic trees, and a group of "sparse" type ganglion cells, consisting mainly of ganglion cells with medium to large dendritic trees.

The complex-type ganglion cells likely correspond to B1 ganglion cells, whereas the sparse cells are likely correlates of $C2_{OFF}$ or A_{OFF} cells described by Sun *et al.* (2002). This classification of the monostratified cells is further supported by recent evidence, showing that $A_{OFF\text{-}S}$ ganglion cells (van Wyk *et al.*, 2009) change in size in a nasal-temporal gradient, indicating that the medium sized sparse ganglion cells correspond to the temporal $A_{OFF\text{-}S}$ and the large sparse to nasal $A_{OFF\text{-}S}$ ganglion cells (Bleckert *et al.*, 2014). Bleckert and colleagues suggested, that previously described ganglion cells (Sun *et al.*, 2002; Badea & Nathans, 2004; Coombs *et al.*, 2006; Völgyi *et al.*, 2009; Farrow *et al.*, 2013) might have been misclassified as own cell type, but are rather small or large A_{ON} or A_{OFF} ganglion cells sampled from the temporal (small cells) or nasal (large cells) retina, respectively. However, the size difference in the dendritic field size of A_{ON} cells appeared as a product of up and down scaling of the dendritic lengths not affecting the number of dendritic segments. If applied to the here analysed monostratified ganglion cells, the data of Bleckert and colleagues is congruent with the classification in two types of ganglion cells. The smaller complex ganglion cells and the medium to large sparse type ganglion cells corresponding to $A_{OFF\text{-}S}$ cells. Indeed the number of dendritic tips shown by Bleckert *et al.* (2014) appears similar to the number of dendritic tips observed at sparse ganglion cells analysed herein.

The smaller complex cells, by contrast, possessed higher numbers of dendritic tips, indicating that these cells belong to another cell type, rather than being temporal A-type ganglion cells. This conclusion was further supported by recent observations in the laboratory, where a large A-type cell was found in direct proximity of a smaller cell with a more complex dendritic tree in a retina flat mount labelled with antibodies against the neurofilament SMI-32. These antibodies selectively label $A_{OFF\text{-}T}$ and $A_{ON\text{-}S}$ ganglion cells (Lin *et al.*, 2004; Coombs *et al.*, 2006; Huberman *et al.*, 2008; Bleckert *et al.*, 2014). The large cell, but not the smaller one, colocalised with the marker SMI indicating that the large cell is indeed an A-type cell, whereas the smaller complex cell belongs

to another type (personal communication, Laura Hüser, Max-Planck-Institute for Brain Research, Frankfurt a. M.).

In summary, the **monostratified** ganglion cell types appear to belong to **two distinct ganglion cell types** determined by the complexity rather than three types as determined by the size of their dendritic trees. The sparse cells most likely correspond to $A_{OFF\text{-}S}$ ganglion cells, whereas the smaller complex cells most likely correspond to B-type ganglion cells (see Table 4.1). A-type ganglion cells in other species have been considered to be homologues to parasol ganglion cells in primate retina, whereas the smaller B-type cells were regarded as homologues to the primate midget ganglion cells, making them interesting research objects for comparative studies of their connectivities.

The analysed **bistratified** ganglion cells found in GFP-O mice had a similar morphology as D2 cells in Sun *et al.* (2002) and likely corresponded to the functional type of ON/OFF-DSGCs (Huberman *et al.*, 2009; Rivlin-Etzion *et al.*, 2011). Furthermore, another direction-selective cell type, the asymmetric monostratified ganglion cells in retinae of **Jam-B** mice, which correspond to C6 ganglion cells in the catalogue of Sun *et al.* (2002) and respond to upward motion (Kim *et al.*, 2008), were included in the analysis. Cells of other studies in the mouse retina, which might correlate to the cells analysed during this thesis, are summarised in Table 4.1. It is noteworthy, that in some cases the branching depth of the ganglion cell types or clusters could not be unambiguously matched to the cells described here. However, it must be taken into account, that most of the studies classifying ganglion cells were performed without markers of the IPL depth, hence the branching depth must rely on an estimate of the IPL thickness, which may be the source of this discrepancy. For the cells described herein the bipolar cell marker used was a reliable marker for S1 of the IPL. Further studies combining physiological and anatomical approaches similar to the study of van Wyk *et al.* (2009) could help to reliably determine different cell types and further studies will be necessary to investigate topographical changes of ganglion cells within the mouse retina.

4.1.2 Mixed bipolar cell input onto OFF-ganglion cells

In the vertebrate retina light signals from photoreceptors are relayed to ganglion cells via bipolar cells. Whereas in the mammalian retina rod photore-

ceptors connect to one bipolar cell type only, despite a few exceptions like type 4 cone bipolar cells, which also contact rods, cone signals segregate onto several parallel channels via about a dozen of distinct cone bipolar cell types (Haverkamp *et al.*, 2008; for a review see Masland, 2001a,b; Wässle, 2004; Wässle *et al.*, 2009a). These cone bipolar cell types differ in their morphology, expression of molecular markers and their physiological properties, which in turn strongly influence the responses of the postsynaptic ganglion cell type (reviewed by Euler *et al.*, 2014).

Probably the most striking example of how the responses of ganglion cells are shaped by their input from certain bipolar cell types is the segregation into ON- and OFF-channels in the IPL: Retinal ganglion cells stratifying in the inner layers of the IPL receive input from ON-bipolar cells and are responsive to light onset, whereas most ganglion cells stratifying in the outer layers of the IPL (S1 and S2) connect to OFF-bipolar cells and respond to the offset of light (Famiglietti & Kolb, 1976). However, the different types of ON- and OFF-bipolar cell types differ also in their physiological properties, such as temporal aspects or tuning to certain colours. Midget bipolar cells in the central primate retina, for instance, relay signals from a single cone onto a single midget ganglion cell, which in turn selectively responds to stimuli of the wavelength the connected cone is sensitive for (e.g. red or green depending on the expressed cone opsin; compare subsection 1.4.2, Fig. 1.5 A). Another way to implement colour opponency in ganglion cells was shown for small bistratified ganglion cells of the primate retina. These ganglion cells receive S-ON signals from S-ON bipolar cells selectively connected to S-cones and yellow-OFF signals through input from bipolar cells connected to L- and M-cones (Fig., 1.6 A) in addition to yellow OFF-surrounds in S-ON bipolar cells generated by H2 horizontal cells (reviewed by Dacey & Packer, 2003).

In the mouse retina only little is known about selective connections between bipolar cell types and ganglion cells. A sophisticated study demonstrated that type 6 bipolar cells provide the dominant input onto $A_{ON\text{-}S}$ cells (Schwartz *et al.*, 2012). Within the here presented work it was investigated if such a dominance or selectivity also occurs in different ganglion cell types within the OFF-layer of the IPL. Five types of OFF-bipolar cells (type 1, 2, 3a, 3b and 4) have been morphologically and physiologically described in the mouse

retina (Ghosh *et al.*, 2004; Mataruga *et al.*, 2007; Breuninger *et al.*, 2011; Baden *et al.*, 2013; Puller *et al.*, 2013). Type 3a and 3b bipolar cells stratify in S2, type 4 terminals branch more broadly in S1 and 2, whereas type 1 and 2 are more restricted to S1 (Fig. 1.2 A; Ghosh *et al.*, 2004). Type 1 bipolar cells in the dorsal retina avoid S-cones and are therefore green-OFF colour-selective bipolar cells. Hence, these cells are thought to be involved in pathways processing blue/green colour opponency. Type 2 bipolar cells in the dorsal retina also display a bias towards green signals, some however receive strong blue input, a phenomenon that is credited to their small dendritic tree, which only rarely samples from the scarce S-cones in that region (Breuninger *et al.*, 2011). Due to their small dendritic tree and axon terminal sizes, type 2 bipolar cells in the mouse were regarded as potential homologues to midget bipolar cells in the primate retina. This hypothesis would imply a selective connection between type 2 bipolar cells and their postsynaptic ganglion cells. Here, type 2 bipolar cells and synaptic ribbons were labelled using antibodies against synaptotagmin-2 and CtBP2 to identify output synapses of type 2 bipolar cells in transgenic mice expressing a fluorescent marker, which was enhanced with antibodies directed against GFP, in ganglion cells. The input from bipolar cells onto these ganglion cells was measured and the percentage of input deriving from type 2 bipolar cells was assessed.

It occurred that the **sparse ganglion cells**, which most likely correspond to $A_{OFF\text{-}S}$ or C2 ganglion cells, receive about 45% of their input from type 2 bipolar cells. The majority of the remaining 55% of bipolar cell input must therefore be provided by other bipolar cell types stratifying in S1 (type 1 and type 4). The same holds true for the **complex ganglion cells**, which received about 43% of their input from type 2 bipolar cells, which also argues for a non-selective connection between the ganglion cell type and multiple bipolar cell types. It cannot be ruled out that either the sparse or the complex cells receive the majority of their remaining input from only one of the candidate bipolar cells providing output in S1, type 1 or type 4 bipolar cells. In this case it would be an interesting question if these ganglion cells avoid the contact to certain bipolar cells within their dendritic field and how such a bias could be developmentally implemented.

However, it is noteworthy that no differences were found in the synaptic connectivity of type 2 bipolar cells, often regarded as midget bipolar cell equivalent (see above) with the complex B-type-like cells and sparse A-like ganglion cells, considered as homologues to midget and parasol ganglion cells in primate. Hence, the here presented results argue against a homology of type 2 bipolar and complex B-type ganglion cells in the mouse retina with the midget bipolar and ganglion cells in the primate retina. Whereas midget ganglion cells selectively connect to midget bipolar cells, the herein analysed complex B-type like ganglion cells sample non or at least less selectively from multiple types of bipolar cells within their dendritic field. However, it cannot be excluded that the midget system in primates might have evolved following topographical specialisation of the retina. Therefore further comparative studies of different species could help to shed light on the evolution of the connectivity neuronal pathways. An example for similar deviations in the connectivity of morphologically corresponding cell types in the mouse and primate is given by DB1 and type 1 bipolar cells. DB1 cells in the primate retina connect non-selectively to multiple cone types (Puthussery *et al.*, 2011)), whereas type 1 cells in the mouse retina sample from M-cones only and avoid contacts to S-cones within their dendritic field (Breuninger *et al.*, 2011). Hence, DB1 cells appear to convey luminosity signals, whereas type 1 cells convey M-cone (green) signals, which can be contrasted to S-cone (blue) signals used for dichromatic colour vision.

One might ask why such a large variety of physiologically different bipolar cell types exists, if their input converges on the same ganglion cell. However, it may allow ganglion cells to compute different aspects, e.g. temporal features of a light stimulus encoded by different bipolar cell types. Many studies investigated the physiology of different bipolar cell types in various species and demonstrated remarkable differences in their cone contacts, colour selectivity and temporal properties, at least in part, mediated by their expression of glutamate receptors (DeVries & Schwartz, 1999; DeVries, 2000; DeVries *et al.*, 2006; Breuninger *et al.*, 2011; Baden *et al.*, 2013; Puller *et al.*, 2013). A striking example of how the physiological properties of a target cell are shaped by the input from different types of bipolar cell is provided by the connectivity of type 2 and type 3a bipolar cells, and OFF-starburst amacrine cells. In this

example the direction-selectivity of the starburst amacrine cells dendrite relies on the different kinetics of the bipolar cells providing input at certain locations of the starburst amacrine cells dendrite (Kim *et al.*, 2014). Therefore ganglion cells could exhibit various complex responses through a computation of bipolar cell input with different properties. This influence on the ganglion cells response properties could also result from less selective contacts to bipolar cells, which are still tuned by a domination of the input from one type over lesser input from other bipolar cell types. A_{ON} ganglion cells, for instance, receive a dominant, but not a pure input from type 6 bipolar cells (Bleckert *et al.*, 2014).

Type 2 bipolar cell input to D2 and C6 cells – presumed ON/OFF- and OFF-DSGCs

Herein it was found that **OFF-DSGCs in Jam-B mice** (C6 ganglion cells) receive only a minority (about 20%) of their input from type 2 bipolar cells, whereas 80% must derive from type 1, type 4 or both bipolar cell types. Hence, these cells are candidates for a weighted bipolar cell input, dominated by one bipolar cell type. Until now it has not been tested if OFF-DSGCs show a strong preference to the offset of green stimuli, which would imply a bipolar cell input dominated by type 1 cells. However, the sense of colour selectivity added to the selective response to upward motion remains elusive. It appears more sensible to expect a major contribution of a bipolar cell type transmitting non-colour selective luminosity signals over a large range of the lights spectrum. Type 4 bipolar cells appear to be a good candidate to provide the majority of the bipolar cell input to OFF-DSGCs, since type 4 cells contact both cone types present in the mouse retina, as well as rod photoreceptors (Haverkamp *et al.*, 2008). The contacts to rod photoreceptors could extend the light sensitivity of the ganglion cell under dim environmental light conditions. The small bistratified ganglion cells, which likely correspond to the functional type of **classical ON/OFF-DSGCs**, also received a slightly smaller amount of their input from type 2 bipolar cells (about 35%). This smaller amount of input might be the result of structural properties of these ganglion cells. The main plexus of the dendritic trees of ON/OFF-DSGCs co-stratify with the dendrites of ON- and OFF-starburst amacrine

cells. Hence, a large part of the OFF-plexus is located slightly below the axon terminals of type 2 bipolar cells, and is likely to sample from bipolar cell types 3a, 3b and maybe type 4 as well. As for the OFF-DSGCs, a major input from bipolar cells conveying luminosity signals is conceivable. ON/OFF-DSGCs could receive non-selective input from all bipolar cell types in their dendritic field to sample the whole spectrum of a moving light stimulus. This hypothesis would also be in agreement with a recent study demonstrating non-direction selective glutamatergic input from bipolar cells onto ON/OFF-DSGCs (Park *et al.*, 2014), which may derive from multiple bipolar cell types.

4.2 Synaptic inhibition on intrinsically photosensitive ganglion cells[1]

4.2.1 Distribution of glycine and $GABA_A$ receptor subunits in the macaque retina

Responses of ganglion cell are massively filtered and modulated through inhibitory synaptic input from GABAergic and glycinergic amacrine cells (for a review see Wässle *et al.*, 2009b; Zhang & McCall, 2012). Melanopsin-expressing ganglion cells have also been described to be subject to such modulations. Physiologically, ipRGCs were shown to respond to GABA and glycine application and to exhibit responses (IPSCs inhibitory postsynaptic currents) to inhibitory synaptic input from amacrine cells (primate: Dacey *et al.*, 2005, rodent: Perez-Leon *et al.*, 2006; Viney *et al.*, 2007; Wong *et al.*, 2007). Further, anatomical studies demonstrated that ipRGCs are located postsynaptic to amacrine cells on the ultrastructural level and using light microscopy (Belenky *et al.*, 2003; Jusuf *et al.*, 2007; Viney *et al.*, 2007). However, these studies only generally touched certain aspects of the presence of inhibition on ipRGCs. The second part of the thesis aimed to further characterise the properties of

[1]Parts of the data and results discussed in the following section have been published as research article in the Neuroscience Journal titled: "Intrinsically Photosensitive Ganglion Cells of the Primate Retina express distinct Combinations of Inhibitory Neurotransmitter Receptors" (Neumann, Haverkamp & Auferkorte, (2011), Neuroscience 199:24-31).

the inhibition on M1 and M2 ipRGCs in the primate retina and to give new insights in the connectivity to amacrine cells.

For this purpose a wide screen for different subunits of $GABA_A$ and glycine receptors on the dendrites of both types of ipRGCs was conducted. These are pentameric ion-channel receptors, consisting of subunits involved in the clustering of the receptors at postsynaptic sites, and different α subunits, which influence their kinetic properties (Ivanova *et al.*, 2006; Weiss *et al.*, 2008; Wässle *et al.*, 2009b). In rodent retina, subunits of inhibitory neurotransmitter receptors are expressed in a laminar distribution (Greferath *et al.*, 1995; Grünert, 1999; Heinze *et al.*, 2007). Subunits of the respective glycine or $GABA_A$ receptors are accumulated in bands within different sublaminae of the IPL, strongly arguing for their involvement in specific retinal subcircuits. In primate retina such laminar distributions of these receptors subunits were less profound. Consistent with a previous study in primate retina (Jusuf *et al.*, 2005), GlyRα subunits were homogeneously distributed throughout the IPL, with the exception of GlyRα1, which was aggregated in two bands in the IPL. The same observation was made for two $GABA_A$ receptor subunits, α2 and α3, which were first described in the primate retina during this thesis (Fig. 3.5 D – F; see also Fig. 1 in Neumann *et al.*, 2011).

In contrast to $GABA_A\alpha$3, $GABA_A\alpha$1 and α2 were also found within the OPL, where photoreceptors connect to horizontal and bipolar cells (Fig. 3.5 A – C). Within the OPL $GABA_A\alpha$1 was clustered beneath the cone pedicles. A previous study suggested a role of $GABA_A\alpha$1 at this site in the S-cone circuitry of the primate retina (Puller *et al.*, 2014). The $GABA_A\alpha$2 expression within the OPL, in contrast, was more diffuse, and the reliability of the labelling in this neuropil needs to be proven in further studies. Also in the rat retina the specificity and role of the $GABA_A\alpha$2 remained dubious. Greferath and colleagues speculated that their antiserum might recognise a peptide on the cone pedicle, which is not related to the GABA receptor per se, since they did not encounter the respective mRNA in the OPL (Greferath *et al.*, 1995). However, the analysis of $GABA_A$ receptor clusters within the OPL was beyond the scope of this thesis, which was focused on the analysis of $GABA_A$ and glycine receptors on ipRGCs further discussed below.

The analysis of inhibitory neurotransmitter receptors on M1 and M2 cells has shown that each ipRGC type expressed particular combinations of receptor subunits. While M1 cells expressed mainly GlyRα2 and GABA$_A\alpha$3, for M2 cells only the density of GABA$_A\alpha$2 was elevated compared to the other subunits tested. The glycine receptors were close to absent on M2 cells. This is in accordance with a previous study in the rodent, which showed M2 cells to be postsynaptic to GABAergic amacrine cells by trans-synaptic tracing (Viney *et al.*, 2007). It needs to be mentioned that only the GlyRα2 and GABA$_A\alpha$3 densities on M1 cells were significantly different to densities found in the rotation controls (Neumann *et al.*, 2011, Fig. 3), indicating that these subunits are preferentially expressed by the cell.

One might argue against the expression of the other receptor subunits on M1 cells and for the complete absence of the analysed receptor types on M2 cells. However, it has to be emphasised that rotation controls are incapable to discriminate between the colocalisation of unrelated signals generated by chance following the signal rotation, e.g. high background staining, and valid colocalisations, which occur at low density. This disadvantage is enhanced if one of the analysed signals, in this case the receptor staining, is found in broad areas compared to the other signal (here the melanopsin staining). Therefore rotation controls may only serve as estimation if a certain subunit is expressed preferentially, like GlyRα2 and GABA$_A\alpha$3 in M1 cells, but cannot be used to exclude the existence of receptors expressed at lower densities. This is especially of importance for M2 cells, which had only low receptor densities compared to M1 cells and where no differences to the densities in the controls were detected. Since these cells were described to be postsynaptic to wide-field amacrine cells (Viney *et al.*, 2007), it seems unlikely that these cells express none of the investigated receptor subtypes. A direct comparison of the density of the receptor subtypes among each other appears to be more sensible in this case (Fig. 3.8). This analysis argues for the expression of GlyRα2, α3 and GABA$_A\alpha$3 on M1 and GABA$_A\alpha$2 and possibly GABA$_A\alpha$3 on M2 cells.

It should be noted here that the densities of GlyRs and GABA$_A$ receptors on ipRGCs exceeded the densities of receptors and synaptic markers on ganglion cells published in earlier studies of the primate retina by far (Lin *et al.*,

2000; Jusuf *et al.*, 2005)[2]. In a control experiment the linear density of the clustering protein was analysed and a linear density of 40 ± 4 gephyrin clusters per 100 µm (mean ± SEM) dendrites was observed on M1 cells (data not shown). A value, which is in accordance with other more recent studies on the density of synapses on retinal ganglion cells (primate: Abbott *et al.*, 2012, mouse: Bleckert *et al.*, 2013), which reported $40-49$ clusters of $GABA_A\gamma2$ receptors in transgenic mice, and $34-43$ gephyrin clusters on various ganglion cell types. Nevertheless, it is struggling that the sum of the densities of different receptor subtypes (e.g. $GABA_A\alpha2$, $GABA_A\alpha3$ and GlyR$\alpha2$) exceeded the density of gephyrin clusters on ipRGCs, which are supposed to be located at most inhibitory synapses. Previous studies in mouse and primate, however, found that a certain percentage of inhibitory receptors are not colocalised with gephyrin (4.2; but see also *mouse:* Haverkamp *et al.*, 2004, *primate:* Abbott *et al.*, 2012). It might be possible that not all splice variants of gephyrin are recognised by the antibodies against gephyrin, since no glycine and only minor GABA receptor staining was observed in gephyrin knock-out mice, indicating that gephyrin is responsible for the clustering of all glycine and some GABA receptors (Fischer *et al.*, 2000).

Furthermore, some GlyRα subunits were shown to colocalise to a certain percentage with other GlyRα subunits (see also section 1.3) (Haverkamp *et al.*, 2004; Jusuf *et al.*, 2007; Heinze *et al.*, 2007). Therefore it appears reasonable to find a lower density of gephyrin than expected from the total sum of all analysed receptor subunits.

The remaining discrepancy of the low densities of receptors found on ganglion cells might be explained by methodological differences. In the early studies conventional fluorescence microscopy instead of confocal microscopy was used for the analysis (Lin *et al.*, 2000; Jusuf *et al.*, 2005). This blur of stray light in the conventional fluorescence microscopy, which is significantly reduced in confocal mircroscopy, might have hampered the detection of small and less intense immunofluorescent clusters on the dendrites of cells.

[2] (9 clusters of GlyRα1; 11 clusters of GlyRs(all) and 16 clusters of gephyrin per 100 µm on parasol ganglion cells and 9 gephyrin clusters per 100 µm on M1 and M2 cells)

Table 4.2: Colocalisation of subunits of $GABA_A$, GlyRs and gephyrin.

Subunits	Colocalisation [%] [mean ± S.D.]	Species	Source
GlyRα1 / GlyRα2	8.6 ± 2.4	marmoset	(Jusuf *et al.*, 2005)
GlyRα1 / GlyRα3	6.2 ± 3.5		
GlyRα2 / GlyRα3	24.3 ± 4.7		
GlyRα1 / GlyRα3	21.5 ± 3.4	mouse	(Haverkamp *et al.*, 2003b)
GlyRα3 / $GlyR_{(all)}$	65.1 ± 4.2		
GlyRα3 / gephyrin	53.9 ± 0.9		
GlyRα2 / gephyrin	46.7 ± 4.4	mouse	(Haverkamp *et al.*, 2004)
GlyRα1 / GlyRα2	9 ± 3.1		
GlyRα2 / GlyRα3	26.7 ± 3.6		
GlyRα2 / GlyRα4	31.5	mouse	(Heinze *et al.*, 2007) reviewed by Wässle *et al.* (2009a)
GlyRα3 / GlyRα4	no sign. coinc		
gephyrin / $GABA_A\gamma$2	about 40 (threshold 0.5 µm)	primate	(Abbott *et al.*, 2012)
gephyrin / $GABA_A\alpha$2	about 40 (threshold 0.5 µm)		

4.2.2 Glycinergic input onto M1 ipRGCs: A8 amacrine cells as presynaptic partner

M1 cells were shown to express preferentially GlyRα2 and possibly GlyRα3. Dendrites of small-bistratified amacrine cells (A8) were located at the majority of synaptic GlyRα2 clusters on M1 cells, indicating that A8 cells provide most of the glycinergic input onto M1 cells in the macaque retina. A possible input via GlyRα3 from A8 cells was not analysed for technical reasons: Immunolabelling of A8 amacrine cells in the macaque retina with antibodies against synaptotagmin-2 required longer fixation times than can be used for reliable GlyRα3 stainings (Neumann, 2010). Additionally, in mouse retina GlyRα2 cluster have been shown to be, at least in part (26%), colocalised with GlyRα3 (Haverkamp *et al.*, 2004), indicating that at least some of the receptors found on M1 cells might correspond to clusters of both GlyRα2 and α3 on the same postsynaptic site.

S-OFF signals were shown to arise from amacrine cells, which invert the signals deriving from S-ON bipolar cells to S-OFF signal via inhibitory synapses in ground squirrel and rabbit retina (Chen & Li, 2012; Sher & DeVries, 2012; Mills *et al.*, 2014). Hence, bistratified A8 amacrine cells could possibly confer a blue-OFF signal to M1, if these amacrine cells receive synaptic input from S-ON bipolar cells. To test this hypothesis, it was analysed if A8 amacrine cells were contacted by terminals of S-ON bipolar cells. No evidence of synaptic contacts between S-ON bipolar cell axons and A8 amacrines was found in the ON-layer of the IPL. Still, synaptic *en passent* input from S-ON bipolar cells onto the dense OFF-plexus of A8 remains conceivable. However, A8 cells receive synaptic input from ON- and OFF-bipolar cells (Neumann & Haverkamp, 2013), which receive most of their input from L- or M- cones. The input from L- and M-cones would likely conceal such a hypothetical input from S-ON bipolar cells.

In summary, the glycinergic input from A8 amacrine cells onto M1 cells is presumably involved in other modulations of M1 cells rather than the transmission of colour signals. In contrast, OFF-bipolar cells could directly transfer S-OFF signals to outer-stratifying ipRGCs. Such a pathway and evidence for it will be discussed in the following paragraph.

4.3 S-cones connect to the OFF-midget system in old-world monkey retina

The midget pathway is well described for M- and L-cones in primate retina. In central retina L- and M- cones are connected to a single OFF- and a single ON-midget bipolar cell (Kolb, 1970), which in turn feed the cone´s signal to an OFF- and ON-midget ganglion cell (Kolb & Dekorver, 1991; Calkins *et al.*, 1994). Via this one-to-one connection the midget system conveys red/green colour and high acuity vision to higher brain areas (reviewed by Martin, 1998; Calkins, 2001). However, if S-cones also feed their signals onto midget bipolar cells is more controversial. S-cones are not connected to the invaginating ON-midget bipolar cells (subsection: 1.4.2, Fig.:1.5 B; Kouyama & Marshak, 1992; Wässle *et al.*, 1994; Kolb *et al.*, 1997; Herr *et al.*, 2003). Most of their invaginations are occupied by S-ON bipolar cells, which are selectively con-

nected to S-cone pedicles and avoid contacts to L- and M-cone pedicles within their dendritic field (Mariani, 1984; Marshak *et al.*, 1990). Also, physiological data demonstrates that ON-midget ganglion cells receive only minor input deriving from S-cones (Field *et al.*, 2010). Furthermore, diffuse ON-bipolar cells, namely DB4 and DB6 cells, appear to connect preferentially to M-and L-cones, avoid contacts to S-cones and mediate yellow ON-signals (Lee *et al.*, 2004; Lee & Grünert, 2007), supporting that S-ON signals are transferred by dedicated S-ON bipolar cells.

How S-cones signals are transferred into the retinal OFF-pathways, especially the OFF-midget pathway, is less clear. Physiological evidence of S-OFF signals were found within the retina (Field *et al.*, 2010) and higher brain areas, such as the LGN (Valberg *et al.*, 1986), and in psychophysical studies (Shinomori & Werner, 2008). The anatomical base of such signals remained contradictory. Human S-cone pedicles were found to possess only few flat contacts, typical for contacts to OFF-bipolar cells (Kolb *et al.*, 1997), supporting the studies showing reduced OFF-bipolar cell contacts to S-cones.

Diffuse bipolar cells connect to all cone types (L-, M- and S-cones) within their dendritic field. The low density of S-cones, however leads to a bias to more connections to cones sensitive for longer wavelengths (Lee *et al.*, 2004; Lee & Grünert, 2007; Puthussery *et al.*, 2011). Similar to the here presented data, Lee & Grünert (2007) analysed the input of OFF-bipolar cells using antibodies directed against GLT-1. Consistent with the results shown herein, a reduction of the GLT-1 labelling at S-cone pedicles compared to M-/L-cone pedicles was demonstrated. However, S-cones are significantly smaller than M-/L-cones (see Fig. 3.14 A, D, G and J), therefore the area of the cone pedicle occupied by OFF-bipolar cells was related to the pedicles size. It occured that the proportion or ratio of the contact area of OFF-bipolar cells to cone pedicle area was similar in M-/L- and S-cones. This suggests that S-cones also provide substantial input to the OFF pathway. Nevertheless, a physiological role of the S-cone input onto diffuse bipolar cells remains uncertain, since the major input to these cells derives from L- and M-cones (see above). However, the majority of the cells labelled by GLT-1 antibodies are FMBs. as was demonstrated double-labelling experiments using antibodies against GLT-1 and Rec in which most GLT-1 labelled bipolar cells were also labelled by Rec (Fig. 3.11). Hence

the GLT-1 labelling at S-cone pedicles suggest that S-cones in the macaque retina feed their signals to OFF-midget pathway.

A study in the marmoset monkey retina by Lee *et al.* (2005), in contrast, does not support the existence of an S-OFF midget pathway in this species. These observations, which are mirrored by studies demonstrating a stronger reduction of GLT-1 labelling, as well as the glutamate receptor-1, which is mainly expressed by FMBs (Puller *et al.*, 2007), at S-cone pedicles in the marmoset compared to the macaque monkey retina (reviewed by Puller & Haverkamp, 2011). Such differences may reflect species differences in connectivity of the midget pathway in retinae of the trichromatic macaque and the marmoset, where trichromatic vision is restricted to some female animals (reviewed by Miyagishima *et al.*, 2013).

Contacts between S-cones and OFF-midget bipolar cells were shown by Klug *et al.* (2003) using electron microscopy and serial reconstructions in the macaque retina. An important disadvantage of ultrastructural reconstructions of (classical) electron microscopy is the small sample size and the ease of making mistakes tracing small neuronal processes through the tissue. For the here presented study an approach using light microscopy was used to analyse the connection between S-cones and FMBs in a wide screen to circumvent the difficulties regarding small sample sizes in electron microscopy. Using antibodies which label OFF-bipolar cells (GLT-1) and FMBs (Rec) contacts between S-cones and FMBs (Rec labelled) and presumable FMBs (GLT-1 labelled) were frequently found (Figs. 3.12 (Rec) and 3.13 (GLT-1)).

Summarising, the data shown in this thesis strongly supports that all cone types in the macaque monkey retina are connected to the OFF-pathways and that S-cones signals are transferred into the OFF-midget system. The anatomical data shown here is consistent with the study of Field *et al.* (2010), who demonstrated in sophisticated experiments S-cone input onto OFF-midget ganglion cells in peripheral macaque retina using multi-electrode arrays. The here presented data also indicates that more central S-cones connect to the midget system, since most of the S-cones shown connected to single- or two-headed FMBs, which are absent or rare in the far periphery (Wässle *et al.*, 1994).

FMBs receiving S-cone input could not only act as anatomical substrate for S-OFF midget ganglion cells, but also for outer-stratifying ganglion cell

photoreceptors (M1 cells). Anatomical evidence supporting synaptic inputs from some, but not all FMBs onto M1 cells was presented (Figs. 3.17 and 3.18). It is a tempting speculation that only FMBs, which contact S-cones provide synaptic output (the S-OFF signal) to M1 ipRGCs, whereas those connected to M- and L-cones are not connected to these ganglion cells.

4.4 Conclusion

The data presented within this thesis supports the idea that some ganglion cells connect to bipolar cells within their dendritic field in a non-selective manner, likely to detect all luminance signals provided via the bipolar cells. In some cases, however, the input onto the ganglion cells appeared to be dominated by a certain bipolar cell type, which is likely to influence the physiological properties of the ganglion cell. In the primate retina ipRGCs were investigated and it was found that the different ipRGC types expressed different subsets of inhibitory neurotransmitters, strongly supporting their involvement in different retinal circuits. The connectivity of outer-stratifying M1 ipRGCs was analysed in detail and the results revealed a pathway which could possibly explain chromatic S-OFF responses within these cells: Bistratified A8 amacrine cells were not confirmed as source of S-OFF signals, but provided the majority of glycinergic synapses found on M1 cells. However no evidence of contacts between A8 amacrine cells and S-ON bipolar cells was found, indicating that these amacrine cells modulate M1 ipRGCs but are unlikely a source of S-OFF signals found in ipRGCs Dacey *et al.* (2005). Instead it was found that S-cones feed their signals into the OFF-pathways via contacts to OFF-bipolar cells, particularly to FMBs. Such S-OFF FMBs are likely the origin of S-OFF signals found in OFF-midget and other ganglion cells. Furthermore, evidence for synaptic input from some FMBs onto M1 dendrites was found. Nevertheless, it is likely that multiple pathways convey S-OFF signals detected in the retina and higher brain areas. Hence, the investigation of circuits processing specific features of visual stimuli remains an interesting field of neuronal research.

Appendix A

Supplemental Data

A.1 Supplemental Figures

In order to investigate, if all S-cone pedicles are contacted by OFF-bipolar cells and to analyse in how far the amount of OFF-bipolar cell contacts differ at S- and M-/L-coness the area of GLT-1 labelling beneath the cone pedicles was measured. For this purpose, the area of cone pedicles identified by CtBP2 or PNA labelling was marked and copied into a new picture. Afterwards the selection was copied into the channel showing the GLT-1 labelling which marks the dendrites of OFF-bipolar cells. The pictures of the GLT-1 area beneath the pedicle were binarised to measure to labelled area. S-cone pedicles were identified by S-opsin labelling, M-/L-cones by the absence of S-opsin immunoreactivity. Supplemental Figures A1 and A2/A3 summarise all analysed S-cone (n = 38) and M-/L-cone pedicles (n = 60), respectively.The analysis was performed in three different tissue samples taken from three different eccentricities. Tissue samples were obtained from two animals (Mk C07 and MkGö). Tissue of two eyes of macaque Mk C07 which was PFA fixed for 30 and 15 min, respectively (Mk C07 30: eccentricity: 4 – 6 mm; Mk C07 15: eccentricity: 6 – 12 mm) and from one eye of macaque Mk Gö, which was PFA fixed for 15 min (Mk Gö 15: far periphery). Whereas the pedicle size of M-/L-cones increased from the most central to the most peripheral tissue sample, S-cone size was larger at 6-12 mm than in the central piece (3–6 mm) but did not change at higher eccentricities. Changes in the cone pedicle size were mirrored by changes of the area occupied by GLT-1 labelled dendrites of OFF-bipolar

cells. The ratio GLT-1 labelled area beneath cone pedicles remained similar at all eccentricties (see also Results section 3.3.3).The tissue and eccentricity of all cone pedicles is indicated in the figure legends.

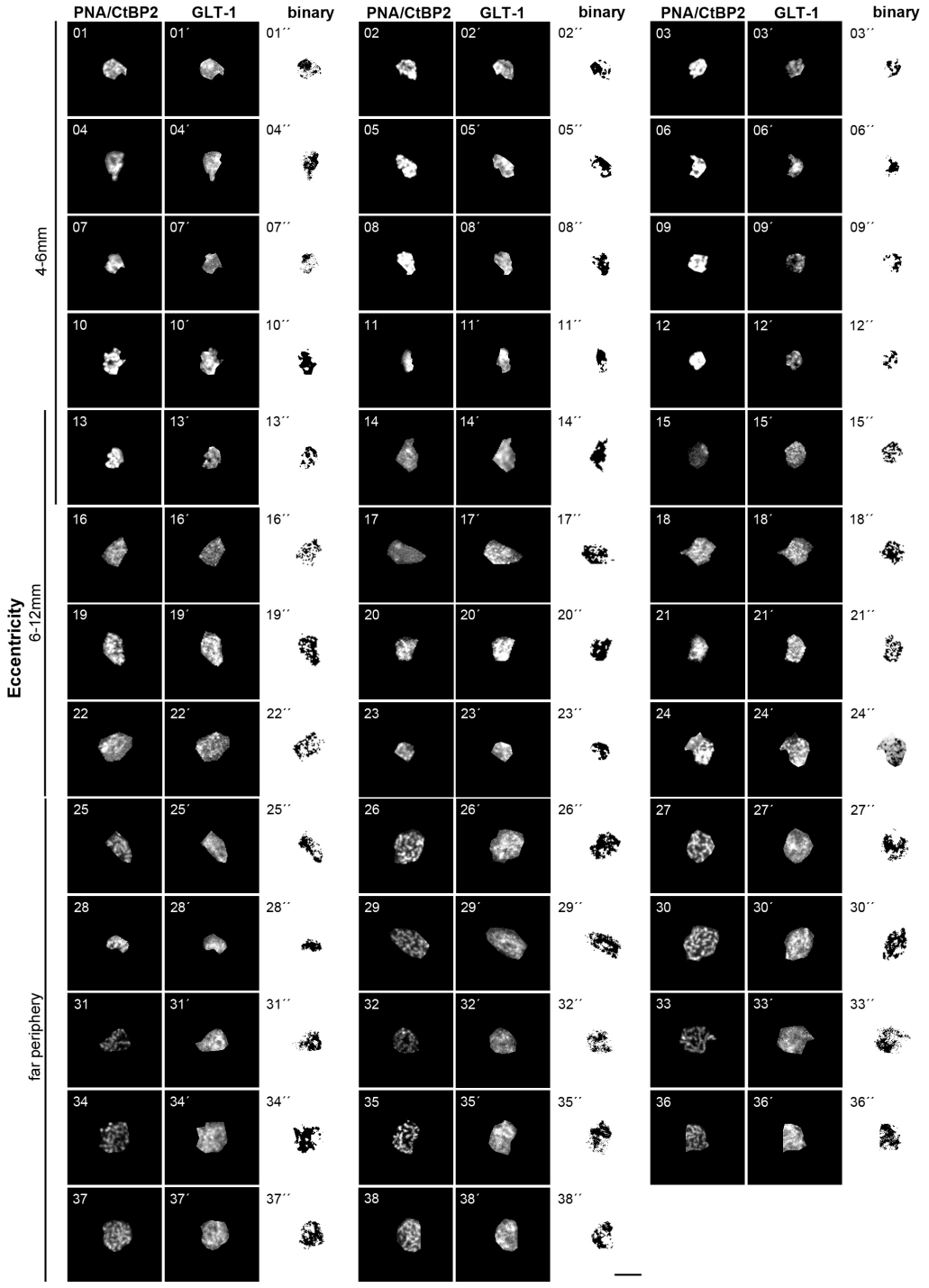

Figure A.1: S-cone pedicles used in the quantitative analysis of OFF-bipolar cell contacts to S- and M-/L- cones. Horizontal sections of macaque retina were triple-immunolabelled against S-opsin, CtBP2 or PNA, and GLT-1. S-cone pedicles were identified by nest-like clusters synaptic ribbons (**1 − 38**) and S-opsin labelling (not shown). The GLT-1 staining at identified cone pedicles is shown in (**1´ − 38´**), the corresponding binary pictures used in the quantitative analysis in (**1´´ − 38´´**). The eccentricity of the tissue samples is indicated on the left (1-13´´: Mk C07 30 (4−6 mm); 14−24´´: Mk C07 15 (6−12 mm); 25-38´´: Mk Gö 15 (far periphery). Scale bar: 38´´(applies to 1−38´´): 5 µm.

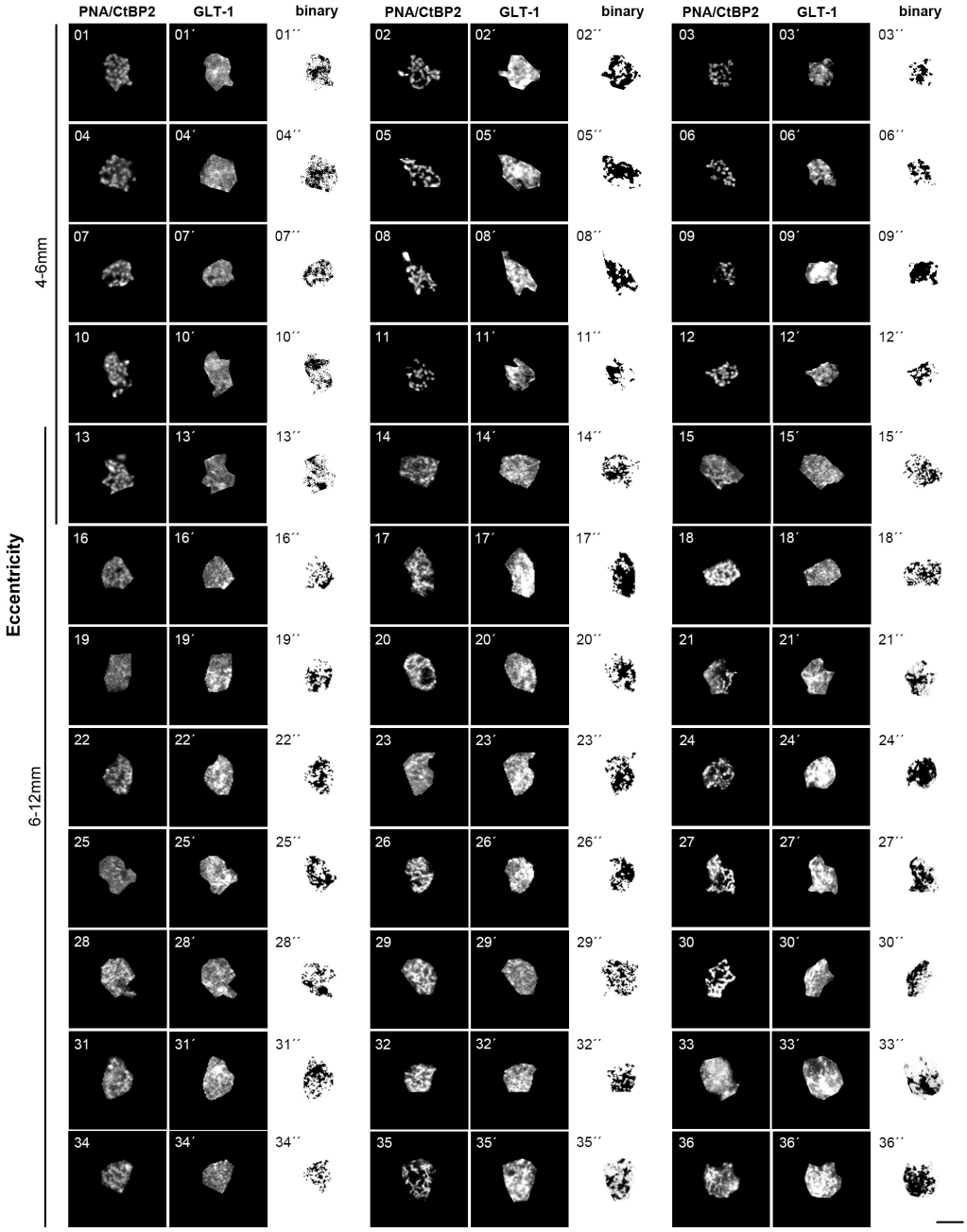

Figure A.2: M-/L-cone pedicles used in the quantitative analysis of OFF-bipolar cell contacts to S- and M-/L- cones. Horizontal sections of macaque retina were triple-immunolabelled against S-opsin, CtBP2 or PNA, and GLT-1. M-/L–cone pedicles were identified by nest-like clusters synaptic ribbons (**1 − 36**) and the absence of S-opsin labelling (not shown). The GLT-1 staining is shown in **(1´ − 36´)**, the corresponding binary pictures used in the quantitative analysis in (**1´´ − 36´´**). The eccentricity of the tissue samples is indicated on the left (1-13´´: Mk C07 30 (4 − 6 mm); 14-36´´: Mk C07 15 (6 − 12 mm) Scale bar: 38´´(applies to 1 − 36´´). Scale bar: 5 µm.

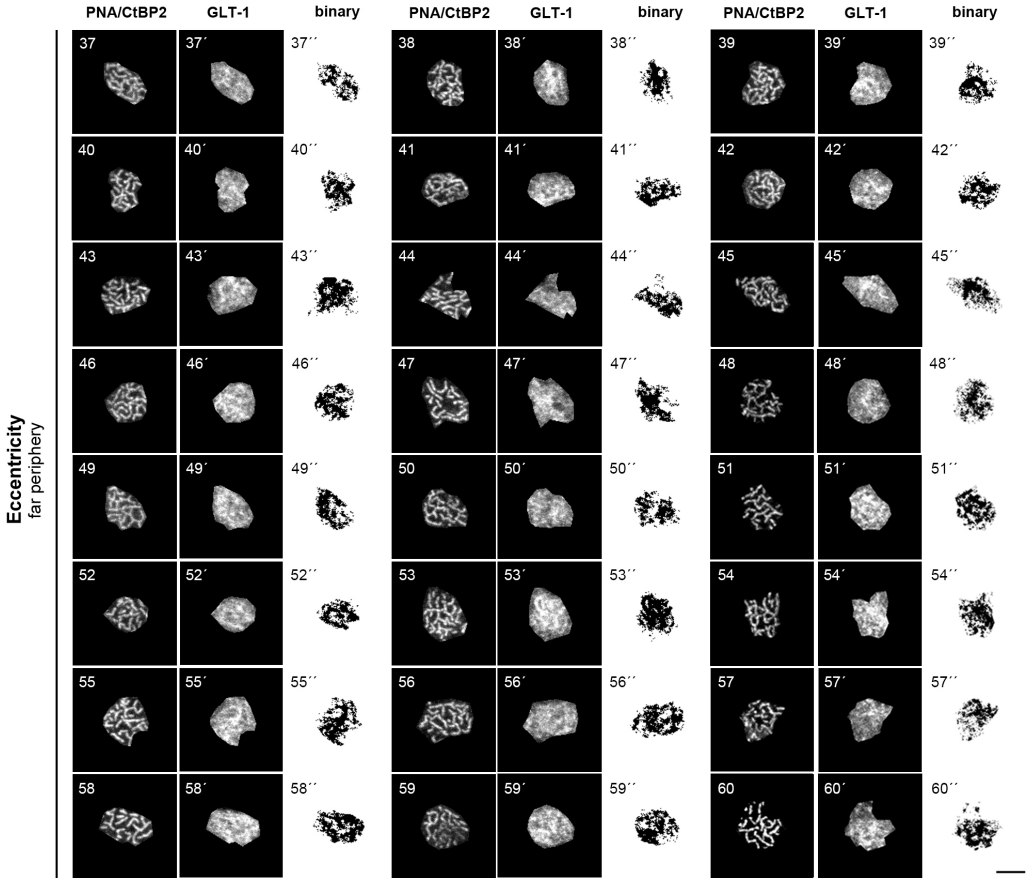

Figure A.3: M-/L-cone pedicles used in the quantitative analysis of OFF-bipolar cell contacts to S- and M-/L- cones (continued Fig. A.2). Horizontal sections of macaque retina were triple-immunolabelled against S-opsin, CtBP2 or PNA, and GLT-1. M-/L–cone pedicles were identified by nest-like clusters synaptic ribbons (**37 − 60**) and the absence of S-opsin labelling (not shown). The GLT-1 staining is shown in (**37´,− 60´**), the corresponding binary pictures used in the quantitative analysis in (**37´´ − 60´´**). The eccentricity of the tissue samples is indicated on the left. All cone pedicles shown in this figure (cone pedicles number 37-60 were taken from the far peripheral tissue sample (Mk Gö 15)).Scale bar: 60“ (applies to 37 − 60´´): 5 µm.

Bibliography

Abbott, C. J., Percival, K. A., Martin, P. R., & Grünert, U. 2012. Amacrine and bipolar inputs to midget and parasol ganglion cells in marmoset retina. *Visual neuroscience*, **29**(3), 157–68.

Ahnelt, P. K. 1998. The photoreceptor mosaic. *Eye*, **12 (Pt 3b)**, 531–40.

Ahnelt, P. K., Kolb, H., & Pflug, R. 1987. Identification of a subtype of cone photoreceptor, likely to be blue sensitive, in the human retina. *The Journal of comparative neurology*, **255**(1), 18–34.

Ammermüller, J., & Kolb, H. 1995. The organization of the turtle inner retina. I. ON- and OFF-center pathways. *The Journal of comparative neurology*, **358**(1), 1–34.

Amthor, F. R., Oyster, C. W., & Takahashi, E. S. 1984. Morphology of on-off direction-selective ganglion cells in the rabbit retina. *Brain research*, **298**(1), 187–90.

Anderson, James R., Jones, Bryan W., Watt, Carl B., Shaw, Margaret V., Yang, Jia-Hui, DeMill, David, Lauritzen, James S., Lin, Yanhua, Rapp, Kevin D., Mastronarde, David, Koshevoy, Pavel, Grimm, Bradley, Tasdizen, Tolga, Whitaker, Ross, & Marc, Robert E. 2011. Exploring the retinal connectome. *Molecular Vision*, **17**, 355–379.

Auferkorte, O. N., Baden, T., Kaushalya, S. K., Zabouri, N., Rudolph, U., Haverkamp, S., & Euler, T. 2012. GABA(A) receptors containing the alpha2 subunit are critical for direction-selective inhibition in the retina. *PLoS One*, **7**(4), e35109.

Badea, T. C., & Nathans, J. 2004. Quantitative analysis of neuronal morphologies in the mouse retina visualized by using a genetically directed reporter. *J Comp Neurol*, **480**(4), 331–51.

Baden, T., Berens, P., Bethge, M., & Euler, T. 2013. Spikes in mammalian bipolar cells support temporal layering of the inner retina. *Current biology : CB*, **23**(1), 48–52.

Baylor, D. A., & Hodgkin, A. L. 1973. Detection and resolution of visual stimuli by turtle photoreceptors. *The Journal of physiology*, **234**(1), 163–98.

Becker, C. M. 1995. Glycine Receptors: Molecular Heterogeneity and Implications for Disease. *The Neuroscientist*, **1**(3), 130–141.

Belenky, M. A., Smeraski, C. A., Provencio, I., Sollars, P. J., & Pickard, G. E. 2003. Melanopsin retinal ganglion cells receive bipolar and amacrine cell synapses. *The Journal of comparative neurology*, **460**(3), 380–93.

Ben-Ari, Y. 2007. [GABA, a key transmitter for fetal brain maturation]. *Medecine sciences : M/S*, **23**(8-9), 751–5.

Ben-Ari, Y., Gaiarsa, J. L., Tyzio, R., & Khazipov, R. 2007. GABA: a pioneer transmitter that excites immature neurons and generates primitive oscillations. *Physiological reviews*, **87**(4), 1215–84.

Benke, D., Michel, C., & Möhler, H. 2002. Structure of $GABA_B$ receptors in rat retina. *Journal of receptor and signal transduction research*, **22**(1-4), 253–66.

Berson, D. M., Pu, M., & Famiglietti, E. V. 1998. The zeta cell: a new ganglion cell type in cat retina. *The Journal of comparative neurology*, **399**(2), 269–88.

Berson, D. M., Isayama, T., & Pu, M. 1999. The Eta ganglion cell type of cat retina. *The Journal of comparative neurology*, **408**(2), 204–19.

Berson, D. M., Dunn, F. A., & Takao, M. 2002. Phototransduction by retinal ganglion cells that set the circadian clock. *Science*, **295**(5557), 1070–3.

Betz, H., & Laube, B. 2006. Glycine receptors: recent insights into their structural organization and functional diversity. *Journal of neurochemistry*, **97**(6), 1600–10.

Blanks, J. C., & Johnson, L. V. 1984. Specific binding of peanut lectin to a class of retinal photoreceptor cells. A species comparison. *Investigative ophthalmology & visual science*, **25**(5), 546–57.

Bleckert, A., Parker, E. D., Kang, Y., Pancaroglu, R., Soto, F., Lewis, R., Craig, A. M., & Wong, R. O. 2013. Spatial relationships between GABAergic and glutamatergic synapses on the dendrites of distinct types of mouse retinal ganglion cells across development. *PLoS One*, **8**(7), e69612.

Bleckert, A., Schwartz, G. W., Turner, M. H., Rieke, F., & Wong, R. O. 2014. Visual Space Is Represented by Nonmatching Topographies of Distinct Mouse Retinal Ganglion Cell Types. *Current biology : CB*.

Bowmaker, J. K., & Dartnall, H. J. 1980a. Visual pigments of rods and cones in a human retina. *The Journal of physiology*, **298**, 501–11.

Bowmaker, J. K., & Dartnall, H. J. 1980b. Visual pigments of rods and cones in a human retina. *The Journal of physiology*, **298**, 501–11.

Bowmaker, J. K., & Hunt, D. M. 2006. Evolution of vertebrate visual pigments. *Current biology : CB*, **16**(13), R484–9.

Bowmaker, J. K., Dartnall, H. J., & Mollon, J. D. 1980. Microspectrophotometric demonstration of four classes of photoreceptor in an old world primate, Macaca fascicularis. *The Journal of physiology*, **298**, 131–43.

Boycott, B. B., & Kolb, H. 1973a. The connections between bipolar cells and photoreceptors in the retina of the domestic cat. *The Journal of comparative neurology*, **148**(1), 91–114.

Boycott, B. B., & Kolb, H. 1973b. The horizontal cells of the rhesus monkey retina. *The Journal of comparative neurology*, **148**(1), 115–39.

Brandstätter, J. H., Greferath, U., Euler, T., & Wässle, H. 1995. Co-stratification of $GABA_A$ receptors with the directionally selective circuitry of the rat retina. *Visual neuroscience*, **12**(2), 345–58.

Breuninger, T., Puller, C., Haverkamp, S., & Euler, T. 2011. Chromatic bipolar cell pathways in the mouse retina. *The Journal of neuroscience : the official journal of the Society for Neuroscience*, **31**(17), 6504–17.

Cadetti, L., Tranchina, D., & Thoreson, W. B. 2005. A comparison of release kinetics and glutamate receptor properties in shaping rod-cone differences in EPSC kinetics in the salamander retina. *The Journal of physiology*, **569**(Pt 3), 773–88.

Calkins, D. J. 2001. Seeing with S cones. *Progress in retinal and eye research*, **20**(3), 255–87.

Calkins, D. J., Schein, S. J., Tsukamoto, Y., & Sterling, P. 1994. M and L cones in macaque fovea connect to midget ganglion cells by different numbers of excitatory synapses. *Nature*, **371**(6492), 70–2.

Caroni, P. 1997. Overexpression of growth-associated proteins in the neurons of adult transgenic mice. *Journal of neuroscience methods*, **71**(1), 3–9.

Chen, S., & Li, W. 2012. A color-coding amacrine cell may provide a blue-off signal in a mammalian retina. *Nature neuroscience*, **15**(7), 954–6.

Cook, J. E., & Becker, D. L. 1995. Gap junctions in the vertebrate retina. *Microscopy research and technique*, **31**(5), 408–19.

Coombs, J., van der List, D., Wang, G. Y., & Chalupa, L. M. 2006. Morphological properties of mouse retinal ganglion cells. *Neuroscience*, **140**(1), 123–36.

Curcio, C. A., Sloan, K. R., Kalina, R. E., & Hendrickson, A. E. 1990. Human photoreceptor topography. *The Journal of comparative neurology*, **292**(4), 497–523.

Curcio, C. A., Allen, K. A., Sloan, K. R., Lerea, C. L., Hurley, J. B., Klock, I. B., & Milam, A. H. 1991. Distribution and morphology

of human cone photoreceptors stained with anti-blue opsin. *The Journal of comparative neurology*, **312**(4), 610–24.

Dacey, D. M. 1993. The mosaic of midget ganglion cells in the human retina. *J Neurosci*, **13**(12), 5334–55.

Dacey, D. M., & Lee, B. B. 1994. The 'blue-on' opponent pathway in primate retina originates from a distinct bistratified ganglion cell type. *Nature*, **367**(6465), 731–5.

Dacey, D. M., & Packer, O. S. 2003. Colour coding in the primate retina: diverse cell types and cone-specific circuitry. *Current opinion in neurobiology*, **13**(4), 421–7.

Dacey, D. M., Lee, B. B., Stafford, D. K., Pokorny, J., & Smith, V. C. 1996. Horizontal cells of the primate retina: cone specificity without spectral opponency. *Science*, **271**(5249), 656–9.

Dacey, D. M., Peterson, B. B., Robinson, F. R., & Gamlin, P. D. 2003. Fireworks in the primate retina: in vitro photodynamics reveals diverse LGN-projecting ganglion cell types. *Neuron*, **37**(1), 15–27.

Dacey, D. M., Liao, H. W., Peterson, B. B., Robinson, F. R., Smith, V. C., Pokorny, J., Yau, K. W., & Gamlin, P. D. 2005. Melanopsin-expressing ganglion cells in primate retina signal colour and irradiance and project to the LGN. *Nature*, **433**(7027), 749–54.

Dacey, D. M., Crook, J. D., & Packer, O. S. 2013. Distinct synaptic mechanisms create parallel S-ON and S-OFF color opponent pathways in the primate retina. *Visual neuroscience*, 1–13.

Dacey, D. M., Crook, J. D., & Packer, O. S. 2014. Distinct synaptic mechanisms create parallel S-ON and S-OFF color opponent pathways in the primate retina. *Visual neuroscience*, **31**(2), 139–51.

Dacey, D.M., Peterson, B.B., Liao, H.-W., & Yau, K.-W. 2006 (May 1, 2006). *Two Types of Melanopsin-Containing Ganglion Cells in the Primate Retina: Links to Dopaminergic Amacrine and DB6 Cone Bipolar Cells.*

Derry, J. M., & Barnard, P. J. 1991. Mapping of the glycine receptor alpha 2-subunit gene and the GABAA alpha 3-subunit gene on the mouse X chromosome. *Genomics*, **10**(3), 593–7.

DeVries, S. H. 2000. Bipolar cells use kainate and AMPA receptors to filter visual information into separate channels. *Neuron*, **28**(3), 847–56.

DeVries, S. H., & Schwartz, E. A. 1999. Kainate receptors mediate synaptic transmission between cones and 'Off' bipolar cells in a mammalian retina. *Nature*, **397**(6715), 157–60.

DeVries, S. H., Li, W., & Saszik, S. 2006. Parallel processing in two transmitter microenvironments at the cone photoreceptor synapse. *Neuron*, **50**(5), 735–48.

Dick, O., tom Dieck, S., Altrock, W. D., Ammermuller, J., Weiler, R., Garner, C. C., Gundelfinger, E. D., & Brandstatter, J. H. 2003. The presynaptic active zone protein bassoon is essential for photoreceptor ribbon synapse formation in the retina. *Neuron*, **37**(5), 775–86.

Dowling, J. E., & Boycott, B. B. 1966. Organization of the primate retina: electron microscopy. *Proceedings of the Royal Society of London. Series B, Containing papers of a Biological character. Royal Society*, **166**(1002), 80–111.

Dumitrescu, O. N., Pucci, F. G., Wong, K. Y., & Berson, D. M. 2009. Ectopic retinal ON bipolar cell synapses in the OFF inner plexiform layer: contacts with dopaminergic amacrine cells and melanopsin ganglion cells. *The Journal of comparative neurology*, **517**(2), 226–44.

Ekesten, B., & Gouras, P. 2005. Cone and rod inputs to murine retinal ganglion cells: evidence of cone opsin specific channels. *Visual neuroscience*, **22**(6), 893–903.

Euler, T., Hausselt, S. E., Margolis, D. J., Breuninger, T., Castell, X., Detwiler, P. B., & Denk, W. 2009. Eyecup scope–optical recordings of light stimulus-evoked fluorescence signals in the retina. *Pflugers Archiv : European journal of physiology*, **457**(6), 1393–414.

Euler, T., Haverkamp, S., Schubert, T., & Baden, T. 2014. Retinal bipolar cells: elementary building blocks of vision. *Nature reviews. Neuroscience*, **15**(8), 507–19.

Famiglietti, E. V. 2008. Wide-field cone bipolar cells and the blue-ON pathway to color-coded ganglion cells in rabbit retina. *Visual neuroscience*, **25**(1), 53–66.

Famiglietti, E. V., Jr., & Kolb, H. 1976. Structural basis for ON-and OFF-center responses in retinal ganglion cells. *Science*, **194**(4261), 193–5.

Farrow, K., Teixeira, M., Szikra, T., Viney, T. J., Balint, K., Yonehara, K., & Roska, B. 2013. Ambient illumination toggles a neuronal circuit switch in the retina and visual perception at cone threshold. *Neuron*, **78**(2), 325–38.

Feng, G., Mellor, R. H., Bernstein, M., Keller-Peck, C., Nguyen, Q. T., Wallace, M., Nerbonne, J. M., Lichtman, J. W., & Sanes, J. R. 2000. Imaging neuronal subsets in transgenic mice expressing multiple spectral variants of GFP. *Neuron*, **28**(1), 41–51.

Field, G. D., Gauthier, J. L., Sher, A., Greschner, M., Machado, T. A., Jepson, L. H., Shlens, J., Gunning, D. E., Mathieson, K., Dabrowski, W., Paninski, L., Litke, A. M., & Chichilnisky, E. J. 2010. Functional connectivity in the retina at the resolution of photoreceptors. *Nature*, **467**(7316), 673–7.

Fischer, F., Kneussel, M., Tintrup, H., Haverkamp, S., Rauen, T., Betz, H., & Wassle, H. 2000. Reduced synaptic clustering of GABA and glycine receptors in the retina of the gephyrin null mutant mouse. *The Journal of comparative neurology*, **427**(4), 634–48.

Fritschy, J. M., Harvey, R. J., & Schwarz, G. 2008. Gephyrin: where do we stand, where do we go? *Trends in neurosciences*, **31**(5), 257–64.

Ghosh, K. K., Bujan, S., Haverkamp, S., Feigenspan, A., & Wässle, H. 2004. Types of bipolar cells in the mouse retina. *J Comp Neurol*, **469**(1), 70–82.

Greferath, U., Grünert, U., Fritschy, J. M., Stephenson, A., Möhler, H., & Wässle, H. 1995. $GABA_A$ receptor subunits have differential distributions in the rat retina: in situ hybridization and immunohistochemistry. *The Journal of comparative neurology*, **353**(4), 553–71.

Grenningloh, G., Schmieden, V., Schofield, P. R., Seeburg, P. H., Siddique, T., Mohandas, T. K., Becker, C. M., & Betz, H. 1990. Alpha subunit variants of the human glycine receptor: primary structures, functional expression and chromosomal localization of the corresponding genes. *The EMBO journal*, **9**(3), 771–6.

Grünert, U. 1999. Distribution of GABAA and glycine receptors in the mammalian retina. *Clinical and experimental pharmacology & physiology*, **26**(11), 941–4.

Grünert, U. 2000. Distribution of GABA and glycine receptors on bipolar and ganglion cells in the mammalian retina. *Microscopy research and technique*, **50**(2), 130–40.

Grünert, U., & Ghosh, K. K. 1999. Midget and parasol ganglion cells of the primate retina express the alpha1 subunit of the glycine receptor. *Visual neuroscience*, **16**(5), 957–66.

Grünert, U., & Wässle, H. 1996. Glycine receptors in the rod pathway of the macaque monkey retina. *Visual neuroscience*, **13**(1), 101–15.

Grünert, U., Martin, P. R., & Wässle, H. 1994. Immunocytochemical analysis of bipolar cells in the macaque monkey retina. *The Journal of comparative neurology*, **348**(4), 607–27.

Grünert, Ulrike, Jusuf, Patricia R., Lee, Sammy C.S., & Nguyen, Dung Than. 2011. Bipolar input to melanopsin containing ganglion cells in primate retina. *Visual Neuroscience*, **28**(1), 39–50.

Grudzinska, J., Schemm, R., Haeger, S., Nicke, A., Schmalzing, G., Betz, H., & Laube, B. 2005. The beta subunit determines the ligand binding properties of synaptic glycine receptors. *Neuron*, **45**(5), 727–39.

Hack, I., & Peichl, L. 1999. Horizontal cells of the rabbit retina are non-selectively connected to the cones. *The European journal of neuroscience*, **11**(7), 2261–74.

Hannibal, J., Kankipati, L., Strang, C. E., Peterson, B. B., Dacey, D., & Gamlin, P. D. 2014. Central projections of intrinsically photosensitive retinal ganglion cells in the macaque monkey. *The Journal of comparative neurology*.

Harvey, R. J., Schmieden, V., Von Holst, A., Laube, B., Rohrer, H., & Betz, H. 2000. Glycine receptors containing the alpha4 subunit in the embryonic sympathetic nervous system, spinal cord and male genital ridge. *The European journal of neuroscience*, **12**(3), 994–1001.

Hattar, S., Liao, H. W., Takao, M., Berson, D. M., & Yau, K. W. 2002. Melanopsin-containing retinal ganglion cells: architecture, projections, and intrinsic photosensitivity. *Science*, **295**(5557), 1065–70.

Haverkamp, S., Grünert, U., & Wässle, H. 2000. The cone pedicle, a complex synapse in the retina. *Neuron*, **27**(1), 85–95.

Haverkamp, S., Grünert, U., & Wässle, H. 2001. The synaptic architecture of AMPA receptors at the cone pedicle of the primate retina. *The Journal of neuroscience : the official journal of the Society for Neuroscience*, **21**(7), 2488–500.

Haverkamp, S., Haeseleer, F., & Hendrickson, A. 2003a. A comparison of immunocytochemical markers to identify bipolar cell types in human and monkey retina. *Visual neuroscience*, **20**(6), 589–600.

Haverkamp, S., Müller, U., Harvey, K., Harvey, R. J., Betz, H., & Wässle, H. 2003b. Diversity of glycine receptors in the mouse retina: localization of the alpha3 subunit. *The Journal of comparative neurology*, **465**(4), 524–39.

Haverkamp, S., Müller, U., Zeilhofer, H. U., Harvey, R. J., & Wässle, H. 2004. Diversity of glycine receptors in the mouse retina: localization of the alpha2 subunit. *The Journal of comparative neurology*, **477**(4), 399–411.

Haverkamp, S., Wassle, H., Duebel, J., Kuner, T., Augustine, G. J., Feng, G., & Euler, T. 2005. The primordial, blue-cone color system of the mouse retina. *The Journal of neuroscience : the official journal of the Society for Neuroscience*, **25**(22), 5438–45.

Haverkamp, S., Specht, D., Majumdar, S., Zaidi, N. F., Brandstätter, J. H., Wasco, W., Wässle, H., & Tom Dieck, S. 2008. Type 4 OFF cone bipolar cells of the mouse retina express calsenilin and contact cones as well as rods. *The Journal of comparative neurology*, **507**(1), 1087–101.

Heinze, L., Harvey, R. J., Haverkamp, S., & Wässle, H. 2007. Diversity of glycine receptors in the mouse retina: localization of the alpha4 subunit. *The Journal of comparative neurology*, **500**(4), 693–707.

Hendrickson, A., & Kupfer, C. 1976. The histogenesis of the fovea in the macaque monkey. *Investigative ophthalmology & visual science*, **15**(9), 746–56.

Hendrickson, A E. 1994. Primate foveal development: a microcosm of current questions in neurobiology. *Investigative Ophthalmology & Visual Science*, **35**(8), 3129–33.

Hendrickson, Anita. 1992. A morphological comparison of foveal development in man and monkey. *Eye*, **6**(2), 136–144.

Herr, S., Klug, K., Sterling, P., & Schein, S. 2003. Inner S-cone bipolar cells provide all of the central elements for S cones in macaque retina. *The Journal of comparative neurology*, **457**(2), 185–201.

Hong, Y. K., Kim, I. J., & Sanes, J. R. 2011. Stereotyped axonal arbors of retinal ganglion cell subsets in the mouse superior colliculus. *J Comp Neurol*, **519**(9), 1691–711.

Hopkins, J. M., & Boycott, B. B. 1997. The cone synapses of cone bipolar cells of primate retina. *Journal of neurocytology*, **26**(5), 313–25.

Hoshi, Hideo, Liu, Wei-Li, Massey, Stephen C., & Mills, Stephen L. 2009. ON Inputs to the OFF Layer: Bipolar Cells That Break the Stratification Rules of the Retina. *The Journal of Neuroscience*, **29**(28), 8875–8883.

Hou, M., Duan, L., & Slaughter, M. M. 2008. Synaptic inhibition by glycine acting at a metabotropic receptor in tiger salamander retina. *The Journal of physiology*, **586**(Pt 12), 2913–26.

Huberman, A. D., Manu, M., Koch, S. M., Susman, M. W., Lutz, A. B., Ullian, E. M., Baccus, S. A., & Barres, B. A. 2008. Architecture and activity-mediated refinement of axonal projections from a mosaic of genetically identified retinal ganglion cells. *Neuron*, **59**(3), 425–38.

Huberman, Andrew D., Wei, Wei, Elstrott, Justin, Stafford, Ben K., Feller, Marla B., & Barres, Ben A. 2009. Genetic Identification of an On-Off Direction- Selective Retinal Ganglion Cell Subtype Reveals a Layer-Specific Subcortical Map of Posterior Motion. *Neuron*, **62**(3), 327–334.

Hunt, D. M., & Peichl, L. 2013. S cones: Evolution, retinal distribution, development, and spectral sensitivity. *Visual neuroscience*, 1–24.

Isayama, T., Berson, D. M., & Pu, M. 2000. Theta ganglion cell type of cat retina. *The Journal of comparative neurology*, **417**(1), 32–48.

Ivanova, E., Müller, U., & Wässle, H. 2006. Characterization of the glycinergic input to bipolar cells of the mouse retina. *The European journal of neuroscience*, **23**(2), 350–64.

Jacobs, G. H. 2008. Primate color vision: a comparative perspective. *Visual neuroscience*, **25**(5-6), 619–33.

Jacobs, G. H. 2009. Evolution of colour vision in mammals. *Philosophical transactions of the Royal Society of London. Series B, Biological sciences*, **364**(1531), 2957–67.

Jusuf, P. R., Haverkamp, S., & Grünert, U. 2005. Localization of glycine receptor alpha subunits on bipolar and amacrine cells in primate retina. *The Journal of comparative neurology*, **488**(2), 113–28.

Jusuf, P. R., Lee, S. C., Hannibal, J., & Grünert, U. 2007. Characterization and synaptic connectivity of melanopsin-containing ganglion cells in the primate retina. *The European journal of neuroscience*, **26**(10), 2906–21.

Kim, I. J., Zhang, Y., Yamagata, M., Meister, M., & Sanes, J. R. 2008. Molecular identification of a retinal cell type that responds to upward motion. *Nature*, **452**(7186), 478–82.

Kim, J. S., Greene, M. J., Zlateski, A., Lee, K., Richardson, M., Turaga, S. C., Purcaro, M., Balkam, M., Robinson, A., Behabadi, B. F., Campos, M., Denk, W., & Seung, H. S. 2014. Space-time wiring specificity supports direction selectivity in the retina. *Nature*, **509**(7500), 331–6.

Kingsmore, S. F., Suh, D., & Seldin, M. F. 1994. Genetic mapping of the glycine receptor alpha 3 subunit on mouse chromosome 8. *Mammalian genome : official journal of the International Mammalian Genome Society*, **5**(12), 831–2.

Klug, K., Herr, S., Ngo, I. T., Sterling, P., & Schein, S. 2003. Macaque retina contains an S-cone OFF midget pathway. *The Journal of neuroscience : the official journal of the Society for Neuroscience*, **23**(30), 9881–7.

Kolb, H. 1970. Organization of the outer plexiform layer of the primate retina: electron microscopy of Golgi-impregnated cells. *Philosophical transactions of the Royal Society of London. Series B, Biological sciences*, **258**(823), 261–83.

Kolb, H., & Dekorver, L. 1991. Midget ganglion cells of the parafovea of the human retina: a study by electron microscopy and serial section reconstructions. *The Journal of comparative neurology*, **303**(4), 617–36.

Kolb, H., Mariani, A., & Gallego, A. 1980. A second type of horizontal cell in the monkey retina. *The Journal of comparative neurology*, **189**(1), 31–44.

Kolb, H., Nelson, R., & Mariani, A. 1981. Amacrine cells, bipolar cells and ganglion cells of the cat retina: a Golgi study. *Vision research*, **21**(7), 1081–1114.

Kolb, H., Linberg, K. A., & Fisher, S. K. 1992. Neurons of the human retina: a Golgi study. *The Journal of comparative neurology*, **318**(2), 147–87.

Kolb, H., Goede, P., Roberts, S., McDermott, R., & Gouras, P. 1997. Uniqueness of the S-cone pedicle in the human retina and consequences for color processing. *The Journal of comparative neurology*, **386**(3), 443–60.

Kong, J. H., Fish, D. R., Rockhill, R. L., & Masland, R. H. 2005. Diversity of ganglion cells in the mouse retina: unsupervised morphological classification and its limits. *J Comp Neurol*, **489**(3), 293–310.

Koulen, P., Brandstätter, J. H., Enz, R., Bormann, J., & Wässle, H. 1998. Synaptic clustering of GABA(C) receptor rho-subunits in the rat retina. *The European journal of neuroscience*, **10**(1), 115–27.

Kouyama, N., & Marshak, D. W. 1992. Bipolar cells specific for blue cones in the macaque retina. *The Journal of neuroscience : the official journal of the Society for Neuroscience*, **12**(4), 1233–52.

Lee, S. C., & Grünert, U. 2007. Connections of diffuse bipolar cells in primate retina are biased against S-cones. *The Journal of comparative neurology*, **502**(1), 126–40.

Lee, S. C., Jusuf, P. R., & Grünert, U. 2004. S-cone connections of the diffuse bipolar cell type DB6 in macaque monkey retina. *The Journal of comparative neurology*, **474**(3), 353–63.

Lee, S. C., Telkes, I., & Grünert, U. 2005. S-cones do not contribute to the OFF-midget pathway in the retina of the marmoset, Callithrix jacchus. *The European journal of neuroscience*, **22**(2), 437–47.

Levick, W. R. 1967. Receptive fields and trigger features of ganglion cells in the visual streak of the rabbit's retina. *The Journal of Physiology*, **188**(3), 285–307.

Li, W., & DeVries, S. H. 2006. Bipolar cell pathways for color and luminance vision in a dichromatic mammalian retina. *Nature neuroscience*, **9**(5), 669–75.

Lin, B., Martin, P. R., Solomon, S. G., & Grünert, U. 2000. Distribution of glycine receptor subunits on primate retinal ganglion cells: a quantitative analysis. *The European journal of neuroscience*, **12**(12), 4155–70.

Lin, B., Wang, S. W., & Masland, R. H. 2004. Retinal ganglion cell type, size, and spacing can be specified independent of homotypic dendritic contacts. *Neuron*, **43**(4), 475–85.

Liu, P. C., & Chiao, C. C. 2007. Morphologic identification of the OFF-type blue cone bipolar cell in the rabbit retina. *Investigative ophthalmology & visual science*, **48**(7), 3388–95.

Lynch, J. W. 2009. Native glycine receptor subtypes and their physiological roles. *Neuropharmacology*, **56**(1), 303–9.

Lynch, J. W. 2014 (Accessed on 03/07/2014). *Glycine receptors: α4 (pseudogene in humans).*

MacNeil, M. A., & Gaul, P. A. 2008. Biocytin wide-field bipolar cells in rabbit retina selectively contact blue cones. *The Journal of comparative neurology*, **506**(1), 6–15.

Majumdar, S., Heinze, L., Haverkamp, S., Ivanova, E., & Wassle, H. 2007. Glycine receptors of A-type ganglion cells of the mouse retina. *Visual neuroscience*, **24**(4), 471–87.

Majumdar, S., Weiss, J., & Wässle, H. 2009. Glycinergic input of wide-field, displaced amacrine cells of the mouse retina. *The Journal of physiology*, **587**(Pt 15), 3831–49.

Marc, R. E., Anderson, J. R., Jones, B. W., Sigulinsky, C. L., & Lauritzen, J. S. 2014. The AII amacrine cell connectome: a dense network hub. *Frontiers in neural circuits*, **8**, 104.

Mariani, A. P. 1984. Bipolar cells in monkey retina selective for the cones likely to be blue-sensitive. *Nature*, **308**(5955), 184–6.

Mariani, A. P., & Hersh, L. B. 1988. Synaptic organization of cholinergic amacrine cells in the rhesus monkey retina. *The Journal of comparative neurology*, **267**(2), 269–80.

Mariani, A. P., Cosenza-Murphy, D., & Barker, J. L. 1987. GABAergic synapses and benzodiazepine receptors are not identically distributed in the primate retina. *Brain research*, **415**(1), 153–7.

Marshak, D. W., Aldrich, L. B., Del Valle, J., & Yamada, T. 1990. Localization of immunoreactive cholecystokinin precursor to amacrine cells and bipolar cells of the macaque monkey retina. *The Journal of neuroscience : the official journal of the Society for Neuroscience*, **10**(9), 3045–55.

Martin, P. R. 1998. Colour processing in the primate retina: recent progress. *The Journal of physiology*, **513 (Pt 3)**, 631–8.

Masland, R. H. 2001a. The fundamental plan of the retina. *Nature neuroscience*, **4**(9), 877–86.

Masland, R. H. 2001b. Neuronal diversity in the retina. *Current opinion in neurobiology*, **11**(4), 431–6.

Mataruga, A., Kremmer, E., & Müller, F. 2007. Type 3a and type 3b OFF cone bipolar cells provide for the alternative rod pathway in the mouse retina. *The Journal of comparative neurology*, **502**(6), 1123–37.

Matzenbach, B., Maulet, Y., Sefton, L., Courtier, B., Avner, P., Guenet, J. L., & Betz, H. 1994. Structural analysis of mouse glycine receptor alpha subunit genes. Identification and chromosomal localization of a novel variant. *The Journal of biological chemistry*, **269**(4), 2607–12.

Milam, A. H., Dacey, D. M., & Dizhoor, A. M. 1993. Recoverin immunoreactivity in mammalian cone bipolar cells. *Visual neuroscience*, **10**(1), 1–12.

Mills, S. L., Tian, L. M., Hoshi, H., Whitaker, C. M., & Massey, S. C. 2014. Three distinct blue-green color pathways in a mammalian retina. *The Journal of neuroscience : the official journal of the Society for Neuroscience*, **34**(5), 1760–8.

Miyagishima, K. J., Grünert, U., & Li, W. 2013. Processing of S-cone signals in the inner plexiform layer of the mammalian retina. *Visual neuroscience*, 1–11.

Neumann, S., & Haverkamp, S. 2013. Characterization of small-field bistratified amacrine cells in macaque retina labeled by antibodies against synaptotagmin-2. *The Journal of comparative neurology*, **521**(3), 709–24.

Neumann, S., Haverkamp, S., & Auferkorte, O. N. 2011. Intrinsically photosensitive ganglion cells of the primate retina express distinct combinations of inhibitory neurotransmitter receptors. *Neuroscience*, **199**, 24–31.

Neumann, Sonja. 2010. *Charakterisierung Synaptotagmin-II immunoreaktiver Amakrinzellen in der Makakenretina.* Diploma Thesis, Johannes Gutenberg Universität.

Nikolic, Z., Laube, B., Weber, R. G., Lichter, P., Kioschis, P., Poustka, A., Mulhardt, C., & Becker, C. M. 1998. The human glycine receptor subunit alpha3. Glra3 gene structure, chromosomal localization, and functional characterization of alternative transcripts. *The Journal of biological chemistry*, **273**(31), 19708–14.

Nikonov, S. S., Kholodenko, R., Lem, J., & Pugh, E. N., Jr. 2006. Physiological features of the S- and M-cone photoreceptors of wild-type mice from single-cell recordings. *The Journal of general physiology*, **127**(4), 359–74.

Park, S. J., Kim, I. J., Looger, L. L., Demb, J. B., & Borghuis, B. G. 2014. Excitatory synaptic inputs to mouse on-off direction-selective retinal ganglion cells lack direction tuning. *The Journal of neuroscience : the official journal of the Society for Neuroscience*, **34**(11), 3976–81.

Peichl, L; Sandmann, D; Boycott BB. 1998. *Comparative anatomy and function of mammalian horizontal cells.* New York: Plenum Press. Pages 147–172.

Peichl, L. 1992. Topography of ganglion cells in the dog and wolf retina. *The Journal of comparative neurology*, **324**(4), 603–20.

Peichl, L. 2005. Diversity of mammalian photoreceptor properties: adaptations to habitat and lifestyle? *Anat Rec A Discov Mol Cell Evol Biol*, **287**(1), 1001–12.

Peichl, L., & Gonzalez-Soriano, J. 1994. Morphological types of horizontal cell in rodent retinae: a comparison of rat, mouse, gerbil, and guinea pig. *Visual neuroscience*, **11**(3), 501–17.

Peichl, L., Ott, H., & Boycott, B. B. 1987a. Alpha ganglion cells in mammalian retinae. *Proceedings of the Royal Society of London. Series B, Containing papers of a Biological character. Royal Society*, **231**(1263), 169–97.

Peichl, L., Buhl, E. H., & Boycott, B. B. 1987b. Alpha ganglion cells in the rabbit retina. *The Journal of comparative neurology*, **263**(1), 25–41.

Perez-Leon, J. A., Warren, E. J., Allen, C. N., Robinson, D. W., & Brown, R. L. 2006. Synaptic inputs to retinal ganglion cells that set the circadian clock. *The European journal of neuroscience*, **24**(4), 1117–23.

Pickard, G. E., & Sollars, P. J. 2012. Intrinsically photosensitive retinal ganglion cells. *Reviews of physiology, biochemistry and pharmacology*, **162**, 59–90.

Provencio, I., Jiang, G., De Grip, W. J., Hayes, W. P., & Rollag, M. D. 1998. Melanopsin: An opsin in melanophores, brain, and eye. *Proceedings of the National Academy of Sciences of the United States of America*, **95**(1), 340–5.

Provis, J. M., Dubis, A. M., Maddess, T., & Carroll, J. 2013. Adaptation of the central retina for high acuity vision: cones, the fovea and the avascular zone. *Progress in retinal and eye research*, **35**, 63–81.

Puller, C., & Haverkamp, S. 2011. Bipolar cell pathways for color vision in non-primate dichromats. *Visual neuroscience*, **28**(1), 51–60.

Puller, C., Haverkamp, S., & Grünert, U. 2007. OFF midget bipolar cells in the retina of the marmoset, Callithrix jacchus, express AMPA receptors. *The Journal of comparative neurology*, **502**(3), 442–54.

Puller, C., Ivanova, E., Euler, T., Haverkamp, S., & Schubert, T. 2013. OFF bipolar cells express distinct types of dendritic glutamate receptors in the mouse retina. *Neuroscience*, **243**, 136–48.

Puller, C., Haverkamp, S., Neitz, M., & Neitz, J. 2014. Synaptic Elements for GABAergic Feed-Forward Signaling between HII Horizontal Cells and Blue Cone Bipolar Cells Are Enriched beneath Primate S-Cones. *PLoS One*, **9**(2), e88963.

Puthussery, T., Gayet-Primo, J., Taylor, W. R., & Haverkamp, S. 2011. Immunohistochemical identification and synaptic inputs to the diffuse bipolar cell type DB1 in macaque retina. *The Journal of comparative neurology*, **519**(18), 3640–56.

Ramón y Cajal, Santiago. 1892. La rétine des vertébrés. *La cellule*, **1**(9).

Ramón y Cajal, Santiago. 1909. *Histologie du systéme nerveux de l´hommes et des vertébrés EDITION FRANÇAISE REVUE & MISE A JOUR PAR L'AUTEUR.* Vol. Tome 1. Paris: Maloine.

Reid, R. C., & Shapley, R. M. 2002. Space and time maps of cone photoreceptor signals in macaque lateral geniculate nucleus. *The Journal of neuroscience : the official journal of the Society for Neuroscience*, **22**(14), 6158–75.

Rivlin-Etzion, M., Zhou, K., Wei, W., Elstrott, J., Nguyen, P. L., Barres, B. A., Huberman, A. D., & Feller, M. B. 2011. Transgenic mice reveal unexpected diversity of on-off direction-selective retinal ganglion cell subtypes and brain structures involved in motion processing. *The Journal of neuroscience : the official journal of the Society for Neuroscience*, **31**(24), 8760–9.

Rockhill, R. L., Daly, F. J., MacNeil, M. A., Brown, S. P., & Masland, R. H. 2002. The diversity of ganglion cells in a mammalian retina. *The Journal of neuroscience : the official journal of the Society for Neuroscience*, **22**(9), 3831–43.

Ryan, S. G., Buckwalter, M. S., Lynch, J. W., Handford, C. A., Segura, L., Shiang, R., Wasmuth, J. J., Camper, S. A., Schofield, P., & O'Connell, P. 1994. A missense mutation in the gene encoding the alpha 1 subunit of the inhibitory glycine receptor in the spasmodic mouse. *Nature genetics*, **7**(2), 131–5.

Sassoè-Pognetto, M., Kirsch, J., Grünert, U., Greferath, U., Fritschy, J. M., Möhler, H., Betz, H., & Wässle, H. 1995. Colocalization of gephyrin and $GABA_A$-receptor subunits in the rat retina. *The Journal of comparative neurology*, **357**(1), 1–14.

Sassoe-Pognetto, M., Wassle, H., & Grunert, U. 1994. Glycinergic synapses in the rod pathway of the rat retina: cone bipolar cells express the alpha 1 subunit of the glycine receptor. *The Journal of neuroscience : the official journal of the Society for Neuroscience*, **14**(8), 5131–46.

Schnapf, J. L., & Copenhagen, D. R. 1982. Differences in the kinetics of rod and cone synaptic transmission. *Nature*, **296**(5860), 862–4.

Schwartz, G. W., Okawa, H., Dunn, F. A., Morgan, J. L., Kerschensteiner, D., Wong, R. O., & Rieke, F. 2012. The spatial structure of a nonlinear receptive field. *Nat Neurosci*, **15**(11), 1572–80.

Sher, A., & DeVries, S. H. 2012. A non-canonical pathway for mammalian blue-green color vision. *Nature neuroscience*, **15**(7), 952–3.

Shinomori, K., & Werner, J. S. 2008. The impulse response of S-cone pathways in detection of increments and decrements. *Visual neuroscience*, **25**(3), 341–7.

Söhl, G., Maxeiner, S., & Willecke, K. 2005. Expression and functions of neuronal gap junctions. *Nature reviews. Neuroscience*, **6**(3), 191–200.

Song, Y., & Slaughter, M. M. 2010. $GABA_B$ receptor feedback regulation of bipolar cell transmitter release. *The Journal of physiology*, **588**(Pt 24), 4937–49.

Stein, J. J., Johnson, S. A., & Berson, D. M. 1996. Distribution and coverage of beta cells in the cat retina. *The Journal of comparative neurology*, **372**(4), 597–617.

Sun, W., Li, N., & He, S. 2002. Large-scale morphological survey of mouse retinal ganglion cells. *J Comp Neurol*, **451**(2), 115–26.

Tom Dieck, S., Altrock, W. D., Kessels, M. M., Qualmann, B., Regus, H., Brauner, D., Fejtova, A., Bracko, O., Gundelfinger, E. D., & Brandstätter, J. H. 2005. Molecular dissection of the photoreceptor ribbon synapse: physical interaction of Bassoon and RIBEYE is essential for the assembly of the ribbon complex. *J Cell Biol*, **168**(5), 825–36.

Valberg, A., Lee, B. B., & Tigwell, D. A. 1986. Neurones with strong inhibitory S-cone inputs in the macaque lateral geniculate nucleus. *Vision research*, **26**(7), 1061–4.

van Wyk, M., Wässle, H., & Taylor, W. R. 2009. Receptive field properties of ON- and OFF-ganglion cells in the mouse retina. *Vis Neurosci*, **26**(3), 297–308.

Vaney, D. I., Nelson, J. C., & Pow, D. V. 1998. Neurotransmitter coupling through gap junctions in the retina. *The Journal of neuroscience : the official journal of the Society for Neuroscience*, **18**(24), 10594–602.

Vidal, M., Morris, R., Grosveld, F., & Spanopoulou, E. 1990. Tissue-specific control elements of the Thy-1 gene. *The EMBO journal*, **9**(3), 833–40.

Viney, T. J., Balint, K., Hillier, D., Siegert, S., Boldogkoi, Z., Enquist, L. W., Meister, M., Cepko, C. L., & Roska, B. 2007. Local retinal circuits of melanopsin-containing ganglion cells identified by transsynaptic viral tracing. *Current biology : CB*, **17**(11), 981–8.

Völgyi, B., Chheda, S., & Bloomfield, S. A. 2009. Tracer coupling patterns of the ganglion cell subtypes in the mouse retina. *J Comp Neurol*, **512**(5), 664–87.

Vugler, A. A., Redgrave, P., Semo, M., Lawrence, J., Greenwood, J., & Coffey, P. J. 2007. Dopamine neurones form a discrete plexus with melanopsin cells in normal and degenerating retina. *Experimental neurology*, **205**(1), 26–35.

Weiss, J., O'Sullivan, G. A., Heinze, L., Chen, H. X., Betz, H., & Wassle, H. 2008. Glycinergic input of small-field amacrine cells in the retinas of wildtype and glycine receptor deficient mice. *Molecular and cellular neurosciences*, **37**(1), 40–55.

Wikler, K. C., & Rakic, P. 1990. Distribution of photoreceptor subtypes in the retina of diurnal and nocturnal primates. *The Journal of neuroscience : the official journal of the Society for Neuroscience*, **10**(10), 3390–401.

Wikler, K. C., Williams, R. W., & Rakic, P. 1990. Photoreceptor mosaic: number and distribution of rods and cones in the rhesus monkey retina. *The Journal of comparative neurology*, **297**(4), 499–508.

Wong, K. Y., Dunn, F. A., Graham, D. M., & Berson, D. M. 2007. Synaptic influences on rat ganglion-cell photoreceptors. *The Journal of physiology*, **582**(Pt 1), 279–96.

Wässle, H. 2004. Parallel processing in the mammalian retina. *Nature reviews. Neuroscience*, **5**(10), 747–57.

Wässle, H., & Boycott, B. B. 1991. Functional architecture of the mammalian retina. *Physiological reviews*, **71**(2), 447–80.

Wässle, H., Grünert, U., Martin, P. R., & Boycott, B. B. 1994. Immunocytochemical characterization and spatial distribution of midget bipolar cells in the macaque monkey retina. *Vision research*, **34**(5), 561–79.

Wässle, H., Koulen, P., Brandstätter, J. H., Fletcher, E. L., & Becker, C. M. 1998. Glycine and GABA receptors in the mammalian retina. *Vision research*, **38**(10), 1411–30.

Wässle, H., Puller, C., Müller, F., & Haverkamp, S. 2009a. Cone contacts, mosaics, and territories of bipolar cells in the mouse retina. *J Neurosci*, **29**(1), 106–17.

Wässle, H., Heinze, L., Ivanova, E., Majumdar, S., Weiss, J., Harvey, R. J., & Haverkamp, S. 2009b. Glycinergic transmission in the Mammalian retina. *Frontiers in molecular neuroscience*, **2**, 6.

Zhang, C., & McCall, M. A. 2012. Receptor targets of amacrine cells. *Visual neuroscience*, **29**(1), 11–29.

Zhang, D. Q., Zhou, T. R., & McMahon, D. G. 2007. Functional heterogeneity of retinal dopaminergic neurons underlying their multiple roles in vision. *The Journal of neuroscience : the official journal of the Society for Neuroscience*, **27**(3), 692–9.

Zhang, Y., Kim, I. J., Sanes, J. R., & Meister, M. 2012. The most numerous ganglion cell type of the mouse retina is a selective feature detector. *Proceedings of the National Academy of Sciences of the United States of America*, **109**(36), E2391–8.

Summary

Before signals of the visual environment are transferred to higher brain areas via the optic nerve, they are processed and filtered in parallel pathways within the retina. In the past a plethora of functionally distinct ganglion cell types responding to certain aspects of the environment, such as direction of movement, contrast and colour have been described. Aim of this thesis was the anatomical investigation of the selectivity in retinal circuits underlying this diversity. For this purpose, mouse and macaque retinae were analysed. OFF-ganglion cells in the mouse retina received their excitatory drive unselectively from all bipolar cell types stratifying within the area of their dendritic trees. Only the input to direction-selective C6 ganglion cells and bistratified D2 ganglion cells appeared to be weighted.

In primates the highly specialised midget-system forms a 1:1 connection from red- and green-sensitive cones onto midget bipolar- and ganglion cells, building the substrate for red/green colour vision. Here it was demonstrated that blue-sensitive (S-) cones also contact OFF-midget bipolars and are, thus, potential candidates to transfer blue-OFF signals to M1 intrinsically photosensitive ganglion cells (ipRGCs). M1 cells received glycinergic input from A8 amacrine cells and express $GABA_A$ receptors containing subunit $\alpha 3$. M2 cells, in contrast, received less inhibitory input.

Zusammenfassung

Bereits in der Retina werden Informationen über Lichtreize aus der Umwelt in parallelen Schaltkreisen bearbeitet und gefiltert, bevor sie über die Axone der Ganglienzellen an höhere visuelle Zentren des Gehirns weitergeleitet werden. Bisher wurde eine Vielfalt an Ganglienzelltypen beschrieben, welche auf bestimmte Aspekte der Umwelt wie Bewegung, Kontrast oder Farbe spezifisch reagieren. Ziel dieser anatomischen Arbeit war es selektive Verschaltungen retinaler Nervenzellen zu untersuchen, die zu diesem vielfältigen Anwortverhalten führen. Als Modellsystem wurden Retinae von Mäusen und Makaken verwendet. In dieser Arbeit wurde gezeigt, dass OFF-Ganglienzellen der Mausretina ihren exzitatorischen Eingang größtenteils unspezifisch, von allen Bipolarzelltypen innerhalb ihres dendritischen Feldes erhalten. Allein für richtungsselektive C6 Ganglienzellen und, in geringerem Maße, für bistratifizierte D2 Ganglienzellen konnte eine ungleichmäßige Gewichtung des Eingangs verschiedener Bipolarzelltypen festgestellt werden.

In der Primatenretina hingegen, ist ein hochspezifisches midget-System beschrieben, welches in zentraler Retina über eine 1:1 Verschaltung von rot- und grün-selektiven Zapfen, midget Bipolar- und Ganglienzellen rot/grün Farbsehen ermöglicht. Im Rahmen dieser Dissertation wurde in Makakenretina gezeigt, dass auch blau-selektive (S-) Zapfen mit OFF-midget Bipolarzellen verknüpft sind und somit eine potentielle Quelle für blau-OFF-Signale der M1 intrinsisch-photosensitiven Ganglienzellen (ipRGCs) darstellen. M1 ipRGCs erhalten über Glyzinrezeptoren Eingang von A8 Amakrinzellen und exprimieren $GABA_A\alpha 3$ Rezeptor Untereinheiten. M2 ipRGCs hingegen werden nur geringfügig inhibitorisch moduliert.

Danksagung

For data protection reasons only in the printed version.
Aus Datenschutzgründen nur in der gedruckten Fassung.

Eidesstattliche Erklärung

Hiermit erkläre ich, Sonja Neumann, diese Doktorarbeit selbstständig verfaßt und keine anderen als die angegebenen Quellen und Hilfsmittel verwendet zu haben.

Mainz, den 16.10.2014

Sonja Neumann

Curriculum Vitae

For data protection reasons only in the printed version.
Aus Datenschutzgründen nur in der gedruckten Fassung.